Ministry of Energy and Water Resources
Geological Survey of Israel

Tel-Aviv University

Magnetic Properties of Carbonate Rocks as a Tool for Estimating Strain near the Dead Sea Transform, Northern Israel

Ran Issachar

Report GSI/25/2013

Jerusalem, October 2013

30 Malkhe Israel St., Jerusalem 95501, Israel

Cover design: Nili Almog

Front Cover: Akbara Rock
Photography: Ran Issachar

Ministry of National infrastructures
Energy and Water Resources
Geological Survey of Israel

Magnetic Properties of Carbonate Rocks as a Tool for Estimating Strain near the Dead Sea Transform, Northern Israel

Ran Issachar

Thesis submitted in partial fulfillment of the requirement for the degree of
M.Sc Geophysical, Atmospheric and Planetary Sciences, Tel-Aviv University.

This work was carried out under the supervision of:
Dr. Tsafrir Levi, Geological Survey of Israel, Jerusalem
Prof. Ram Weinberger, Geological Survey of Israel, Jerusalem
Prof. Shmuel Marco, Department of Geophysical, Atmospheric and Planetary Sciences,
Tel-Aviv University

Report GSI/25/2013 Jerusalem, December 2013

Abstract

To improve the knowledge of the strain field along the Dead-Sea Transform (DST) system in northern Israel, I measured and analyzed the magnetic properties of ~400 samples of Eocene rocks from the Rosh-Pinna, Mt. Gilboa and the HaOnn-Cliffs areas. Analyses of XRD diffraction, thin-sections and scanning electron microscopy (SEM) images indicate that the Eocene Bar-Kokhba Formation consists of crystalline calcite and the amounts of *Fe, Mn, Mg, Al* and *Si* are very low. The Bar-Kokhba rocks are diamagnetic with low-field average bulk-susceptibility of $k_m = -10.95 \pm 1.01[\mu SI]$, indicating that the magnetic susceptibility is exclusively controlled by calcite crystals. The orientations of the anisotropy of magnetic susceptibility (AMS) k_3 axes are co-axial with preferred crystal orientation of the calcite *c-axes* and suggesting the maximum shortening axes. I show that the anisotropy parameters (P` and Δk) are associated with the relative magnitudes of the finite strains accumulated in the rocks. The AMS of ~300 samples from the Eocene Bar-Kokhba Formation in the Rosh-Pinna region reveals ~N-S maximum horizontal shortening that is most likely associated with the DST activity. The strain magnitudes next to the DST are generally heterogeneous and in most cases not associated with distinct structures.

An isolation method of magnetic phases, developed in this study, reveals that the paramagnetic phase of *Fe*-bearing minerals above 500 ppm content mask the diamagnetic phase of calcite-bearing rocks, and dominate the AMS. The diamagnetic phase was successfully isolated from the AMS of multi-phases rock, in one study case, and reveals P' values in the range between 1.01 to 1.04 .

The Eocene chalks of the Adulam, Timrat and Maresha Formations have weak diamagnetic to weak paramagnetic low-field susceptibility. The AMS of the Timrat Formation consists of three magnetic phases: diamagnetic of calcite, paramagnetic of clay-rich minerals and ferrimagnetic of magnetite grains. Using integrative techniques in the isolation method the contribution of the sub-phases to the total AMS was evaluated. I infer that the principal axes of the total AMS in Timrat Formation are indicative of preferred crystal orientation of the calcite diamagnetic phase.

Content

List of figures

List of tables

Glossary of magnetic terminology

AMS - Anisotropy of Magnetic Susceptibility.

AARM - Anisotropy of Anhysteretic Remanent Magnetization.

IRM - Isothermal Remanent Magnetization.

k - Magnetic susceptibility.

H - Magnetic field.

M - Magnetization.

H_d - Demagnetization field.

k_1, k_2, k_3 - Maximum, intermediate and minimum principal susceptibilities respectively.

k_m - Low-field Bulk susceptibility

P - Anisotropy degree.

P` - Corrected anisotropy degree.

Δk - Susceptibility difference.

T- Anisotropy shape factor.

L - Magnetic lineation.

F - Magnetic foliation.

k_t - The total susceptibility tensor of a specimen.

$\hat{k}$ - Normalized susceptibility tensor (k_m in the norming factor).

k_f, k_p, k_d - Ferromagnetic, paramagnetic, and diamagnetic susceptibilities tensors respectively.

c_f, c_p, c_d - Respective ferromagnetic, paramagnetic, and diamagnetic percentages respectively.

kT – Temperature dependence susceptibility.

1. Introduction

1.1. Background and significance

Elastic and inelastic strains that commonly accumulate close to plate boundaries are mainly released by seismic and aseismic movements along fault planes. The rocks in the surrounding areas are deformed in different styles of deformation structures. Knowledge of the strain field that developed during the geological time provides insight into the tectonic evolution of plate boundaries and helps in understanding the mechanisms and the nature of the processes associated with plate movements. The mutual dependence of the strain field, around continental plate-bounding transform faults on the regional stress field and mechanical properties of host rocks and the faults are only partially known. The importance of studying the strain fields and nature of deformation is growing due to the heavily dense population and human activities in close proximity to the continental transforms such as in California and the northern parts of Israel. Previous studies done in northern Israel are commonly based on the study of meso-scale kinematic indicators such as faults, joint sets, and folds (Eyal, 1996; Eyal and Reches, 1983; Hatzor and Reches, 1990; Reches, 1987; Reches and Hoexter, 1981; Ron and Eyal, 1985). These methods are commonly used by structural geologists and depend on finding meso-structures, which are sometimes hard to observe. In order to complement meso-structure methods, efforts are invested in finding microscopic deformation indicators. The texture of rocks in many cases can indicate the principal axes of the strain field (Rutter and Rusbridge, 1977). Neutron and X-ray diffraction are common methods used to determine the texture of deformed rocks (Wenk et al., 1984). Studies show that anisotropy of magnetic susceptibility (AMS) can also serve as a texture indicator of deformed rocks. The AMS is a rapid and more straight-forward method that sums up the magnetic contribution of all the components of the rock and presents an average magnetic fabric (Borradaile, 1988). The correlation between the magnetic fabric and the rock texture can be done when the magnetically-dominated minerals are known. Literature on the magnetic susceptibility of rocks is widely available (Borradaile, 1987; Borradaile, 1988; Borradaile, 1991; Borradaile and Henry, 1997; Borradaile and Jackson, 2004; Borradaile and Jackson, 2010; Hrouda, 1982; Hrouda, 1993; Hrouda et al., 2000; Hrouda and Jezek, 1999; Jackson and Tauxe, 1991; Tarling and Hrouda, 1993). The advance analytical tools and techniques enable accurate reproducible measurements of diamagnetic and weak paramagnetic rocks. Both AMS and strain are second-rank tensors, leading to

attempts of correlating AMS and strain (Borradaile, 1987; Borradaile, 1991; Hirt et al., 2000; Hrouda, 1993; Kligfield et al., 1982; Tauxe, 1998). The AMS axes show, in many deformed environments, a fair to good correlation with the directions of the principal strain axes (Borradaile, 1987; Borradaile, 1988; Borradaile, 1991; Borradaile and Henry, 1997; Hrouda et al., 2009; Latta and Anastasio, 2007; Mamtani and Sengupta, 2009; Pares et al., 1999; Soto et al., 2007; Tarling and Hrouda, 1993). Plastic deformation can produce strong preferred crystal orientation and strong correlation of the AMS axial orientations (Borradaile and Jackson, 2010). For high symmetry crystals principal susceptibilities and crystal axes are parallel (Nye, 1957). The alignment of calcite crystallographic *c*-axes parallel to the shortening direction is directly inferred from the magnetic fabric (Owens and Rutter, 1978; Schmidt et al., 2006; Wenk et al., 1987). Previous works determined principal strain field directions from AMS measurements of carbonate rocks by correlating the AMS to the preferred crystal orientation of the calcite crystals in the rock (de Wall et al., 2000; Hamilton et al., 2004; Levi and Weinberger, 2011).

In this study I try to determine the strain field near the Dead-Sea-Transform (DST) in northern Israel. The DST extends along ~1000 km, from the northern ends of the Red-Sea-rift to the Taurus convergence zone in Turkey, accommodating strike-slip motion along the plate boundary between the Arabian plate and the Sinai sub-plate (or African plate) (Figure 1) with ~105 km of left-lateral offset since the Early-Middle Miocene (Freund, 1970; Garfunkel, 1981; Joffe and Garfunkel, 1987; Quennell, 1956). The texture of calcite crystals in Eocene carbonate rocks is estimated, using the AMS method, and correlated to the principal directions of the regional strain field. Calcite has weak diamagnetic response that can be easily overprinted by paramagnetic and ferromagnetic minerals involved in the rock (Borradaile, 1988). Based on the above, I searched for rocks that contain negligible amounts of second-phase minerals and crystal impurities, lower than 400ppm. I focused on the magnetic fabrics of the Bar-Kokhba Formation, consisting of limestone that was identified from preliminary analysis as a pure calcite-bearing rock. In addition, I focused on the Eocene chalks of the Timrat, Adulam and Maresha formations that are widely spread along the DST. Based on preliminary results, the Adulam and Maresha formations are identified as weak diamagnetic or weak paramagnetic rocks. In this study I apply an isolation method of magnetic phases on the Bar-Kokhba and Timrat rocks in order to investigate the effect of paramagnetic/ferromagnetic minerals on the total AMS of carbonate rocks.

1.2. Objectives

Aiming to improve the understanding of the deformation and strain distribution on the one hand, and to broaden the knowledge on the magnetic properties of calcite-bearing rocks on the other, the objectives of this study were:

1) To improve the understanding of the spatial and temporal variations of the strain field associated with the deformation adjacent to the DST in northern Israel (Rosh-Pinna area). This objective is achieved by measuring the AMS of pure calcite-bearing rocks as proxies for the strain field next to the DST.

1) To develop a process method for isolating the effect of paramagnetic/ferromagnetic minerals on the magnetic properties of carbonate rocks. This would help to better understand the possibilities and limitations using the AMS of carbonate rocks as a strain proxy. By applying this method on Bar-Kokhba rocks which consist of multi magnetic phases associated with young chemical alteration processes, I could evaluate the effect of the second-phase minerals on the AMS.
2) To investigate the AMS of weak diamagnetic and weak paramagnetic chalks that crop out next to the DST. Correlating the AMS of these formations to the strain field could promote the understanding of the spatial and temporal variations of the strain field within the DST.

1.3. Geological setting

1.3.1 Strain fields around the Dead-Sea Transform

The DST extends along ~1000 km, from the northern ends of the Red Sea rift to the Taurus convergence zone in Turkey, passing through the Gulf of Elat-Aqaba, the Jordan valley, Lebanon and Syria. The DST accommodates strike-slip motion along the plate boundary between the Arabian plate and the Sinai sub-plate (or African plate) (Figure 1). A host of stratigraphic, structural and geochronological evidence suggests ~105 km of left-lateral offset across the southern parts of the DST since the Early-Middle Miocene (Bartov et al., 1980; Freund, 1970; Garfunkel, 1981; Joffe and Garfunkel, 1987; Quennell, 1956). The estimated slip rate, based on tectonic modeling and long-term geological considerations, range from 6 to 10 mm/yr (Joffe and Garfunkel, 1987), while current GPS-based models indicate a relative plate motion of 4-5 mm/yr (ArRajehi et al., 2010; Le Beon et al., 2008; Reilinger et al., 2006). Geological observations suggest that two distinct paleostrain regimes operated in the Sinai sub-plate (Eyal, 1996; Eyal and Reches, 1983): (1) WNW – ESE shortening and NNE – SSW extension, beginning in the Turonian, is associated with the development of the Syrian Arc fold belt (Krenkel, 1924); and (2) NNW – SSE shortening and ENE – WSW extension that was active from middle Miocene to recent, and is associated with the left-lateral motion along the DST. Garfunkel (1981) showed that the directions of the principal stresses adjacent to the DST are probably deflected toward the fault trace. He suggested that the deflection is greatest near rhomb-shape grabens, where the DST acts as a weak zone (e.g., "free boundary"). Ron and Eyal (1985) inferred, from combined analysis of mega- and meso-structures, a strain field characterized by NNW – SSE horizontal shortening in the Tiberias area. Studies within the Korazim block suggests that the striking geometry north to the Sea-of-Galilee has changed during the last million years (Heimann and Ron, 1993; Rotstein and Bartov, 1989). As a result the area absorbed deformation in the form of right-lateral slips and counterclockwise rotation within the Korazim block. Weinberger et al. (2009), who investigated the style of deformation between the Hula basin in northern Israel and the Lebanese restraining bend in southern Lebanon found evidence for the transition from an early (Miocene–lower Pliocene) phase of pure strike-slip motion, with NW – SE regional shortening, to a late (Pleistocene to Recent) phase of convergent strike slip with E – W shortening.

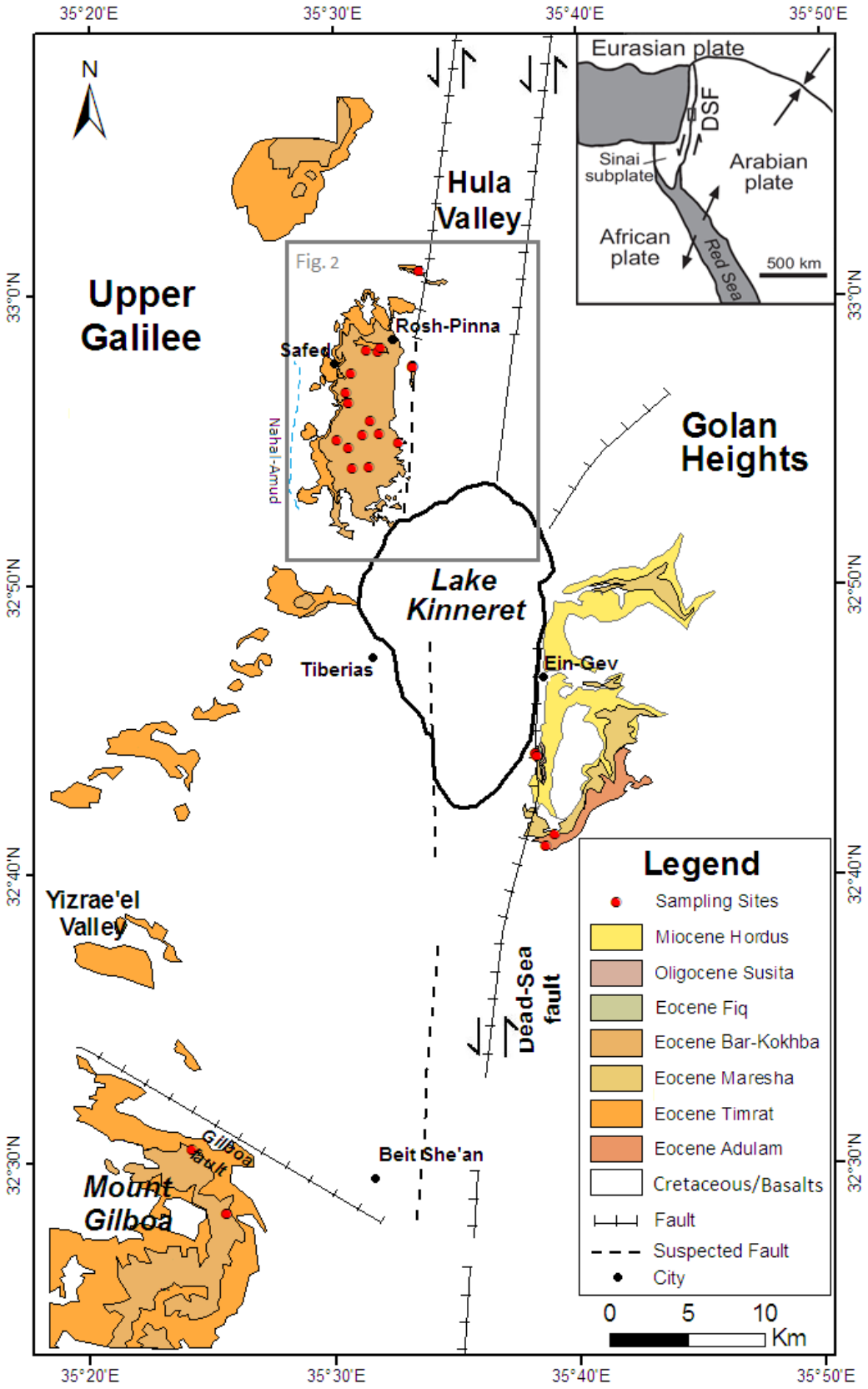

Figure 1. Geological map of the study area. Faults after Weinstein (2011). Red dots mark the sampling sites.

1.3.2 Structure and lithology of the Rosh-Pinna area

The ~75 km^2 Rosh-Pinna area consists of Eocene limestones and chalks (Figure 2). The Rosh-Pinna area is bounded on the east by the Korazim block (Sneh and Weinberger, 2006), which is mainly covered by Plio-Pleistocene basalts (Heimann, 1990). From the west, the Nahal-Amud creek serves as the western boundary of the Rosh-Pinna area; typically Galilee Cretaceous rocks are exposed west of it (Levitte, 2001). The Timrat Formation is exposed at the base of the Rosh-Pinna creek and in the western slopes of the Rosh-Pinna area. The layers dip slightly to the southeast; in the eastern parts the attitude of the layers is almost horizontal. No major fault structures or fold systems are found within the Rosh-Pinna area.

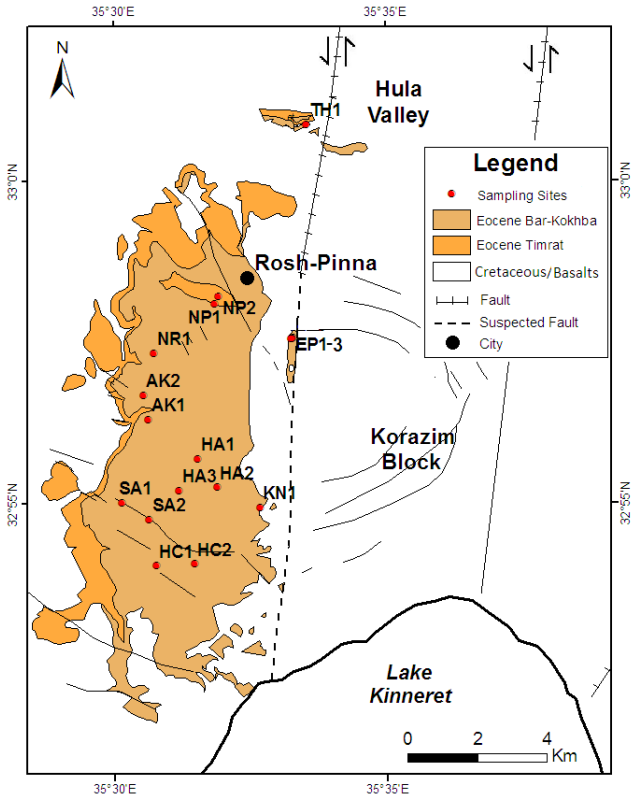

Figure 2. Geological map of the study area. Faults after Weinstein (2011). Red dots mark the sampling sites.

1.4. AMS and deformation of carbonate rocks

1.4.1. Magnetic anisotropy of carbonate rocks

The magnetic susceptibility (k) relates the applied magnetic field (H) to an induced magnetization (M) by $\begin{bmatrix} M_x \\ M_y \\ M_z \end{bmatrix} = \begin{bmatrix} k_{xx} & k_{xy} & k_{xz} \\ k_{xy} & k_{yy} & k_{yz} \\ k_{xz} & k_{yz} & k_{zz} \end{bmatrix} \begin{bmatrix} H_x \\ H_y \\ H_z \end{bmatrix}$ (Borradaile and Jackson, 2004). In anisotropic materials the shape of the susceptibility is described by three principal values k_{max} (k_1), k_{int} (k_2), and k_{min} (k_3), which correspond to the maximum, intermediate and minimum magnetic susceptibility magnitudes, respectively (Borradaile and Jackson, 2004). The orientations of the principal susceptibilities are usually presented on the lower hemisphere of an equal-area projection. There is a wide variety of parameters that have been used to describe the axial magnitude relationships of the susceptibility ellipsoid (Jelinek, 1981):

1) Mean susceptibility or bulk susceptibility, $k_m = \frac{k_1+k_2+k_3}{3}$.
2) Anisotropy degree, $P = \frac{k_1}{k_3}$, and corrected anisotropy degree, $P` = e^{\sqrt{2((n_1-n)^2+(n_2-n)^2+(n_3-n)^2)}}$ where; n_1, n_2 and n_3 are the natural logarithms of the principal susceptibilities and $n = \frac{n_1+n_2+n_3}{3}$.
3) Shape of anisotropy, $U = \frac{2k_2-k_1-k_3}{k_1-k_3}$, and or shape factor, $T = \frac{2n-n_1-n_3}{n_1-n_3}$, where $U\ or\ T = -1$ represents prolate ellipsoid, $U\ or\ T = 0$ represents sphere and $U\ or\ T = +1$ represents oblate ellipsoid.
4) Susceptibility difference, $\Delta k = k_1 - k_3$.
5) Magnetic lineation, $L = \frac{k_1}{k_2}$.
6) Magnetic foliation, $F = \frac{k_2}{k_3}$.

Both AMS and strain are second-rank tensors, leading to attempts to correlate AMS and strain (Borradaile, 1987; Borradaile, 1991; Hirt et al., 2000; Hrouda, 1993; Kligfield et al., 1982; Tauxe, 1998). The AMS axes show a fair to good correlation with the directions of the principal strain axes in many deformed environments (Borradaile, 1987; Borradaile, 1988; Borradaile, 1991; Borradaile and Henry, 1997; Hrouda et al., 2009; Latta and Anastasio, 2007; Mamtani and Sengupta, 2009; Pares et al., 1999; Soto et al., 2007; Tarling and Hrouda, 1993). Studies show that new magnetic fabric develops in rocks during deformation

(Almqvist et al., 2009; Borradaile and Jackson, 2004; Cogne and Perroud, 1988; Dietrich and Song, 1984; Hirt et al., 1988; Jayangondaperumal et al., 2010; Soto et al., 2009) but the correlation between the strain field and the magnetic fabric depends on the minerals that form the rock. Limited success and no reliable correlation has been established between the magnitudes of the AMS axes of diamagnetic and low-paramagnetic rocks and the strain magnitudes (Borradaile and Jackson, 2010; Latta and Anastasio, 2007; Parés and B.A., 2004). One major cause for the unsuccessful attempt to correlate magnitudes of the AMS axes with the magnitudes of strain axes is that the former are mainly governed by the amounts of strong magnetic minerals (ferromagnetic, ferrimagnetic and strong paramagnetic) in the rock (Borradaile and Henry, 1997). Nevertheless, Borradaile and Alfrod (1988) found a correlation between the change in the anisotropy degree P and the bulk strain ratio. The AMS anisotropy degree of iron-free carbonate rocks is presumed to have a stronger dependency on the magnitude of strain than on the bulk susceptibility, k_m (Almqvist et al., 2010).

In general, magnetic anisotropy is controlled by grain-shape anisotropy and by crystal anisotropy (Borradaile and Jackson, 2010). Grain-shape anisotropy is mostly effective in strong magnetic rocks, due to the nature of the demagnetizing field (H_d), when the AMS of low magnetic rocks, such as carbonate rocks, is controlled entirely by crystal anisotropy (see *Appendix I*). Crystal anisotropy is reflected by a preferred crystal orientation in the rock texture. Preferred crystal orientation in carbonate rocks may develop due to three different mechanisms: (1) crystallization under non-hydrostatic stress field (Kamb, 1959); (2) plastic deformation (Hobbs et al., 1976); and (3) crystal growth in veins and dikes. The third is not pertinent to this study. The theory of preferred crystal orientation due to crystallization under non-hydrostatic stress field was developed by Kamb (1959) and later by Patterson (1973) and McKenzie et al. (1996). Field-work and laboratory studies have confirmed and broadened these relationships (Hounslow, 2001; Neumann, 1969; Tullis and Yund, 1982). When crystallization takes place under stress, the weakest *c-axis* of calcite tends to align with the greatest principal pressure axis (Kamb, 1959), other carbonates belonging to the same crystal system show similar responses to stress (McKenzie et al., 1996; Patterson, 1973). Preferred crystal orientation as a result of plastic deformation by slip is directly related to the mechanics of dislocation glide (Hobbs et al., 1976). The theoretical basis for the development of preferred orientation by slip and consequent rotation is well established (Bishop, 1954; Bishopa, 1953; Bishopa and Hilla, 1951; Calnan and Clews, 1950; Calnan and

Clews, 1951; Taylor, 1938). Textural analyses show that calcite *c-axis* points to the shortening direction under pure shear and simple shear (Wenk et al., 1987). Laboratory experiments, performed on pure-calcite marbles and single calcite crystals, reveal a very good correlation between the preferred *c-axis* directions of calcite measured with neutron and X-ray diffraction and the easy-magnetizing directions as obtained from AMS measurements (Chadima et al., 2004; de Wall et al., 2000; Kligfield et al., 1982; Owens and Rutter, 1978; Siegesmund et al., 1995). Calcite was shown to be very sensitive to strain in compaction experiments, the AMS attains saturation (maximal P' value) at about 40% shortening, and gets to its half value after deformation of 15-20% shortening (Owens and Rutter, 1978). Calcite twinning and other plastic deformation of crystals (Evans and Elmore, 2006; Rutter et al., 1994; Wenk et al., 1987) have long been used for petrofabric studies as sensitive indicators of incremental strain axes and are essentially parallel to the causative paleo-strain axes (Hamilton et al., 2004). It is well known that over a wide range of temperatures, calcite aggregates can be deformed experimentally by intercrystalline gliding. Commonly, samples that are subjected to axial compression result in coaxial finite strain and the alignment of the *c-axis* parallel to the shortening direction (Owens and Rutter, 1978). A series of compaction experiments of synthetic calcite-muscovite samples reveals that the strength of the diamagnetic anisotropy and the susceptibility difference generally increases with the shortening rate, and is not significantly influenced by the muscovite content (Schmidt et al., 2009). Pure calcite crystals are evidently magnetically anisotropic with susceptibility values of -13.8 [μSI] along the *c*-axis and - 12.4 [μSI] along the *a/b* plane (Nye, 1957; Owens and Rutter, 1978). More recently Schmidt et al. (2006) found bulk-susceptibility of calcite at a room temperature of $k_m = -12.09 \pm 0.5\ [\mu SI]$, and susceptibility difference of $\Delta k = 1.10 \pm 0.01\ [\mu SI]$ (Schmidt et al., 2006). Calcite has a prolate AMS shape, using the absolute values of the principals susceptibilities for diamagnetic materials ,($K_1 = |k_3| > K_2 = |k_2| > K_3 = |k_1|$) (Borradaile and Jackson, 2010; Schmidt et al., 2006), with $T = -1$ and $P` = 1.113$ (Owens and Bamford, 1976). In this study the AMS axes of diamagnetic rocks are described by the assigned values of the principal susceptibilities, hence, the minimum susceptibility (k_3) refers to the most negative susceptibility value. In addition, the AMS parameters (P, P', L, F, T, Δk) are calculated based on the absolute (unsigned) values of the principal susceptibilities. This convention is recommended for describing the orientations of the principal axes and their magnitudes (for more details see Hrouda, 2004).

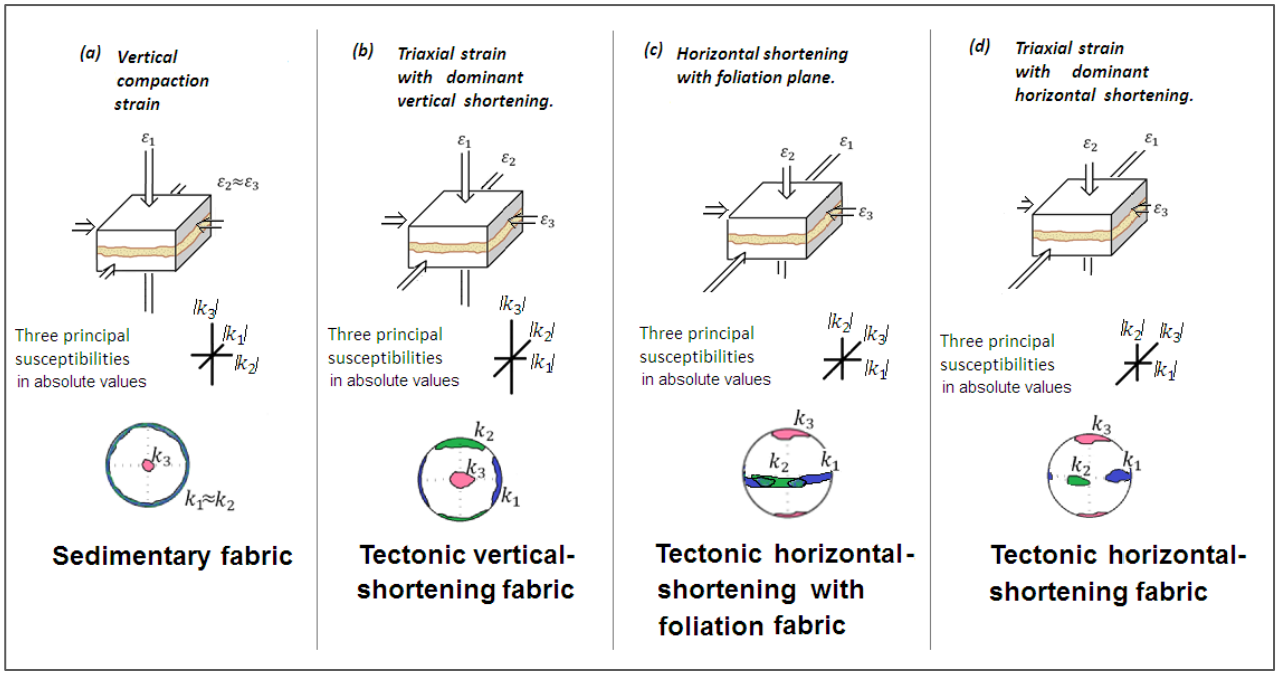

Figure 3. Coaxial deformation path for diamagnetic carbonate rock, demonstrating the transition from sedimentary AMS fabric to different types of tectonic fabrics.

1.4.2. Magnetic fabrics of geological environments

Generally, the corrected anisotropy degree (P'), and the susceptibility-difference (Δk) of deformed calcite-bearing diamagnetic rocks are expected to be lower than those of a single calcite crystal, because perfect alignments in sedimentary rocks are rare (Hrouda, 2004).

Under sedimentation and lithostatic pressure conditions, the orientation of some of the calcite *c-axes* are expected to align parallel to the maximum vertical shortening (ε_1) (Hrouda, 2004). In such cases, the AMS has well-grouped k_3 axes oriented vertical to bedding, and scattered k_1 and k_2 axes parallel to bedding. The magnitudes of the principal susceptibility reflect the strain field with $k_1 \approx k_2 > k_3$, and therefore L>F (using the absolute values of the principal susceptibilities for diamagnetic materials). This magnetic fabric is hereafter termed a sedimentary fabric (Figure 3a).

Under tectonic stress, the AMS axes are co-axial with the principal strain directions ($\varepsilon_1 \geq \varepsilon_2 \geq \varepsilon_3$), where ε_1, ε_2 and ε_3 are the maximum, intermediate and minimum shortening axis, respectively. Under these conditions, generally k_1, k_2 and k_3 are parallel to ε_3, ε_2 and ε_1, respectively, and the AMS fabric is 'normal' (k_3 parallel to *c*-axes) (Borradaile and Jackson, 2010).

Under triaxial strain, when the vertical shortening is dominant the principal susceptibility axes are expected to be well-grouped with k_3 axes perpendicular to the bedding planes, k_2 axes parallel to the bedding planes in ε_2 direction, and k_1 axes parallel to the bedding planes and to minimum shortening (ε_3). This magnetic fabric is hereafter termed a tectonic vertical-shortening fabric (Figure 3b).

In dominant horizontal shortening with foliation plane, k_3 axes are perpendicular to the foliation planes and k_1 and k_2 axes are parallel to the foliation (Pares and van der Pluijm, 2003). The magnetic fabric shows well-grouped k_3 axes perpendicular to the foliation planes, and scattered k_1 and k_2 axes with overlapping of the 95% confidence ellipses. These magnetic fabrics are hereafter termed a tectonic horizontal-shortening with foliation fabric (Figure 3c).

Under triaxial strain where the horizontal shortening is dominant the principal susceptibility axes are expected to be well-grouped with k_3 axes parallel to the horizontal maximum shortening axis (ε_1), k_2 axes parallel ε_2 direction and k_1 parallel to the minimum shortening (ε_3). This magnetic fabric is hereafter termed a tectonic horizontal-shortening fabric (Figure 3d).

When a sample contains more than 400 ppm of Fe2+ or Mn2+ (iron-rich calcite) (Ihmle et al., 1989; Rochette, 1988; Schmidt et al., 2006), ions substitutions form within the crystal structure and inverse AMS fabric (k_1 parallel to *c*-axes) is produced (Rochette, 1988; Ihmle et al., 1989). Under these conditions, calcite becomes less diamagnetic, or more paramagnetic (Almqvist et al., 2009; Rochette, 1988; Schmidt et al., 2006; Schmidt et al., 2007) and the AMS is represented by an oblate AMS ellipsoid (Schmidt et al., 2006).

1.5. Isolation of magnetic phases in carbonate rocks

1.5.1. Background

The AMS is the sum of the magnetic contribution of all the components of the rock and presents an average magnetic fabric (Borradaile, 1988). These components can have different magnetic properties and quite often the AMS of a single mineral is of interest for isolating its susceptibility.

Various experimental techniques were developed using the difference in the physical properties of different magnetic phases in order to identify and characterize the sub-fabrics of the AMS (Martin-Hernandez and Ferre, 2007). There are methods that are based on measurements at different temperatures, using the temperature dependence of paramagnetics according to the Currie-Weiss law (Morrish, 1965). Other methods are based on measuring the magnetic remanence, using the ability of ferromagnetic and ferrimagnetic minerals to retain stable permanent magnetization (Jackson and Tauxe, 1991). Other methods are based on measurements in high fields, or using frequency dependency (Martin-Hernandez and Ferre, 2007). This study applies three experimental techniques (AARM, IRM and temperature-dependent susceptibility measurements; for more details see sections 1.6.*3*-*5*). Generally all the methods have serious limitations, in empirical as well as theoretical aspects, especially in identifying and isolating magnetic sub-phases from the AMS (Hrouda et al., 2000).

In this study I suggest an isolation method, based on a combination of analytical and experimental techniques, in order to isolate the calcite diamagnetic contribution to AMS of carbonate rocks.

The susceptibility tensor of a specimen (k_t) is described with sufficient accuracy as the sum of all the susceptibilities contributed by the minerals contained (Henry and Daly, 1983; Hrouda et al., 2000):

$$k_t = c_f k_f + c_p k_p + c_d k_d \qquad 1.1$$

when:

$$c_f + c_p + c_d = 1 \qquad 1.2$$

where k_f, k_p and k_d are tensors of ferromagnetic, paramagnetic, and diamagnetic susceptibilities respectively, and c_f, c_p and c_d are the respective percentages (Hrouda et al., 2000).

Consider a rock consisting of two dominant magnetic phases: a diamagnetic phase marked with sub index $_d$ and a paramagnetic (or ferromagnetic) phase marked with sub index $_p$. In general, the susceptibility tensor (k) can be constructed from the product of normalized tensor ($\hat{k}$) and bulk susceptibility (k_m), which is also called a norming factor (Jelinek, 1977):

$$k = k_m \cdot \hat{k} \qquad 1.3$$

Then rewriting Eq 1.1 for the two phases (c_p and c_d) in that form:

$$k_{m_t} \cdot \hat{k}_t = c_p\, k_{m_p} \cdot \hat{k}_p + c_d\, k_{m_d} \cdot \hat{k}_d \qquad 1.4$$

If the interest is in one magnetic phase, the diamagnetic phase in our case, it can be estimated using the following expression:

$$k_{m_d} \cdot \hat{k}_d = \frac{1}{1-c_p}\, k_{m_t} \cdot \hat{k}_t - \frac{c_p}{1-c_p}\, k_{m_p} \cdot \hat{k}_p \qquad 1.5$$

Since the susceptibility tensors are normalized it can effectively be argued that the total bulk susceptibility is the sum of the bulk susceptibilities of the components:

$$k_{m_t} \cong c_p\, k_{m_p} + c_d\, k_{m_d} \qquad 1.6$$

Using Eq. 1.2 (for c_p and c_d) we can write:

$$k_{m_t} \cong (k_{m_p} - k_{m_d})c_p\ + k_{m_d} \qquad 1.7$$

Generally, the values of the paramagnetic/ferromagnetic bulk susceptibilities are much greater than the value of the diamagnetic bulk susceptibility, $km_p \gg km_d$, therefore Eq. 1.7 will take the form:

$$k_{m_t} \cong k_{m_p}\, c_p\ + k_{m_d} \qquad 1.8$$

Using Eq. 1.5 and 1.8 it is possible to isolate the AMS sub-fabric of the calcite diamagnetic phase of multi-phase carbonate rock.

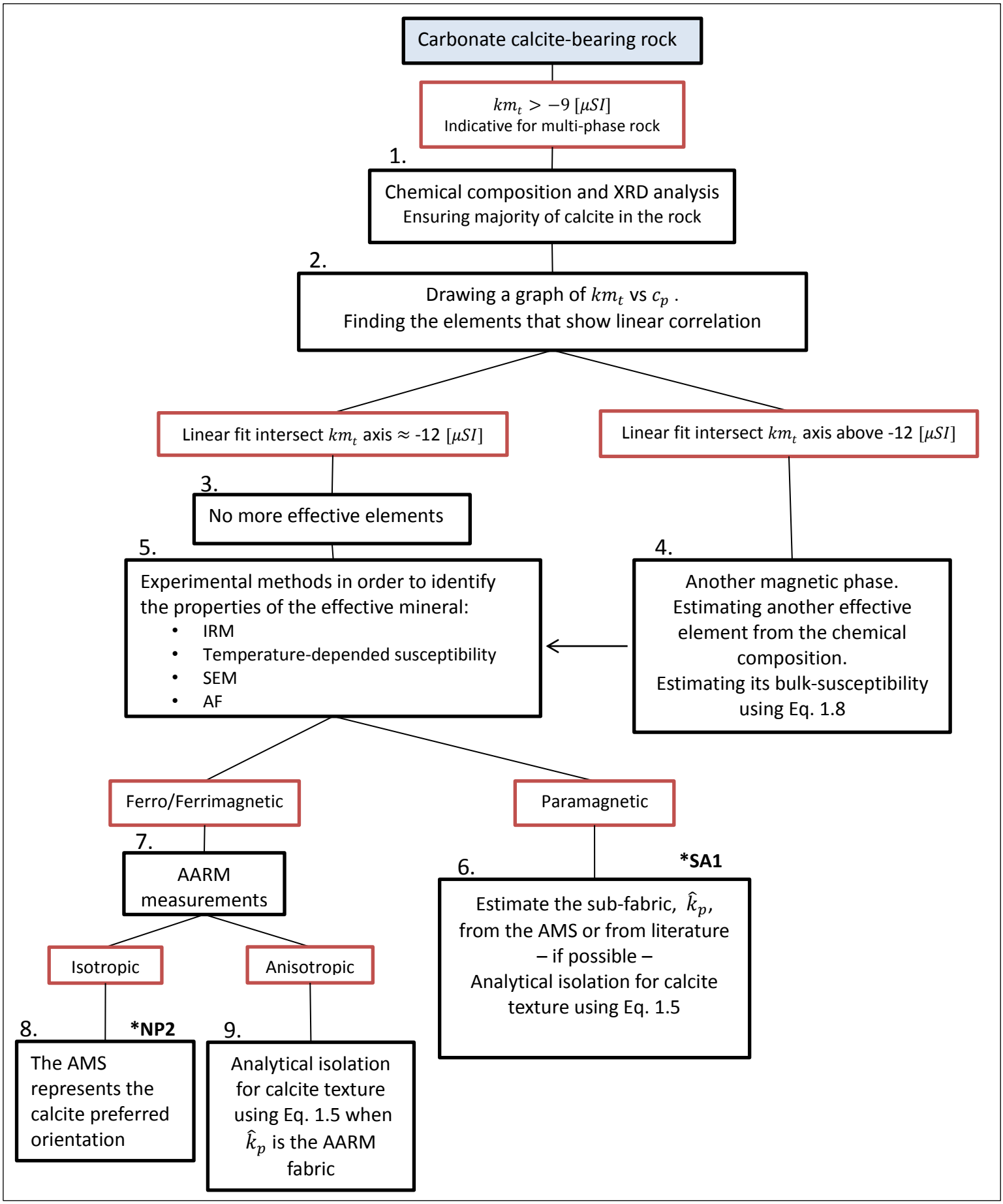

Figure 4. Flow diagram, for the identification and isolation of the AMS sub-fabrics in carbonate rocks.

*SA1 and *NP2 relates to two study cases dealt with in this paper

1.5.2. Working hypothesis and testing procedures

The existence of magnetic phase in addition to a calcite diamagnetic phase, and a para/ferromagnetic sub-fabric in the AMS is suspected when the bulk-susceptibility of carbonate rock specimen (k_{m_t}) is greater than -9 [μSI]. According to Equation 1.5, in order to isolate the AMS sub-fabric of the calcite diamagnetic phase three independent quantities should be estimated; the respective percentages of the para/ferromagnetic phase (c_p), the bulk-susceptibility of the para/ferromagnetic phase (k_{m_p}) and the normalized tensor of the para/ferromagnetic phase ($\hat{k}_p$). Chemical composition analysis can be used to estimate the respective percentages (c_p) of the elements involved in the rock (Schmidt et al., 2006). By preforming chemical composition analysis for group of specimens (of the sampling site) the relations between the specimens' bulk-susceptibilities (k_{m_t}) and the respective amounts of certain elements (c_p) can be estimated. Equation 1.8 predicts a linear correlation between k_{m_t} and c_p for the element carrying the para/ferromagnetic phase, where the slope represents k_{m_p} and the intersection with the k_{m_t} axis represents k_{m_d}. If the linear fit intersects the k_{m_t} axis around -12 [μSI], namely $k_{m_d} \approx -12$ [μSI], then it is assumed that this particular element is carrying the para/ferromagnetic phase. If the linear fit intersects the km_t axis above -12 [μSI], namely $k_{m_d} > -12$ [μSI], then it is assumed that there is another element carrying another para/ferromagnetic phase. The difficulty rises in the estimation of the normalized tensor ($\hat{k}_p$) because of the unknown physical properties of the magnetic phase. Various experimental techniques are available to identify the physical properties of the magnetic phases involved (Martin-Hernandez and Ferre, 2007). If the magnetic phase (c_p) is ferromagnetic or ferrimagnetic, then the anisotropy of anhysteretic remanent magnetization (AARM) can be used to estimate the normalized tensor $\hat{k}_p$ (for more details see section 1.6.3). However, If the magnetic phase (c_p) is paramagnetic, then no experimental method is available to estimate its magnetic principal axes (Martin-Hernandez and Ferre, 2007). Nevertheless, it may be possible to estimate $\hat{k}_p$ from the AMS measurements (exemplified in section 2.5) or to estimate its contribution to the AMS theoretically from the literature.

Figure 4 presents a flow diagram of the testing procedure for the identification and isolation of the AMS sub-fabrics in carbonate rocks according to the working hypothesis presented above. In this study I use isothermal-remanent-magnetization acquisition curves (IRM),

temperature-dependent susceptibility measurements and scanning electron microscopy techniques (for more details see sections *1.6.3-5*) to identify the physical properties of the magnetic phases involved in multi-phase carbonate rocks. I show two examples that use of this process, one for a Bar-Kokhba limestone (SA1 site) that contains second-phase minerals derived from chemical alteration (section 2.5), and the second for Timrat chalk (NP2 site) that contains magnetite grains and clay minerals within the rock texture (section 2.6).

1.6. Methods

1.6.1. Studied localities and sampling strategy

The majority of samples were taken from the Bar-Kokhba Formation in the Rosh-Pinna area (Figure 2). To compare different structural areas and different rock formations I took samples from two more different areas: three from Bar-Kokhba Formation in Mt. Gilboa area and five in the southern parts of the HaOnn-Cliffs area from different Eocene and Oligocene formations (Figure 1).

The sampling sites were distributed in different localities based on their distances from the main segments of the DST. I tried to avoid adjacency to local structures (subsidiary faults, folds) in order to examine the strain field that was influenced directly by the DST. I tried to collect 15-20 specimens from each site in order to have a statistically satisfactory sampling. The geology of the surrounding area, the nature of the rock, and the site coordinates were documented for every sampling site. The specimens were drilled with 2.5 cm core-drill. The drilling direction, the orientation and the name of the specimen were marked on every core (Figure 5). The cylindrical cores were cut to ~2 cm long samples (at the Geological Survey of Israel). Because of inaccuracies in the cutting process the volume of each sample was measured separately.

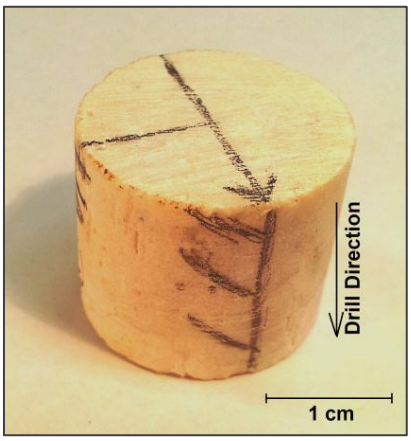

Figure 5. Rock core from the Bar-Kokhba Formation sampled for AMS measurements. Marks indicate the drilling direction.

1.6.2. AMS measurements and analysis

Mathematically, the estimation of the susceptibility tensor of a sample is satisfied by six measurements however, a larger number of directions is preferred to achieve a better accuracy for estimating measurement errors (Hext, 1963). A common design for measuring direction is proposed by Jelinek (1977) for 15 measured directions. Practically, the use of that design is cumbersome and slow because each specimen needs to be flipped manually in each direction. Hence, the spinning specimen method was subsequently developed (Jelinek, 1995), whereby the specimen is measured while it spins about three perpendicular axes. The spinning specimen method is faster, and also more accurate than the manual method. In this study the AMS was measured by the spinning specimen method with KLY-4S Kappabridge, at the magnetic fabric laboratory of the Geological Survey of Israel (GSI). The

sensitivity of the Kappabridge is on the order of 1 x 10^{-8} [SI], enabling the measurement of samples with mean susceptibility on the order of 1 [μSI]. The weak magnetic response of carbonate rocks requires rigorous consideration (Hamilton et al., 2004), the Kappabridge must be precisely calibrated and the susceptibility of the specimen-holder has to be measured several times (three times at least) before each measurement session. It was found that the Kappabridge is very sensitive to room temperature and to the magnetic environments. We therefore kept the room temperature stable and minimized the metallic objects in the laboratory. The measurements were repeated several times to ensure repetition. From each group of susceptibility tensors, of specimens belonging to same sampling site, the mean tensor and its 95% confidence intervals of the principal axes were calculated according to Jelinek's (1978). To verify whether the difference between the principal susceptibilities, determined by the measurements, compared to the measuring errors are great enough for the specimen to be considered as anisotropic, the F-test was performed (Jelinek, 1977). In this study, I considered only specimens that passed the F-test (>3.9) with 95% confidence (meaning that within the error distribution statistically 95 out of 100 specimens would be anisotropic) or its principal axes were within the total site mean-tensor 95% confidence intervals. The AMS magnitudes and principal axes and the anisotropy parameters were calculated using the software package *Anisoft42*, which relies on Jelinek's (1981) and Hrouda (2004). In this study the AMS axes of diamagnetic rocks are described by the assigned values of the principal susceptibilities, hence, the minimum susceptibility (k_3) refers to the most negative susceptibility value. In addition, the AMS parameters (*P*, *P'*, *L*, *F*, *T, Δk*) are calculated based on the absolute (unsigned) values of the principal susceptibility, which means that the largest absolute magnitude is the maximum susceptibility. This convention is recommended for describing the orientations of the principal axes and their magnitudes (for more details see Hrouda, 2004).

1.6.3. AARM measurements

The Anisotropy of Anhysteretic Remanent Magnetization (AARM) is a method to estimate the magnetic fabric of minerals that obtain remanent magnetization (Borradaile and Stupavsky, 1995; Jackson, 1991; Jackson and Tauxe, 1991; McCabe et al., 1985). The sample is subjected to a direct magnetic field under the presence of a stronger alternating magnetic field. The alternating field is slowly reduced and the direct field is held constant. In that way

the sample is magnetized in the direction of the direct field. The magnetization vector, carried by the sample, is measured. By repeating this process six (or more) times, when each time the sample is magnetized by different polarity direction, the remanence susceptibility tensor (k_r) is constructed. In order to examine the anisotropy of ferromagnetic/ferrimagnetic minerals and its contribution to the magnetic properties of the rock, AARM measurements were performed on selected samples from the Bar-Kokhba limestones and Timrat chalks. The samples were magnetized using the AMU-1A magnetizer and then demagnetized with the LDA-3A demagnetizer and the magnetization vector was measured using the JR-6A spinner magnetometer. The AARM orientations and parameters were calculated using the software package *Arem2W*.

1.6.4. *IRM*

The IRM (Isothermal Remanent Magnetization) acquisition curves are constructed by exposing the sample to increasing values of high pulse fields and measuring its magnetization each time. By demagnetizing the rock sample and then exposing it to a high pulse field the sample is magnetized. The ratio between the high pulse field and the remanent magnetization obtained by the rock is dependent on the minerals involved in the rock. Since ferromagnetic and ferrimagnetic minerals have a unique IRM signature, IRM acquisition curves can be used to identify the ferromagnetic and ferrimagnetic minerals in the rock (Fuller et al., 1988; Stockhausen, 1998). For that purpose the IRM of a selected number of samples were measured. Natural Remanent Magnetization was measured using a shielded three axes 2G 750R SRM cryogenic magnetometer, with integrated Alternating Field (AF) coils, at the paleomagnetic laboratory of the Institute of Earth Science, the Hebrew University of Jerusalem. Each sample was subjected to stepwise demagnetization with increasing intensity starting at 5 [mT] and going up to 90 [mT]. Then the samples were exposed to a high pulse field using the ASC model IM10-30 Impulse Magnetizer, starting with a field of 25 [mT] up to 200 [mT] with increments of 25 [mT], then steps of 50 [mT] up to 400 [mT] and steps of 100 [mT] up to 1600 [mT]. After each step the IRM was measured using the Magnetometer in order to create an acquisition curve of Isothermal Remanence Magnetization (IRM)

1.6.5. Temperature-dependent susceptibility measurements

Diamagnetic substances exhibit no temperature dependence of the magnetic susceptibility. Other magnetic properties (such as paramagnetism, ferromagnetism, ferrimagnetism etc.) usually exhibit temperature dependence according to the Curie-Weiss law (Ballet et al., 1985; Beausoleil et al., 1983; Hirt et al., 1995; Hrouda and Jelinek, 1990). Since minerals have unique temperature dependence signatures, temperature dependence susceptibility measurements are useful to define and estimate the contribution of minerals (Cifelli et al., 2004; Hirt et al., 1995; Hirt and Gehring, 1991; Hrouda et al., 1997; Jover et al., 1989; Schultzkrutisch and Heller, 1985). To test the contribution and identify the dominant paramagnetic and ferromagnetic minerals in the rock, magnetic susceptibility measurements at variable temperatures were performed on selected samples. The measurements were performed at low temperatures, ranging from the temperature of liquid nitrogen (-192°) to 700°. For measuring susceptibility in high temperatures I use an agico CS3 furnace, and a CS-L cryostat for low temperatures.

1.6.6. Chemical composition

Chemical composition analyses were performed on selected number of samples to determine the relative content of trace elements. In order to estimate the relations between the magnetic properties and the respective amounts of certain elements in the rock for the isolation method, 8 to 11 samples were analyzed in each site. The chemical composition analysis was performed using ICP-OES optima 3300 at the Geological Survey of Israel. The content of *Fe* and *Mn* were measured using an ICP-MS Elan 6000 (at the Geological Survey of Israel) to achieve higher accuracy because of the special sensitivity of calcite magnetic properties to Fe^{+2} and Mn^{+2} ions (Schmidt et al., 2006).

1.6.7. XRD Measurements

To evaluate the proportion of calcite crystals, the mineralogical composition was determined by X-ray diffraction (Philips PW1730/1710, and PW1830/3710, $CuK\alpha_1$). Ground rock powders were side-packed into aluminum holders. Semi-quantitative composition was estimated by comparison with calibration curves and with the corresponding chemical data (IR and K concentrations).

1.6.8. Thin-Sections

In order to study the depositional environment and the petrology of the rocks, a number of representative thin-sections were analyzed using an optical microscope.

1.6.9. Scanning Electron Microscope (SEM)

To get a good understanding of the rocks micro-structure and to determine the chemical composition of specific points of interest within the rock, a limited number of selected samples were investigated using electron microscopy. This investigation was conducted using a Scanning Electron Microscope (SEM), model FEI Quanta 450, at the Geological Survey of Israel (GSI).

The following detectors were used:

1. Everhart Thornley detector (secondary electrons). Purpose – surface topology.
2. Backscattered electron detector (backscattered electrons). Purpose – differences in elemental composition.
3. Energy-dispersive X-ray spectroscopy (EDS): Oxford Instruments X-max 20 SDD (Silicon Drift Detector). Purpose - elemental analysis and chemical characterization.

The results are presented in three ways.

1. Secondary electron image (labeled LFD or ETD on image caption bottom) which displays surface texture, morphology, and surface roughness.
2. Backscatter electron image (labeled BSED on image caption bottom) which displays differences in atomic/molecular density and highlight chemical composition differences. In a backscatter image the shade of grey indicates molecular/atomic density. Heavier elements are whiter, and lighter elements are darker.
3. EDS Spectra of the number (intensity) and energy level of X-rays enables elemental composition to be determined.

2. Results

2.1. General

The AMS of 402 samples from 25 sites in the Rosh-Pinna, Mt. Gilboa and the HaOnn-Cliffs areas were measured and analyzed (Figure 1). Table 1 presents the AMS results and anisotropy parameters of all samples. Table 2 presents the selected samples for the regional study, samples that passed the anisotropy test (F-test) with over 95% confidence value (>3.9) (Jelinek, 1977) or presented principal axes within the total site mean-tensor 95% confidence intervals (meaning that their magnetic fabric is in agreement with the total site fabric). The susceptibilities of all samples indicate they all belong to the diamagnetic and weak-paramagnetic phases (Figure 6). The values of the bulk-susceptibilities are close to the values of pure calcite crystals, suggesting that the impurities and second-phase minerals concentrations are low. The susceptibilities of Eocene chalk rocks (Adulam, Timrat and Maresha formations) are close to zero, which means that the AMS comprises more than one magnetic phase (Borradaile and Henry, 1997).

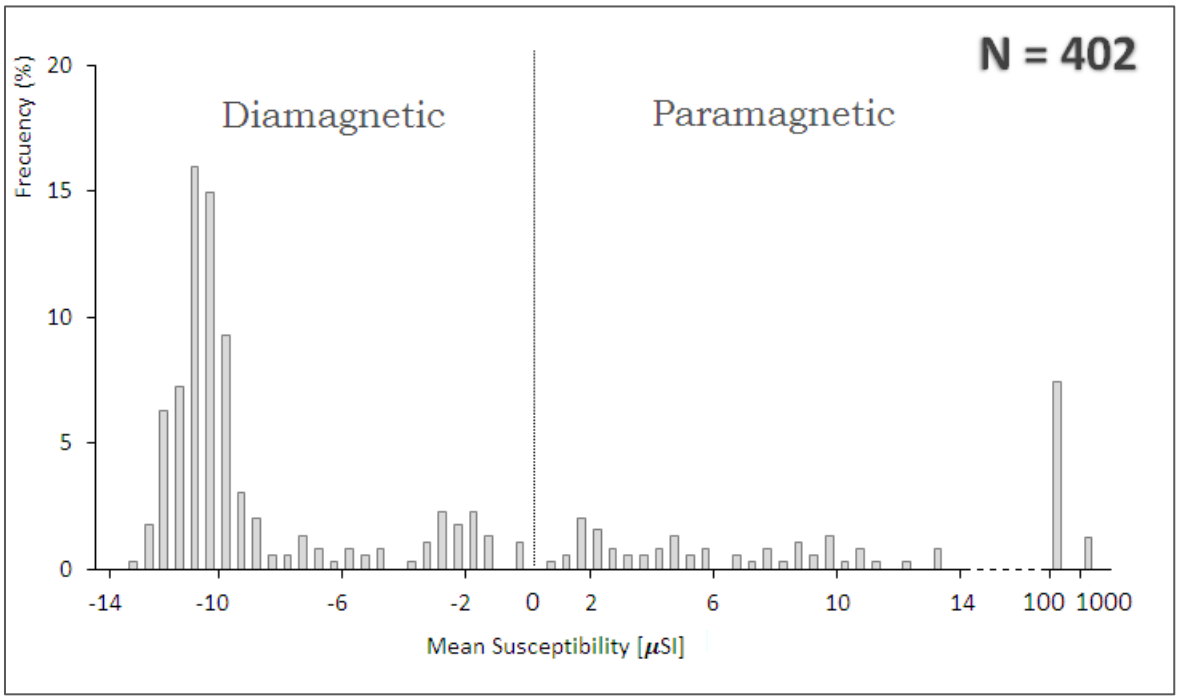

Figure 6. Percentage frequency diagram of the bulk-susceptibility (km) of all samples N=402. Note a high peak in the diamagnetic region of -10 to -11 $[\mu SI]$ bulk-susceptibility values.

Table 1. Magnetic properties of all specimens from low-field AMS measurements. The anisotropy parameters are the average parameters for the sites.

Location	Site Name	Stratigraphic unit	No. of sample (N)	Mean susceptibility [μSI]	Corrected anisotropy Degree (P')	Susceptibility difference Δk [μSI]	Shape parameter (T)	Magnetic foliation (F)	Magnetic lineation (L)
Rosh-Pinna Area	EP1	Bar-Kokhba	10	-6.29	1.029	0.170	-0.308	1.007	1.020
	EP2	Bar-Kokhba	15	-8.90	1.059	0.210	-0.225	1.014	1.039
	EP3	Bar-Kokhba	18	-11.64	1.016	0.149	0.154	1.009	1.006
	KN1	Bar-Kokhba	19	-11.27	1.009	0.094	0.007	1.004	1.004
	TH1	Bar-Kokhba	12	-9.38	1.009	0.076	-0.148	1.004	1.005
	HA1	Bar-Kokhba	12	-10.73	1.010	0.106	-0.213	1.004	1.006
	HA2	Bar-Kokhba	11	-11.05	1.008	0.089	-0.051	1.004	1.004
	HA3	Bar-Kokhba	20	-10.42	1.008	0.079	-0.087	1.004	1.004
	HC1	Bar-Kokhba	18	39.36	1.034	0.212	-0.154	1.017	1.016
	HC2	Bar-Kokhba	18	-9.98	1.006	0.051	0.116	1.003	1.002
	SA1	Bar-Kokhba	19	5.65	1.036	0.282	0.188	1.017	1.017
	SA2	Bar-Kokhba	22	-10.96	1.005	0.056	0.015	1.003	1.002
	AK1	Bar-Kokhba	9	-9.80	1.011	0.095	-0.106	1.004	1.006
	AK2	Bar-Kokhba	20	-10.71	1.009	0.094	-0.291	1.003	1.006
	NR1	Bar-Kokhba	18	-11.26	1.014	0.152	-0.232	1.005	1.008
	NP1	Bar-Kokhba	10	-11.44	1.006	0.065	-0.020	1.003	1.003
	NP2	Timrat	22	0.48	1.133	0.161	0.126	1.076	1.048
Mt. Gilboa Area	MG1	Bar-Kokhba	16	-11.38	1.028	0.294	-0.586	1.005	1.021
	MG2	Bar-Kokhba	13	-9.10	1.023	0.122	-0.187	1.007	1.015
	MG3	Bar-Kokhba	13	-11.17	1.007	0.079	0.078	1.004	1.003
HaOmn Cliffs Area	PK1	Fiq	26	22.30	1.006	0.114	0.234	1.004	1.002
	MH1	Maresha	10	10.44	1.011	0.096	0.097	1.006	1.005
	MH2	Susita	13	9.64	1.085	0.642	0.276	1.052	1.029
	AD1	Adulam	19	-3.07	1.034	0.096	-0.148	1.014	1.019
	MR1	Maresha	18	3.16	1.042	0.087	0.049	1.022	1.019

Table 2. Magnetic properties of selected specimens from low-field AMS measurements of samples that either passed the anisotropy test "F-test" within 95% confidence (Jelinek, 1977) or presented principal directions oriented within the site confidence ellipses. The anisotropy parameters are the average parameters for the sites.

Location	Site Name	Stratigraphic unit	No. of sample (N)	Mean susceptibility [μSI]	Corrected anisotropy Degree (P')	Susceptibility difference Δk [μSI]	Shape parameter (T)	Magnetic Foliation (F)	Magnetic Lineation (L)
Rosh-Pinna Area	EP1	Bar-Kokhba	4	-10.06	1.023	0.229	-0.538	1.005	1.017
	EP3	Bar-Kokhba	13	-12.52	1.013	0.160	0.137	1.007	1.005
	KN1	Bar-Kokhba	16	-11.31	1.009	0.097	0.05	1.002	1.004
	TH1	Bar-Kokhba	12	-9.38	1.009	0.076	-0.148	1.004	1.005
	HA1	Bar-Kokhba	11	-11.07	1.011	0.110	-0.21	1.005	1.006
	HA2	Bar-Kokhba	11	-11.03	1.008	0.089	-0.051	1.004	1.004
	HA3	Bar-Kokhba	17	-11.5	1.007	0.073	-0.101	1.003	1.004
	HC1	Bar-Kokhba	7	-8.21	1.028	0.225	-0.383	1.007	1.020
	SA2	Bar-Kokhba	19	-11.02	1.005	0.057	0.002	1.003	1.002
	AK2	Bar-Kokhba	17	-11.81	1.009	0.096	-0.288	1.003	1.006
	NR1	Bar-Kokhba	15	-11.22	1.012	0.130	-0.277	1.004	1.007
	NP1	Bar-Kokhba	9	-11.72	1.006	0.064	-0.035	1.003	1.003
	NP2	Timrat	16	4.88	1.085	0.108	0.03	1.040	1.041
Mt. Gilboa Area	MG1	Bar-Kokhba	16	-11.40	1.028	0.294	-0.586	1.005	1.021
	MG2	Bar-Kokhba	8	-10.80	1.012	0.127	-0.248	1.004	1.007
	MG3	Bar-Kokhba	13	-11.20	1.007	0.079	0.078	1.004	1.003
HaOnn Cliffs Area	PK1	Fiq	26	22.30	1.006	0.120	0.234	1.004	1.002
	MH1	Maresha	6	8.84	1.010	0.083	0.122	1.006	1.004
	MH2	Susita	12	9.73	1.088	0.664	0.274	1.054	1.030
	AD1	Adulam	17	-3.04	1.035	0.099	-0.139	1.014	1.019
	MR1	Maresha	13	3.60	1.035	0.087	0.155	1.021	1.013

2.2. Rosh-Pinna area

The AMS of 272 samples from 16 sites from the Eocene Bar-Kokhba Formation, and 1 site from the Early Eocene Timrat Formation, from the Rosh-Pinna area (Fig. 2) were measured and analyzed. The rocks from four sites of the Bar-Kokhba Formation (EP2, AK1, SA2 and HC2) contain red veins related to young surface weathering processes and were excluded from the regional study. The influence of the veins on the magnetic properties are discussed in Section 2.5. Figure 7 shows optical microscopy images of thin-sections from sites NP1 and KN1. The rocks consist of marine shells fragments and foraminifera, interpreted as a result of transportation and sliding events during diagenesis. XRD analysis preformed on sample from the NP1 site a yields diffraction pattern indicative of more than 95% calcite ($CaCO_3$) crystals.

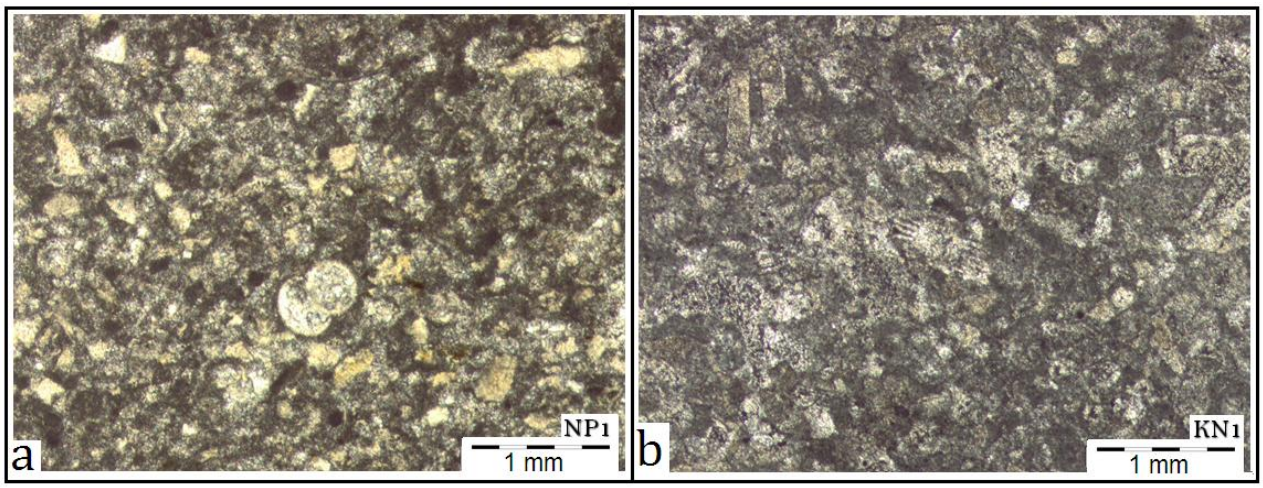

Figure 7. Optical microscopy images of thin-sections of Eocene Bar-Kokhba Formation limestone from the Rosh-Pinna area. (a) NP1 site and (b) KN1 site. Note uniform matrix, composed of fragments of marine shells, interpreted as a result of transportation and sliding events during diagenesis

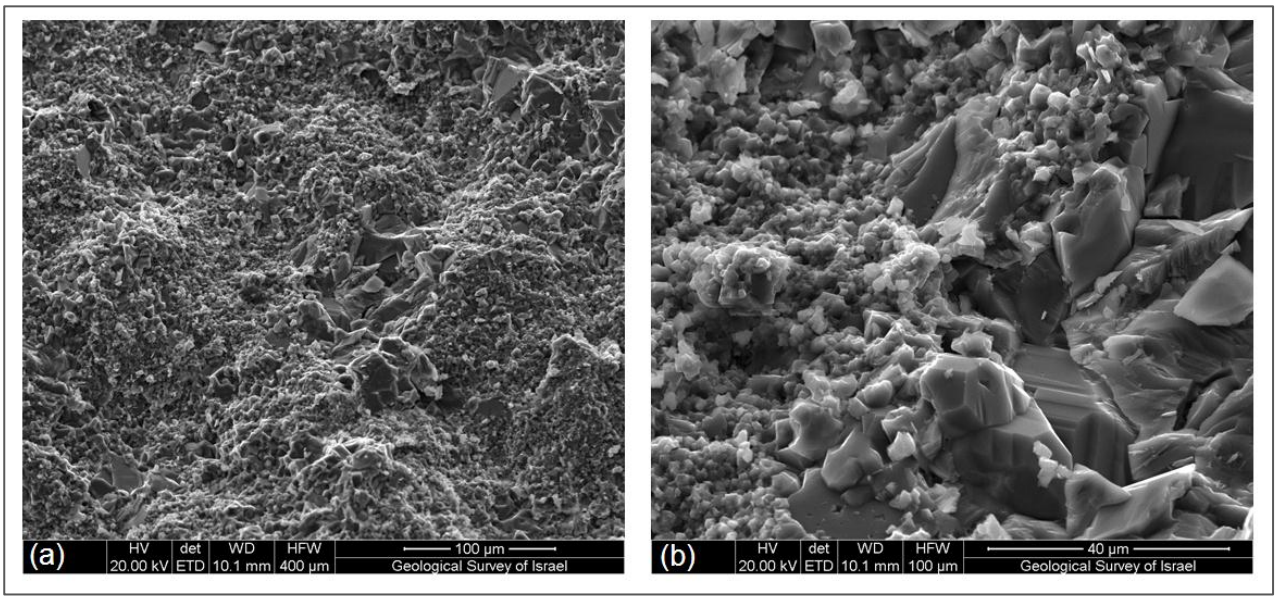

Figure 8. Scanning Electron Microscope (SEM) images of the Eocene Bar-Kokhba Formation limestone sample from the NP1 site. (a) 400 micro-meter view and (b) 100 micro-meter view. The images show calcite crystalline texture.

Table 3. Chemical content and bulk-susceptibility (k_m) of selected samples. The results are in ppm except Ca* which is in 10^4ppm

Site Name	Location	Stratigraphic unit	k_m[μSI]	Si	Al	Ca*	Mg	Fe	Mn
EP3	Rosh-Pinna	Bar- Kohba	-12.75	<1000	<200	55.5	1000	<50	<10
KN1	Rosh-Pinna	Bar- Kohba	-11.46	<1000	4000	55.0	2000	70	<10
NP1	Rosh-Pinna	Bar- Kohba	-11.66	2000	500	55.0	2700	300	-
HC1	Rosh-Pinna	Bar- Kohba	-10.03	< 1000	400	55.9	1400	≤ 50	< 10
HA3	Rosh-Pinna	Bar- Kohba	-11.22	< 1000	≤ 200	55.9	1200	≤ 50	≤ 10
NR1	Rosh-Pinna	Bar- Kohba	-11.64	< 1000	2400	55.9	2000	100	< 10
SA2	Rosh-Pinna	Bar- Kohba	-11.08	≤ 1000	300	56.0	1300	<200	-
MG1	Mt. Gilboa	Bar- Kohba	-12.31	< 1000	200	55.9	1000	< 50	≤ 10
MG3	Mt. Gilboa	Bar- Kohba	-11.37	2000	0	55.0	2000	110	<10

Figure 8 presents SEM images of a sample from the NP1 site showing calcite crystalline texture. The grain size ranges between a few to a couple of dozen micrometers. This texture appears throughout the specimen while no irregularities or different texture spots are observed. Table 3 presents the results of the chemical composition analysis of selected samples from the Rosh-Pinna Bar-Kokhba sites, which confirms the major calcium content and the minor content of other elements in the rock.

Table 2 presents results of AMS measurements preformed on 151 samples from Bar-Kokhba limestones in the Rosh-Pinna area. The rocks are all diamagnetic with mean susceptibility of $k_m = -10.89 \pm 1.16\ [\mu SI]$. This value is sufficiently close to the measured value of pure calcite crystals, leading to the conclusion that the AMS is controlled by calcite. Figure 9 shows the corrected anisotropy degree (P') and the shape parameter (T). The corrected anisotropy degree (P`) of 95% of the samples has P` values lower than 1.02 whereas 60% has P` values lower than 1.01 , indicating that the preferred crystal orientation in the rock is weak. The shape of the AMS (T) is getting closer to -1 with the growth of the corrected anisotropy degree (P'), reflects the development of preferred crystal orientation of calcite in the rock (Borradaile and Jackson, 2010).

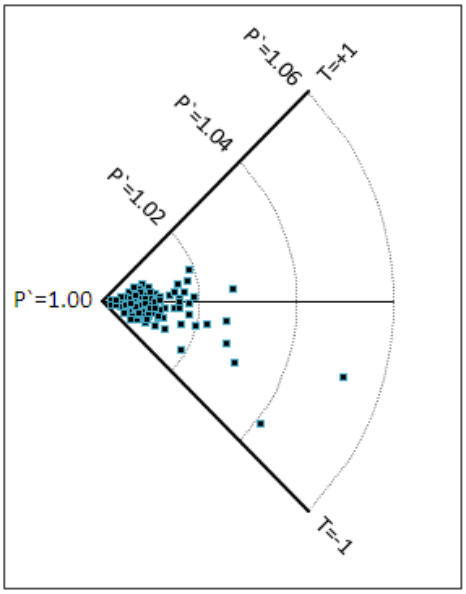

Figure 9. Corrected anisotropy degree (P') and shape parameter (T). AMS data of Bar-Kokhba limestones from the Rosh-Pinna area, presented on a π/4 segment polar plot. P' is represented by the radius and T by the arc length. Plot first introduced by Borradaile and Jackson (2004).

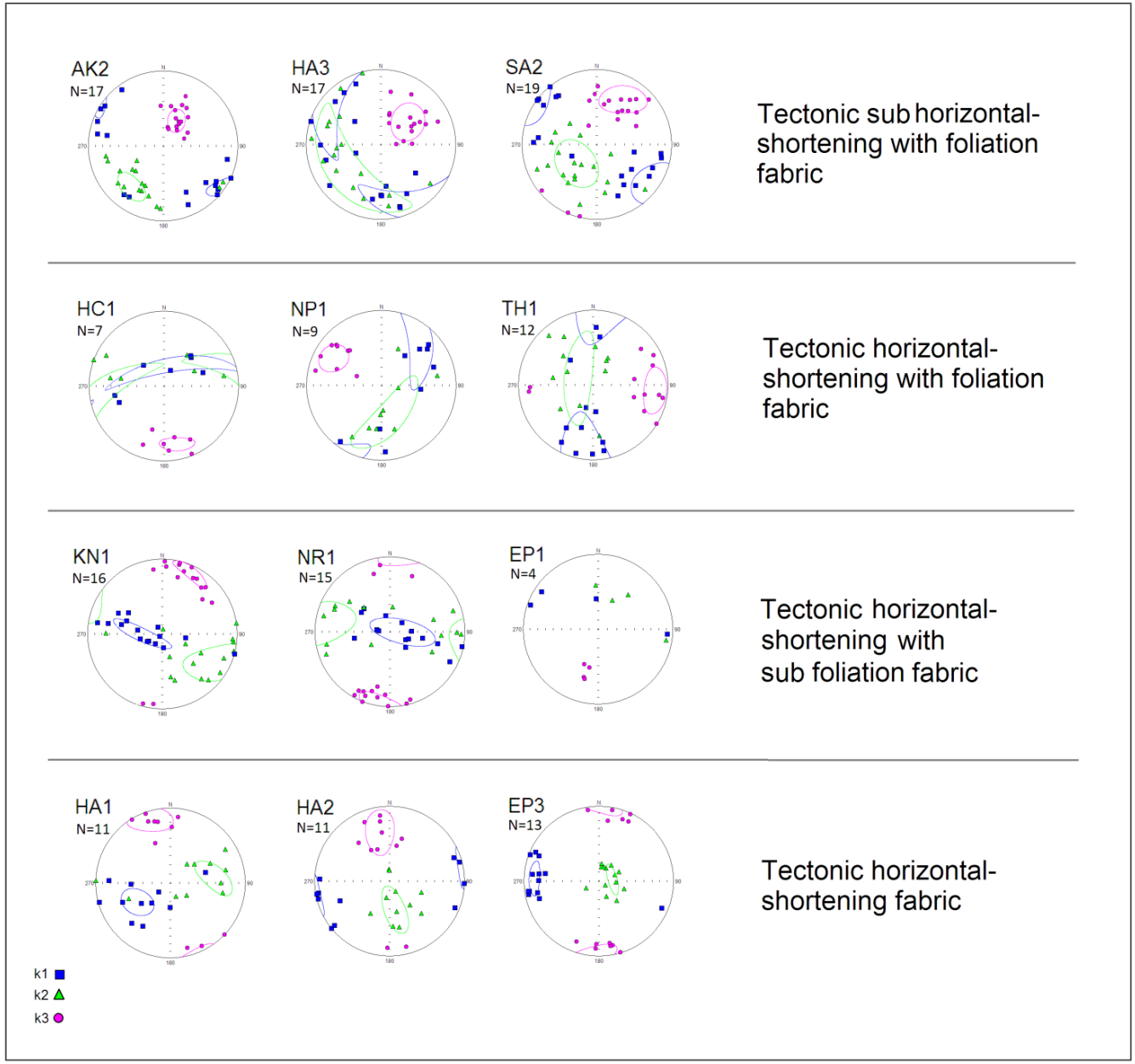

Figure 10. AMS fabrics of the Rosh-Pinna area. Lower-hemisphere, equal-area projection of AMS principal axis and 95% confidence ellipses.

Figure 10 shows the projection of AMS principal axes and the 95% confidence interval of the mean tensor. All sites indicate tectonic fabrics with well-grouped k_3 axes. Magnetic fabrics of AK2, HA3 and SA2 sites are classified as Tectonic sub horizontal-shortening with foliation fabric, the principal directions of the mean tensors are similarly oriented. Magnetic fabrics of HC1, NP1 and TH1 sites are classified as tectonic horizontal-shortening with foliation fabric, as indicated by the 95% confidence interval of the mean tensor. Magnetic fabrics of KN1, NR1 and EP1 sites are classified as tectonic horizontal-shortening with sub foliation. Magnetic fabrics of EP3, HA1 and HA2 sites are classified as tectonic horizontal-shortening fabric. Figure 11 shows that the cumulative rose diagram of the AMS axis. k_3 has predominant horizontal orientation in ~N-S, k_1 has predominant horizontal orientation in ~W-E and k_2 shows no predominant horizontal orientation.

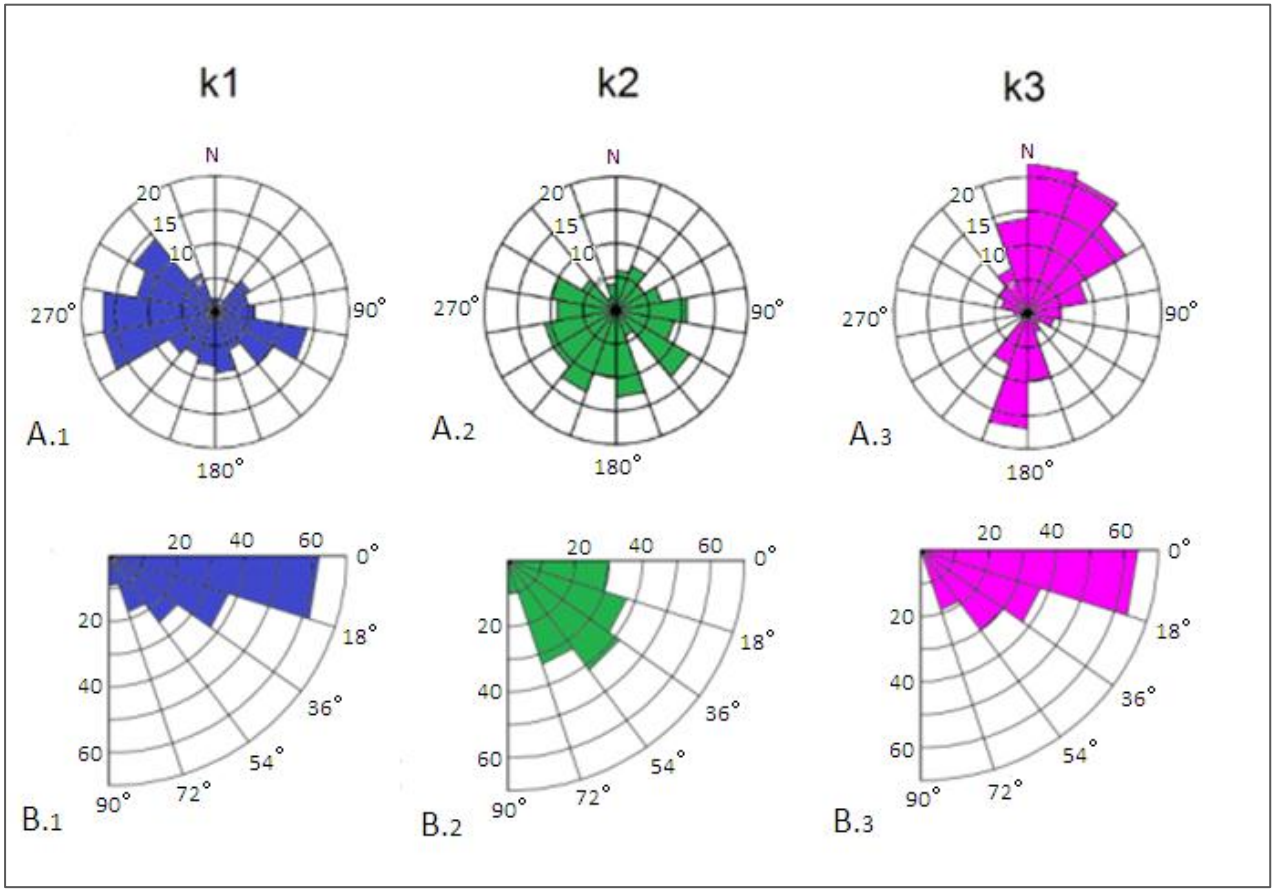

Figure 11. Cumulative rose diagrams of AMS principal directions in the Rosh-Pinna area, all samples statistics, N=151. (A.1), (A.2) and (A.3) represent declination distribution of k1, k2 and k3 respectively. (B.1), (B.2) and (B.3) represent inclination distribution of k1, k2 and k3 respectively.

2.3. Mt. Gilboa area

Samples from three sites at the top of Mt. Gilboa where measured and analyzed. The rocks defined as limestones, belong to the Eocene Bar-Kokhba Formation. Figure 12 shows optical microscopy images of thin-sections from the MG1 and MG3 sites. The image of the MG1 site (Figure 12a) shows that the rock is composed of unbroken Nummulite shells and foraminifera, suggesting that the rock did not undergo significant transportation and sliding during its diagenesis. The shell pores and contact spaces are filled with cement. On the other hand, the image of the MG3 site shows a relatively uniform matrix, composed of fragments of marine shells (Figure 12b), which are interpreted as a result of transportation and sliding events during diagenesis. XRD analysis performed on one of the samples from the MG1 site shows a diffraction pattern indicating that the rock is composed of more than 95% calcite ($CaCO_3$) crystals. Table 3 that shows the chemical composition of selected samples, confirms that calcium-carbonate is the main forming mineral (the large content of Ca), and the minor presence of other elements in the rocks.

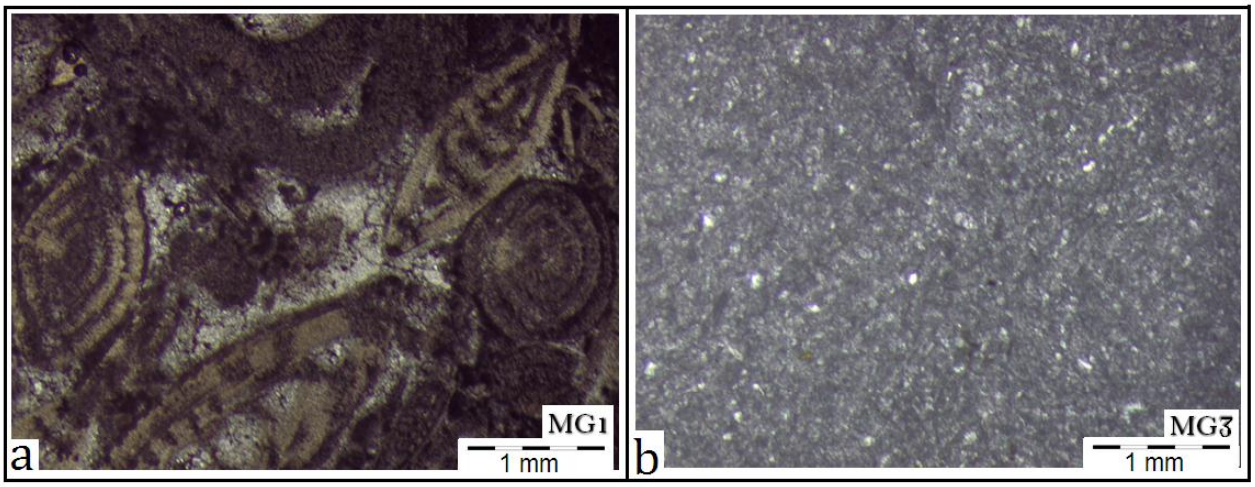

Figure 12. Optical microscopy images of thin-sections of Eocene Bar-Kokhba Formation limestone from the Mt. Gilboa area. (a) MG1 site, the rock is composed of whole Nummulite and foraminifera shells. The shell pores and contact spaces are filled with cement. (b) MG3 site, uniform matrix composed of fragments of marine shells, interpreted as a result of transportation and sliding events during diagenesis.

Table 2 presents the results of AMS measurements of samples from the MG1, MG2 and MG3 sites. The rocks are characterized by diamagnetic response with bulk susceptibility (k_m) of $-11.18 \pm 1.09\ [\mu SI]$, very close to the value of calcite crystal (Schmidt et al., 2006). These results indicate that the magnetic properties are controlled by a diamagnetic phase of calcite. Figure 13 shows the corrected anisotropy degree (P') and the shape parameter (T). The shape (T) of the AMS getting closer to -1 with the growth of the corrected anisotropy degree (P'), reflects the development of preferred crystal orientation of calcite in the rock (Borradaile and Jackson, 2010). The L parameter is greater than the F parameter in the MG1 and MG2 sites (Table 2) (Since the absolute values of the susceptibilities are used for the calculation of the anisotropy parameters, L > F reflects the fact that the difference in the magnitudes between k_3 and k_2 is greater than between k_2 and k_1). The preferred crystal orientation is reflected by the magnetic fabric. Figure 14 shows the projection of AMS principal axes and the 95% confidence interval of the mean tensor, indicating tectonic fabrics with well-grouped k_3 axes. The magnetic fabrics of the MG1 and MG2 sites are classified tectonic vertical-shortening fabric, the principal directions of the mean tensors are identically oriented where the mean k_3 axis is oriented sub-vertically in 345°/02°. The magnetic fabric of the MG3 site is classified as tectonic sub horizontal-shortening fabric.

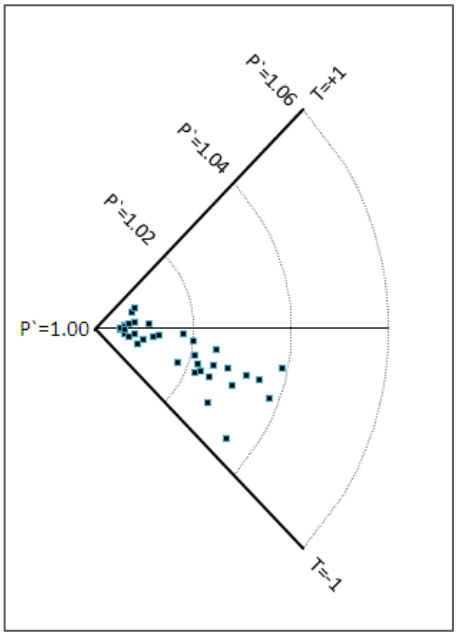

Figure 13. Corrected anisotropy degree (P') and shape parameter (T). AMS data of Bar-Kokhba limestones from the Mt. Gilboa area, presented on a π/4 segment polar plot. P' is represented by the radius and T by the arc length. Plot first introduced by Borradaile and Jackson (2004).

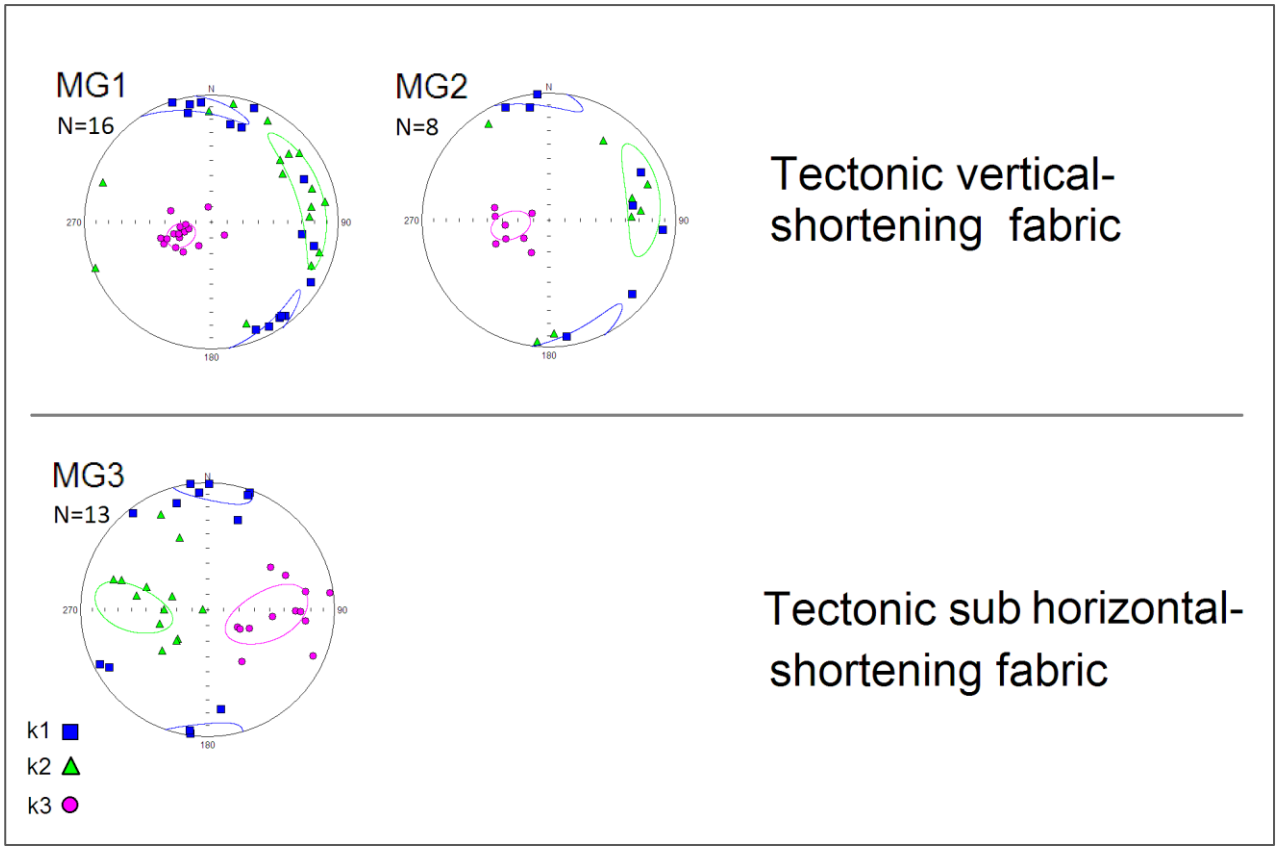

Figure 14. AMS fabrics of the Mt. Gilboa sites. Lower-hemisphere, equal-area projection of AMS principal axes and 95% confidence ellipses.

2.4. HaOnn-Cliffs area

Samples from five different sites in the southern parts of the HaOnn-Cliffs area (Figure 1) were measured and analyzed. The rocks were classified as sedimentary rocks from Early Eocene to Early Oligocene formations. Sites AD1 and MR1 are located on the southern slopes of the Golan-Heights north to the Yarmouk-Valley; the layers slightly dip in a SE direction. The AD1 site consists of soft chalks, of Early Eocene Adulam Formation, consist of micro-size marine shells and foraminifera. Table 4 presents the results of the chemical composition analysis of selected samples from the HaOnn-Cliffs area. The rock of the AD1 site has large amounts of *Ca*, indicative of calcite as major constituent of the rock. Relatively large amounts of *Si*, *Al* and *Mg* contained in the rock, indicate existent clay-minerals. Table 2 shows the magnetic properties and anisotropy parameters from AMS measurements. The bulk susceptibility values of the AD1 site indicate weak diamagnetic response with an average of $k_m = -3.04 \pm 0.46$ $[\mu SI]$. The AMS is anisotropic where the average anisotropy degree is P`=1.035.

Table 4. Chemical content and bulk-susceptibility (k_m) of selected samples from the HaOnn-Cliffs area. The results are in ppm except Ca* which is in 10^4ppm.

Site Name	Location	Formation	k_m [μSI]	Si	Al	Mg	Fe	Mn	Ca*
PK1	HaOnn-Cliffs	Fiq	17.62	17000	4000	7000	37.5	65	52.5
AD1	HaOnn-Cliffs	Adulam	-3.15	18000	3000	8000	860	<10	52.0
MR 1	HaOnn-Cliffs	Maresha	3.51	51000	6300	10000	1500	20	50.9
MH 1	HaOnn-Cliffs	Maresha	9.61	35000	7200	19300	2270	42	30.7
MH 2	HaOnn-Cliffs	Susita	9.46	250000	2700	15500	1130	75	24.0

Figure 15 shows the projection of AMS principal axes and the 95% confidence interval of the mean tensor. The magnetic fabric of the AD1 site indicates tectonic vertical-shortening fabric with well-grouped k_3 axes in a sub-vertical direction and loosely-grouped k_1 and k_2 axes on a sub-horizontal plane. The MR1 site rocks, from the late Eocene Maresha Formation, are soft chalk consisting of micro marine shells and foraminifera. It is located near the AD1 site, higher in the geological section. The chemical composition (Table 4) indicates calcite as major constituent of the rock. The large amounts of *Si*, *Al* and *Mg* content indicate clay-minerals. The AMS measurements indicate weak, positive magnetic response with average bulk susceptibility of $k_m = 3.60 \pm 2.41$ [μSI] (Table 2). The majority of the samples are anisotropic where the average anisotropy degree is P`=1.035. The magnetic fabric (Figure 15) indicates tectonic vertical-shortening fabric with well-grouped k_3 axes in a sub-vertical direction and scatter of k_1 and k_2 axes on a sub-horizontal plane. The MH1 and MH2 sites are located on the lower slopes of the HaOnn-Cliffs, a few meters from each other. The soft, white color chalk of the MH1 site, of Early to Middle Eocene Maresha Formation consist of micro marine shells and foraminifer. The rock was difficult to sample because it disintegrated. Chemical composition (Table 4) shows relatively low amounts of *Ca*. AMS measurements indicate positive magnetic response with average bulk susceptibility of $k_m = 8.84 \pm 1.23$ [μSI] (Table 2). The majority of the samples are anisotropic where the average anisotropy degree is P`=1.010. The magnetic fabric (Figure 15) indicates tectonic vertical shortening fabric with clustering of principal susceptibilities when k_3 is horizontal oriented in a 243°/04° direction, k_2 is oriented in a 343°/64° direction and k_1 is oriented in a 151°/25° direction. The rocks of MH2 site consists of a few millimeters grain size, sharp angular detritus of the Oligocene Susita Formation. Chemical composition (Table 4) shows relatively low amounts of *Ca*. AMS measurements indicate positive magnetic response with average bulk susceptibility of $k_m = 9.73 \pm 5.16$ [μSI] (Table 2). All samples are anisotropic

with an average anisotropy degree of P`=1.088, and all measured samples pass the anisotropy F-test with high values (tens to hundreds). The magnetic fabric (Figure 15) indicates tectonic vertical shortening fabric with well-grouped k_3 principal axes in 015°/19° direction, and moderately-grouped k_2 and k_1 axes in 144°/60° and 278°/21° direction respectively. The PK1 site, located on the lower slopes of the HaOnn-Cliffs, 2 km north of the MH1/2 sites is from the Upper-Eocene Fiq Formation. The layers display a sharp inclination where the tendency is in a 260°/62° direction. Chemical composition (Table 4) is indicative of calcite rock. Large amounts of *Si*, *Al* and *Mg* suggest clay-minerals. AMS measurements indicate positive magnetic response with average bulk-susceptibility of $k_m = 22.30 \pm 10.40$ $[\mu SI]$ (Table 2). The samples are anisotropic with an average anisotropy degree of P`=1.006. The magnetic fabric (Figure 15) indicates tectonic vertical shortening fabric with well-grouped k_3 axes oriented in a 051°/05° direction and moderately-grouped k_2 and k_1 axes oriented in 191°/82° and 321°/05° direction respectively.

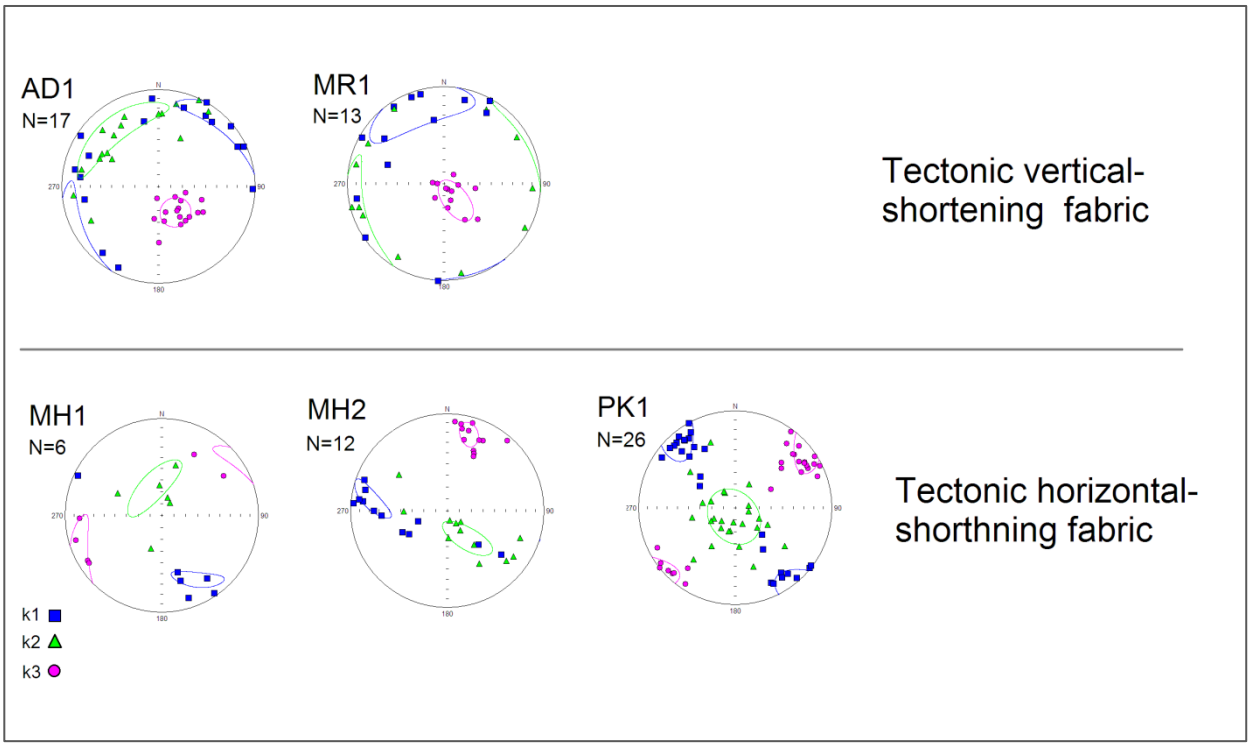

Figure 15. AMS fabrics of the HaOnn-Cliffs area. Lower-hemisphere, equal-area projection of AMS principal axis and 95% confidence ellipses.

2.5. Isolation of diamagnetic phase in Bar-Kokhba rocks

Figure 17b shows a sample of Bar-Kokhba rock that contains reddish color material due to chemical alterations related to young geomorphological processes. Samples from four sites of the Rosh-Pinna area (EP2, AK1, SA1 and HC2) show this alteration, both as filling of small cracks (veins) and more-massively within the original rock. The susceptibility of these samples reaches positive values and their AMS indicate an isotropic fabric (Figure 16). Table 5 presents the results of AMS measurement for the SA1 site, indicating wide dispersion in the bulk susceptibility (k_m) values, ranging from *-10* to *+109* [μSI]. Figure 18 illustrates this dispersion by comparison between the altered samples from the SA1 and unaltered sample from SA2 site. . The k_m values of the SA1samples are widely dispersed between -10 and +25 [μSI] with one sample at +109 [μSI]. In contrast, the k_m values of the SA2 samples site are all grouped around the value of -11 [μSI]. The P` values of the SA1samples are generally higher than the P` values of samples from site SA2. Table 6 shows the chemical composition of selected samples from site SA1. The rocks contain large amounts of *Fe, Mg* and *Al*. The distinct appearance of the alteration products implies that the elements associated with it were available as second-phase minerals and not as crystal impurities within the former rock. Sample SA1-10 shows a jump both in *Fe* content and in k_m (Table 6), suggesting that the *Fe* content is the most influential factor on magnetic properties.

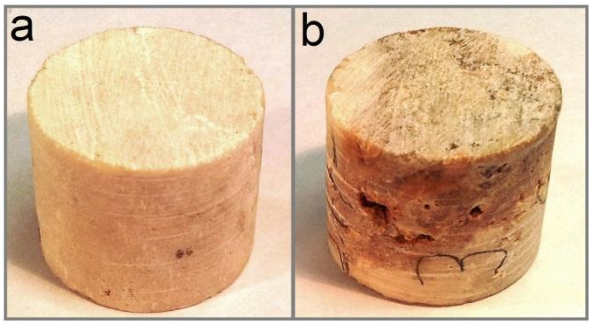

Figure 17. (a) Typical Bar-Kokhba rock, white homogeneous color. (b) Bar-Kokhba s pink to reddish color material related to young surface processes of chemical alteration. Cylinder diameters are 2.5 cm.

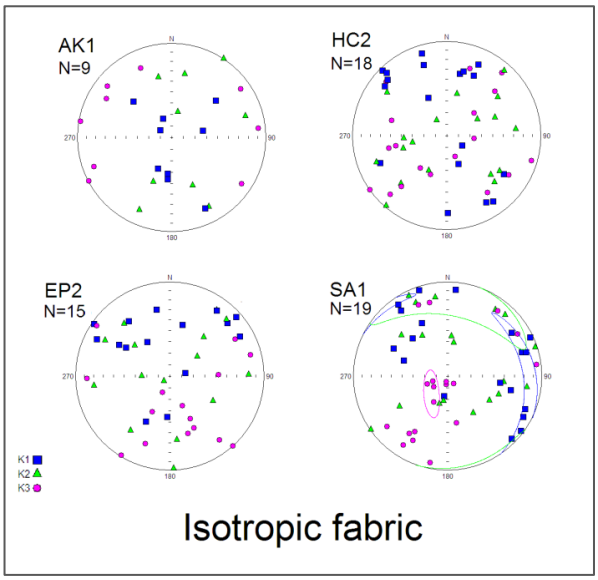

Figure 16. AMS fabrics of altered Bar-Kokhba rocks, indicating isotropic fabric. Lower-hemisphere, equal-area projection of AMS principal axis.

Table 5. Magnetic properties and AMS parameters of all the samples of site SA1.

Sample Name	Mean susceptibility [μSI]	Corrected anisotropy Degree (P')	Susceptibility difference Δk [μSI]	Shape parameter (T)	Magnetic Foliation (F)	Magnetic Lineation (L)
SA1-1	10.88	1.044	0.459	0.294	1.028	1.015
SA1-2	4.99	1.041	0.196	0.371	1.027	1.013
SA1-3	-1.53	1.150	0.213	-0.218	1.056	1.088
SA1-4	16.15	1.006	0.086	0.716	1.005	1.001
SA1-5	12.90	1.044	0.522	-0.702	1.006	1.035
SA1-6	-0.98	1.201	0.180	-0.090	1.087	1.105
SA1-7	-4.90	1.019	0.091	-0.525	1.004	1.014
SA1-8	22.50	1.017	0.334	0.948	1.015	1.000
SA1-9	-10.66	1.011	0.113	-0.381	1.003	1.007
SA1-10	109.70	1.018	1.739	0.805	1.014	1.002
SA1-11	-7.31	1.018	0.126	-0.320	1.006	1.012
SA1-12	-10.73	1.016	0.157	-0.811	1.001	1.013
SA1-13	-10.23	1.011	0.112	-0.246	1.004	1.007
SA1-14	-9.71	1.018	0.170	-0.270	1.006	1.011
SA1-15	-10.51	1.006	0.066	0.178	1.004	1.003
SA1-16	22.96	1.017	0.364	0.880	1.015	1.001
SA1-17	-10.17	1.009	0.091	0.310	1.006	1.003
SA1-18	-7.63	1.013	0.099	0.239	1.008	1.005
SA1-19	-7.21	1.024	0.164	-0.488	1.006	1.017

Figure 19 shows relation a between k_m and the *Fe* percentages (c_p), however the low linear fit, $R^2 = 0.57$, implies weak correlation. Figure 20 shows susceptibility-difference (Δk) versus the *Fe* content of samples from Bar-Kokhba limestones. Although no clear correlation is observed, there is an increase of the susceptibility-difference s with *Fe* content. Figure 21 shows the projection of the principal axes of AMS and AARM measurements. The AARM measurements, performed on six samples containing relatively large amounts of *Fe* content, reveal no anisotropy of anhysteretic remanent magnetization (Figure 21b), the F-tests are low and the magnetic fabric shows no grouping of principal directions. Therefore, the ferromagnetic/ferrimagnetic minerals within the rock are magnetically isotropic. The AMS fabric (Figure 21a) shows scattered principal axes.

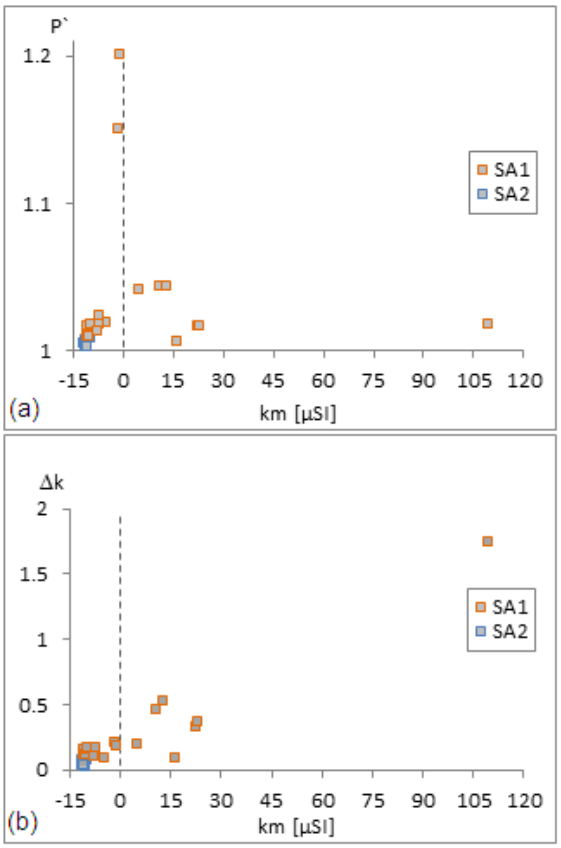

Figure 18. (a) Corrected anisotropy degree (P') versus bulk susceptibility (km) of the SA1 and SA2 sites. (b) Susceptibility difference (Δk=k1-k3) versus bulk susceptibility (km) of SA1 and SA2.

Figure 22 shows the AMS fabric of site AS1 separated to two groups: *Group a*; samples with bulk susceptibility lower than -4.90 ($k_m < -4.90\ [\mu SI]$) and *Group b*; samples with bulk susceptibility greater than -1.53 ($k_m > -1.53[\mu SI]$). The fabric of *Group a* (Figure 22a) shows poorly-grouped k_3 axes, with a mean oriented $\sim$NNE $-$ SSW , and scattered k_1 and k_2 axes that form a magnetic foliation. The fabric of *Group b* (Figure 22b) shows well-grouped k_3 axes oriented vertically, and scattered k_1 and k_2 axes on the horizontal plane; this fabric represents the more altered samples (containing more second-phase minerals).

Table 6. Chemical content and bulk-susceptibility (k_m) of selected samples from site SA1. The results are in ppm except Ca* which is in 10^4ppm.

Sample	Stratigraphic unit	k_m [μSI]	Si	Fe	Mg	Al	Ca*
SA1-1	Bar-Kokhba	10.88	3000	1100	1200	2000	55.3
SA1-2	Bar-Kokhba	4.99	3000	1600	5000	1500	55.4
SA1-6	Bar-Kokhba	-0.98	≤ 1000	400	1200	700	55.5
SA1-7	Bar-Kokhba	-4.90	<1000	320	1000	1000	55.4
SA1-8	Bar-Kokhba	22.49	5000	1300	1000	2500	55.3
SA1-10	Bar-Kokhba	109.70	8000	5800	1500	3800	55.1
SA1-11	Bar-Kokhba	-7.31	≤ 1000	300	800	400	55.9
SA1-12	Bar-Kokhba	-10.73	< 1000	800	800	1500	55.8
SA1-13	Bar-Kokhba	-10.22	< 1000	500	800	200	56.0
SA1-14	Bar-Kokhba	-9.71	1000	175	2000	<100	56.0
SA1-15	Bar-Kokhba	-10.50	≤ 1000	200	600	300	56.0

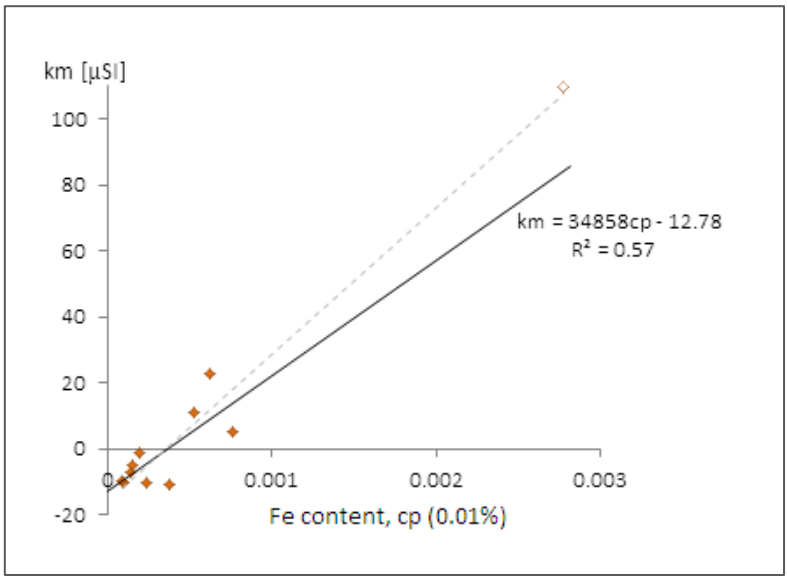

Figure 19. Bulk susceptibility (km) versus *Fe* content in 0.01% (cp) of samples from the SA1 site. The linear fit marked with solid line includes only the filled diamonds.

The analytical isolation method (chapter 1.5) is used here in order to isolate the diamagnetic fabric of the samples of the SA1 site. From the linear fit of k_m versus *Fe* content (c_p) (Figure 19), the respective percentage of *Fe* content is estimated for the entire samples of SA1 site. According to Eq. 1.8 the slope of the graph represent the bulk susceptibility of the paramagnetic/ferromagnetic phase (km_p), and the intersect point with the k_m axis represents the bulk susceptibility of the diamagnetic phase (km_d). The graph yields $km_p = 34858\ [\mu SI]$ and $km_d = -12.78\ [\mu SI]$.

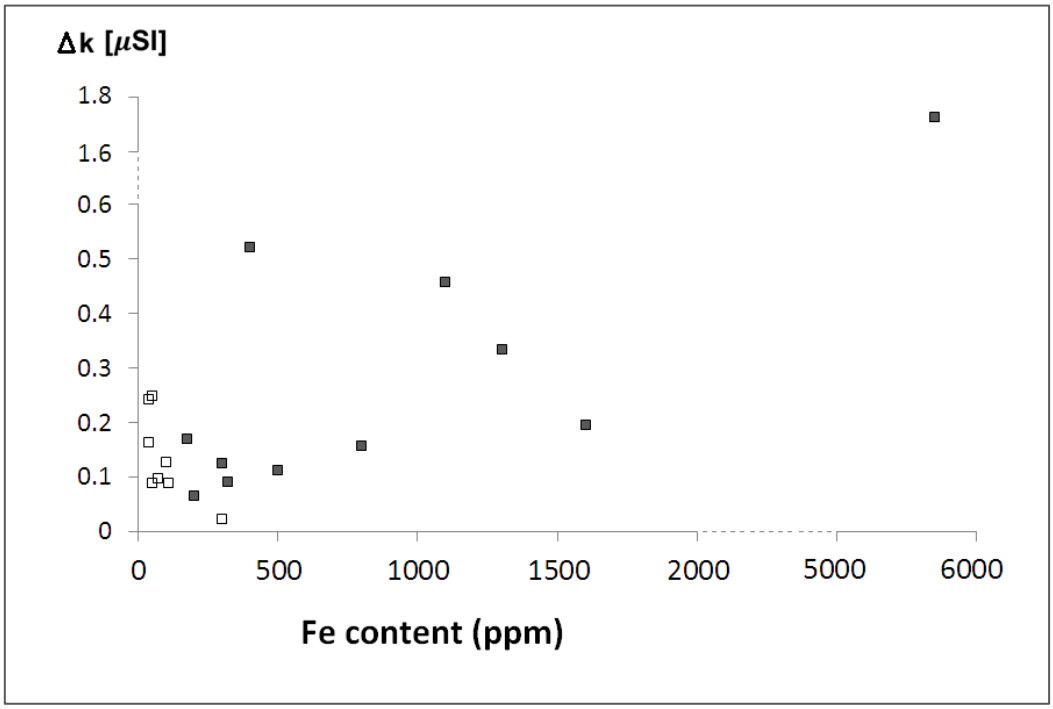

Figure 20. Susceptibility difference (Δk) versus *Fe* content of samples from the Bar-Kokhba Formation. Empty squares refer to the values from Table 3, filled squares refer to values from Table 6.

The value of km_d is very close to the value of a single calcite crystal (Schmidt et al., 2006), hence it is assumed that the *Fe* is the only effective element (beside *Ca*) controlling the AMS of SA1 site. The incompatibility of the AARM fabric with the AMS fabric of *group b* implies that the *Fe* mineral in the rock is paramagnetic. For the isolation method, the normalized AMS tensor of sample SA1-10 will be considered as representing the paramagnetic tensor $\hat{k}_p$ (because it has the sufficiently higher susceptibility $km = 109[\mu SI]$). The bulk susceptibility km_p is estimated from the linear fit of k_m vs. c_p (Figure 19). Using Eq. 1.5 the diamagnetic phase ($km_d \cdot \hat{k}_d$) of the samples is isolated.

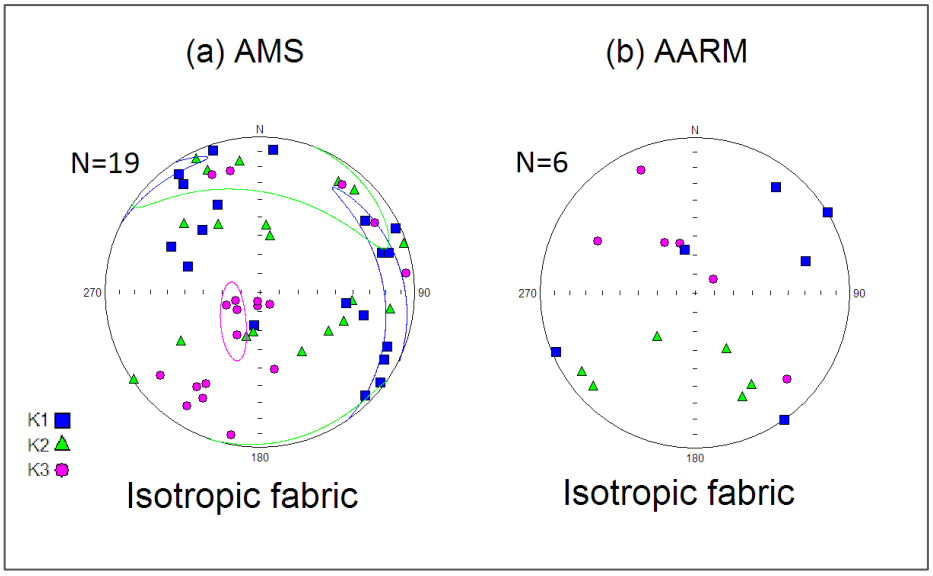

Figure 21. AMS and AARM fabrics of site SA1. Lower-hemisphere, equal-are projection of (a) AMS principal axis and 95% confidence ellipses and (b) AARM principal axis. The AARM fabric represent an isotropic fabric since the fabric shows scattering and all of the measurements failed the anisotropic F-tests.

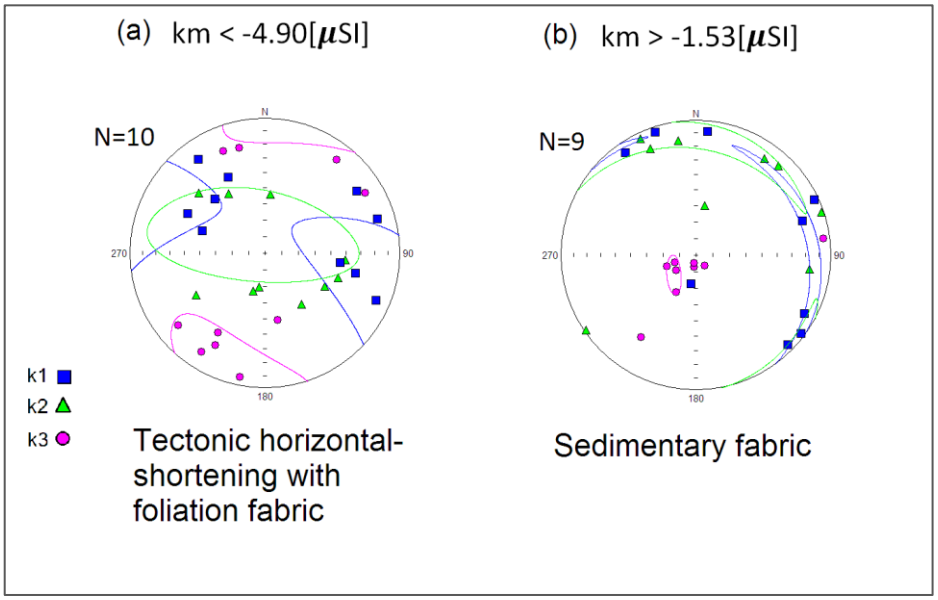

Figure 22. AMS fabrics of site SA1 divided in two: (a) samples with bulk susceptibility lower than -4.90 [μSI]. (b) samples with bulk susceptibility larger than -1.53 [μSI]. Lower-hemisphere, equal-area projection of AMS principal axis and 95% confidence ellipses.

Table 7 and Figure 24 present the AMS parameters resulting from the isolation method. The bulk-susceptibilities of the samples are uniform and very close to the value of single a calcite crystal. However, it is important to emphasize that they are dependent on, and result from the linear fit of k_m vs. c_p (Figure 19). The P` values are low, between 1.00 to 1.02 , and two samples have P'~1.045. The anisotropy shape (T) does not grow with P' (Figure 24) and generally ranges evenly between -0.7 and 0.8. Figure 23 shows the projection of AMS principal axes and the 95% confidence interval of the mean tensor as resulting from the isolation method. The magnetic fabric is classified as tectonic horizontal-shortening fabric. All three principal axes (k_1, k_2 , k_3) are moderately-grouped, where mean k_1 is oriented in 149°/82° direction, mean k_2 in the 310°/08° direction and mean k_3 in the 040°/03° direction.

Table 7. Magnetic properties and AMS parameters of sampling site SA1 as emerging from the isolation method.

Sample No.	Mean susceptibility [μSI]	Corrected anisotropy Degree (P')	Susceptibility difference Δk [μSI]	Shape parameter (T)	Magnetic Foliation (F)	Magnetic Lineation (L)
1.	-12.79	1.020	0.253	0.316	1.013	1.007
2.	-12.78	1.013	0.165	0.030	1.007	1.006
3.	-12.78	1.009	0.115	-0.636	1.002	1.007
4.	-12.79	1.043	0.537	0.580	1.034	1.009
5.	-12.79	1.046	0.574	-0.295	1.016	1.029
6.	-12.78	1.010	0.127	0.417	1.007	1.003
7.	-12.79	1.020	0.253	0.421	1.014	1.006
8.	-12.82	1.016	0.203	0.802	1.014	1.002
9.	-12.79	1.019	0.241	0.364	1.013	1.006
10.	-12.78	1.015	0.195	0.253	1.010	1.006
11.	-12.78	1.007	0.089	-0.442	1.002	1.005
12.	-12.78	1.013	0.165	-0.150	1.006	1.007
13.	-12.78	1.014	0.178	-0.618	1.003	1.011
14.	-12.78	1.010	0.127	-0.334	1.003	1.007
15.	-12.78	1.014	0.178	-0.703	1.002	1.012
16.	-12.78	1.007	0.089	0.110	1.004	1.003
17.	-12.78	1.008	0.102	0.019	1.004	1.004
18.	-12.78	1.008	0.106	-0.383	1.003	1.006
19.	-12.78	1.016	0.203	-0.512	1.004	1.012
Ave.	-12.78	1.016	0.205	-0.040	1.008	1.008
Mean	-12.78	1.012	0.153	0.144	1.007	1.005

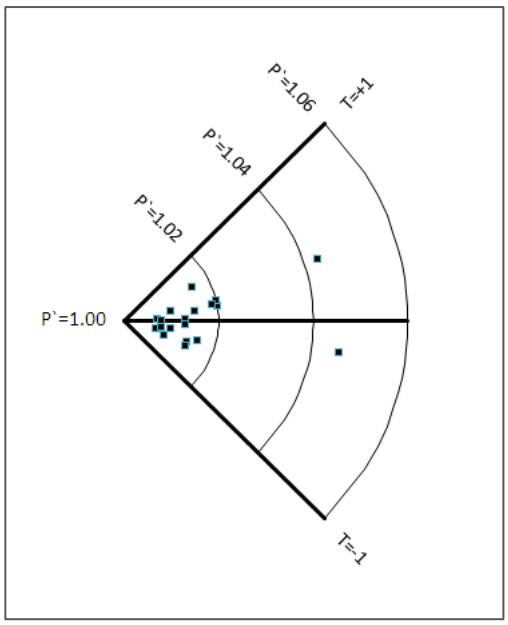

Figure 24. Corrected anisotropy degree (P') and shape parameter (T). AMS data of SA1 diamagnetic sub-fabric, results from isolation method. The data is presented on a π/4 segment polar plot. P' is represented by the radius and T by the arc length. Plot first introduced by Borradaile and Jackson (2004).

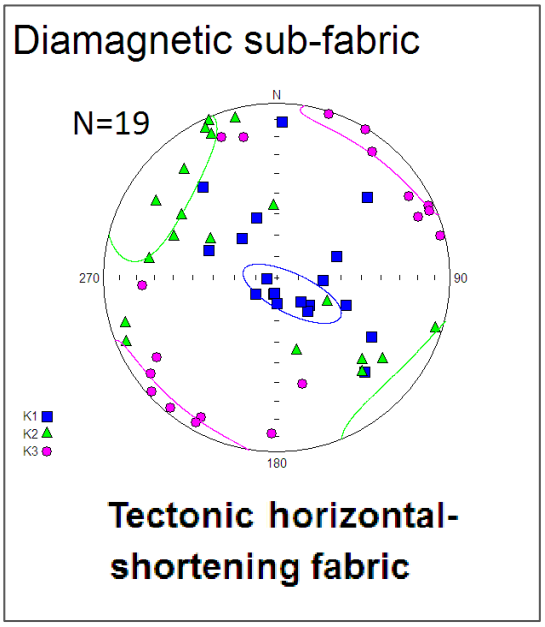

Figure 23. AMS tectonic horizontal-shortening fabric of site SA1 as emerging from the isolation method. This magnetic fabric represents the diamagnetic sub-fabric of the site's AMS (Figure 21a) Lower-hemisphere, equal-area projection of AMS principal axis and 95% confidence ellipses.

2.6. Identification of magnetic phases in the Timrat Formation

The Early Eocene Timrat Formation is exposed at the base of the Rosh-Pinna Creek and in the eastern slopes of the study area (Figure 2). The rocks from the NP2 site, located at the bottom of Rosh-Pinna creek, are determined as soft chalk of the Timrat Formation. XRD analysis performed on two samples from the NP2 site yields a diffraction pattern indicating that the rock is composed of more than 95% calcite ($CaCO_3$) crystals. Figure 26 shows optical microscopy images of thin-section from one sample. The rock is porous and homogenous, composed of micro-size marine foraminifera, distinct golden dots are observed within the rock. Figure 26 shows SEM images, the rock matrix is composed of micro size crystals (less than one micron), and a large amount of foraminifera. Using the Scanning Electron Microscope EDS technology the composition of the distinct dots and the surrounding material were analyzed. The secondary electron image (Figure 27a) shows a large grain which is heavier than the rock matrix. EDS spectra of this grain (Figure 27b) show high peaks of *Fe* and *O* while the matrix spectra (Figure 27c) is characterized by high

peaks of *Ca*, *C* and *O*), implying that the distinct dots are Fe-oxide minerals. Table 8 shows the results of chemical composition analysis of selected samples, indicating large amounts of *Fe*, *Si*, *Mg* and *Al* in the rocks of the Timrat formation (compared to Bar-Kokhba limestones in Table 3). Table 9 and Figure 28 show the magnetic properties and anisotropy parameters from AMS measurements. The bulk susceptibility is between *-2* to *+7* [μSI], where most of the samples are close zero ($-2 < k_m < 2$), suggesting that the magnetic properties are controlled by more than one magnetic phase (Hamilton et al., 2004; Hrouda, 2004). Figure 29 shows the projection of AMS and AARM principal axes and the 95% confidence interval of the AMS mean tensor. The AMS fabric (Figure 29a) is classified as tectonic vertical-shortening fabric. All principal directions are well-grouped, where mean k_1 is oriented in a 076°/14° direction, mean k_2 in a 166°/02° and mean k_3 in a 264°/75° direction. AARM measurement preformed on 9 samples (Figure 29b) reveal no anisotropy of anhysteretic remanent magnetization, the F-tests (of AARM measurements) are low and the magnetic fabric shows no gather of principal directions.

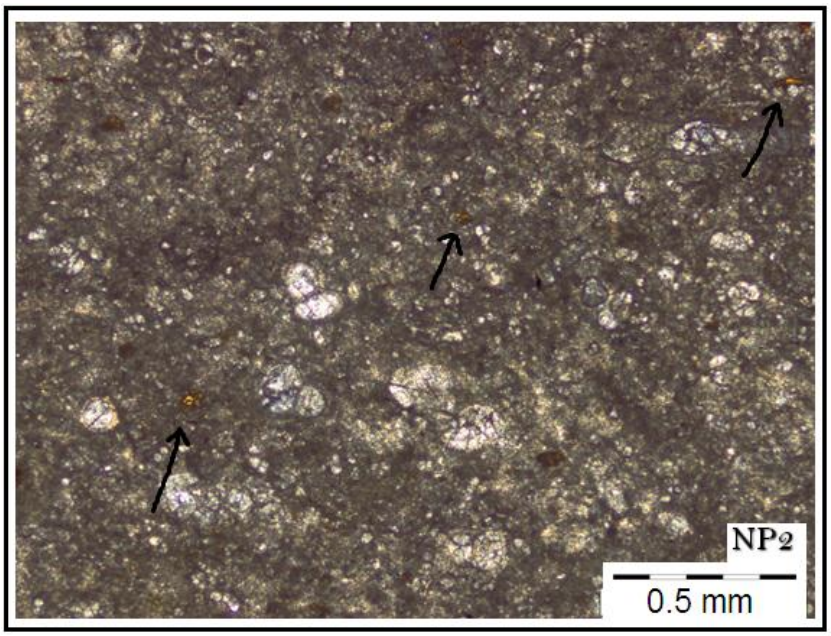

Figure 25. Optical microscopy pictures of thin-sections of a sample from site NP2. The rock is Eocene chalk of the Timrat Formation from the Rosh-Pinna creek. The medium is porous and homogeneous, composed of micro-size marine foraminifera. Arrows mark distinct golden dots observed within the rock.

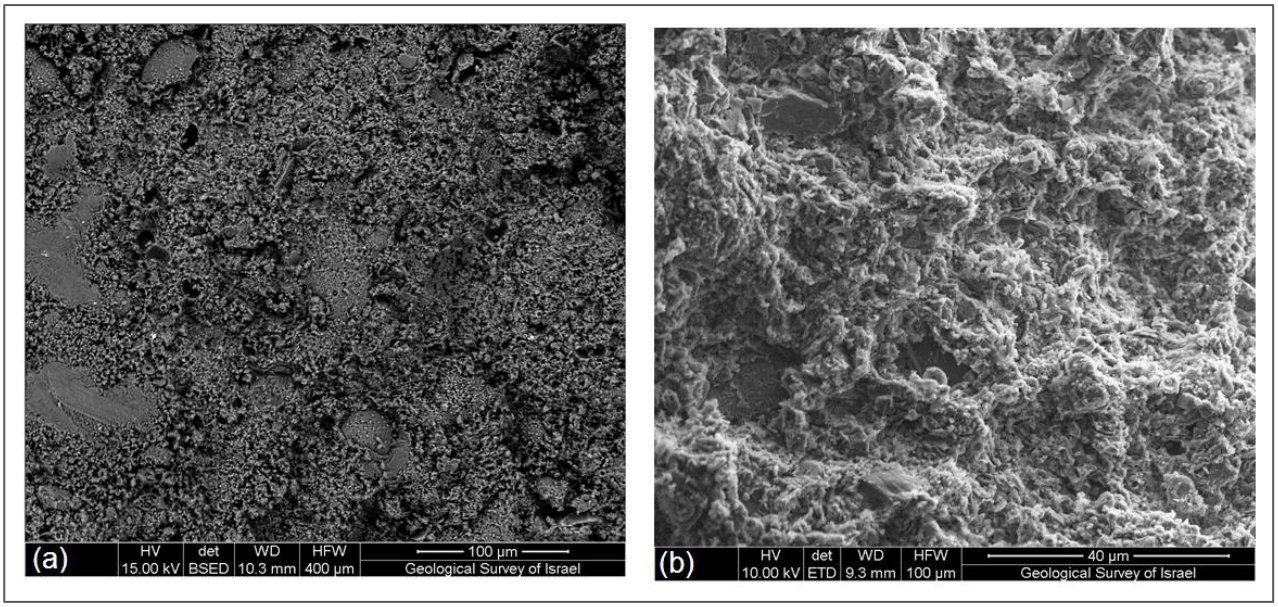

Figure 26. Scanning Electron Microscope (SEM) images of the Eocene Timrat Formation chalk of NP2 site from Rosh-Pinna Creek. (a) 400 micro-meter view and (b) 100 micro-meter view. The images reflect calcite crystalline texture built from micro size foraminifers.

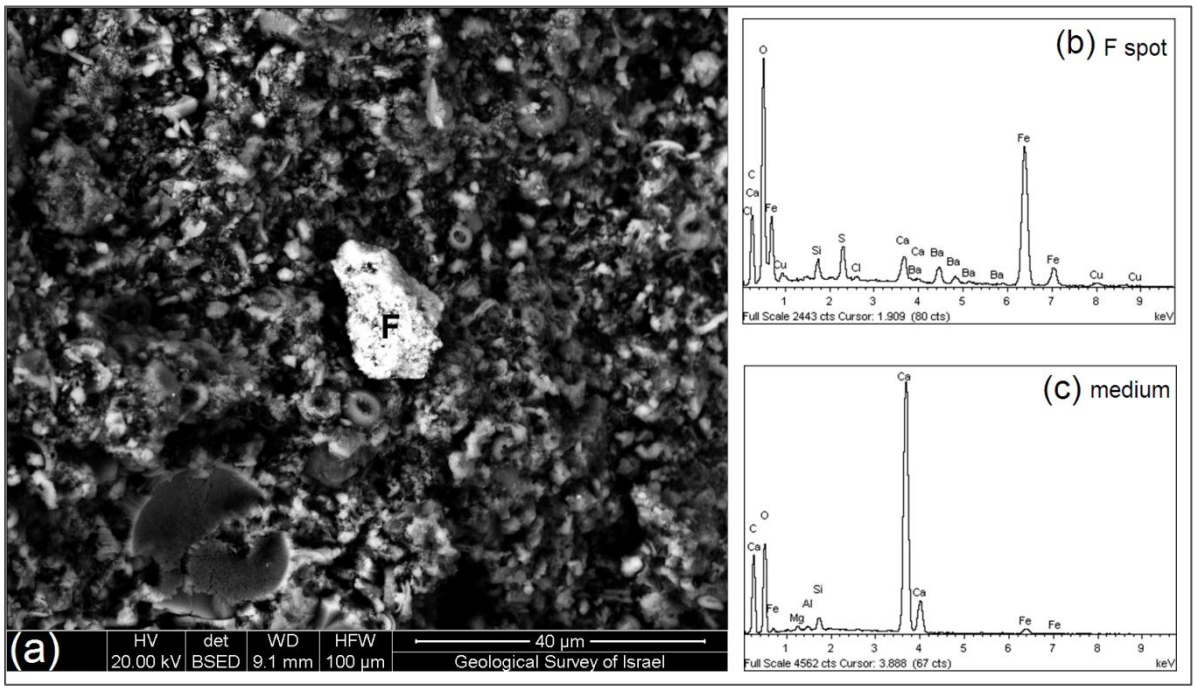

Figure 27. (a) Secondary Electron Images of Eocene chalk, Timrat Formation, from NP2 site in the Rosh-Pinna creek. In this image heavier elements appear brighter.(b) Elemental composition EDS Spectra, (intensity and energy level of X-rays)of the bright grain, identified by peaks of *Fe*, *O* and *C*. (c) Elemental composition EDS Spectra, (intensity and energy level of X-rays)of random spot of surrounding matrix, identified by peaks of *Ca*, *O* and *C.*

Table 8. Chemical content and bulk-susceptibility (k_m) of selected samples from site NP2. The results are in ppm except Ca* which is in 10^4ppm.

Sample	Stratigraphic unit	k_m [μSI]	Si	Al	Mg	Fe	Mn	Ca*
NP2-1	Timrat	-1.05	25000	6300	5400	850	27	53.5
NP2-2	Timrat	-0.53	25000	5700	5500	950	28	53.5
NP2-5	Timrat	0.81	27000	6600	5700	1050	32	53.6
NP2-7	Timrat	-1.77	23000	5000	5000	600	20	52.3
NP2-9	Timrat	1.50	34000	8300	5900	1150	33	53.0
NP2-13	Timrat	-1.37	21000	5000	5300	2000	-	52.7
NP2-17	Timrat	2.27	26000	6400	5800	1900	20	53.4
NP2-23	Timrat	7.22	33000	7500	6000	4500	-	51.7

Table 9. Magnetic properties and AMS parameters of all samples from NP2 site.

Sample Name	Mean Susceptibility [μSI]	Anisotropy Degree (P')	Susceptibility difference Δk [μSI]	Shape parameter (T)	Magnetic Foliation (F)	Magnetic Lineation (L)
NP2-1	-1.05	1.149	0.143	-0.393	1.042	1.099
NP2-2	-0.53	1.25	0.117	-0.025	1.115	1.121
NP2-4	-1.48	1.06	0.086	-0.217	1.023	1.036
NP2-5	0.81	1.113	0.084	0.411	1.076	1.031
NP2-7	-1.77	1.054	0.091	-0.424	1.015	1.037
NP2-8	-1.39	1.092	0.117	-0.57	1.018	1.068
NP2-9	1.50	1.117	0.165	-0.167	1.047	1.066
NP2-10	-1.66	1.064	0.101	-0.215	1.024	1.038
NP2-11	-1.34	1.063	0.078	0.521	1.045	1.014
NP2-12	-1.61	1.048	0.074	-0.358	1.015	1.032
NP2-13	-1.37	1.074	0.096	0.138	1.041	1.031
NP2-14	1.03	1.104	0.097	0.528	1.075	1.023
NP2-16	1.66	1.067	0.102	0.477	1.047	1.016
NP2-17	2.27	1.069	0.151	-0.189	1.027	1.04
NP2-23	7.22	1.019	0.129	0.502	1.014	1.004
NP2-24	5.51	1.018	0.093	0.456	1.012	1.005

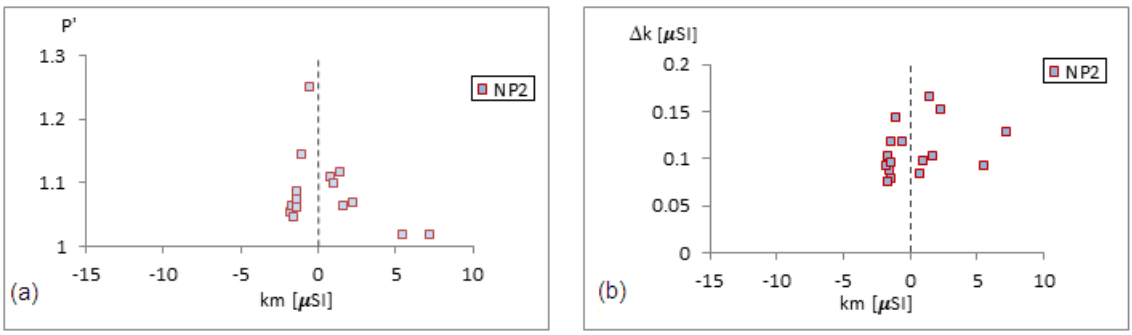

Figure 28. NP2 site (Timrat Formation) magnetic parameters from AMS measurements. (a) corrected anisotropy degree (P') versus bulk susceptibility (km). (b) Susceptibility difference (Δk=k1-k3) versus bulk susceptibility (km).

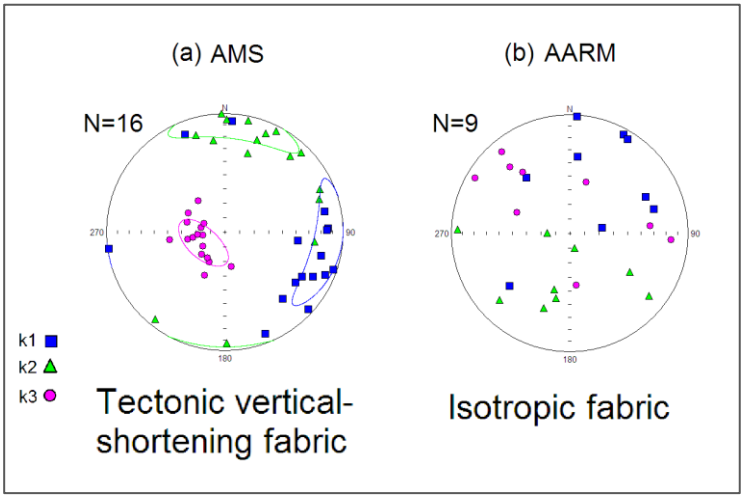

Figure 29. AMS and AARM fabrics of NP2 site. Lower-hemisphere, equal-area projection of (a) AMS principal axis and 95% confidence ellipses and (b) AARM principal axis. The AARM fabric represent an isotropic fabric since the fabric shows scattering and all of the measurements failed the anisotropic F-tests.

Figure 30 shows thermomagnetic curves of high and low temperature susceptibility measurements performed on two samples from the NP2 site. No clear evidence of Fe-oxide minerals such as magnetite (Fe_3O_4) or hematite (Fe_2O_3) is observed. Figure 31, shows the IRM acquisition curves for sample NP2-24, revealing flat saturation just below 200 [mT], indicative of PSD (pseudo-single domain) or small MD (multidomain) magnetite grains (Borradaile et al., 2010; Lanci et al., 2001; Weinberger et al., 1997). Figure 32 presents good linear correlation between bulk-susceptibility (k_m) and the respective *Fe* content (respective percentage, c_f), where $R^2 = 0.93$. The slope of the linear fit suggests that the *Fe*-oxide mineral has bulk-susceptibility of $km_f = 4865\ [\mu SI]$ and the intersection with k_m axis is at $-2.17\ [\mu SI]$. From the IRM acquisition curves, the SEM results and the slope of the linear fit, I deduce that the distinct grains are magnetite grains. Magnetite is ferrimagnetic and its susceptibility greatly depends on the applied field, temperature and grain size (Borradaile and Jackson, 2004; Mullins, 1977). Magnetite presents anhysteretic remanent magnetization, therefore, the isotropic AARM fabric (Figure 29b) indicates that the magnetite grains in the rock have no preferred orientation, and hence no influence on the principal AMS axes. The intersection of the linear fit with k_m axis at $-2.17\ [\mu SI]$ (Figure 32) implies that the rock AMS is controlled by another magnetic phase, beside the calcite crystals diamagnetic phase and the magnetite grains ferrimagnetic phase (step 4 in Figure 4). The large amounts of *Si* content in the rock, emerging from the chemical analysis (Table 8), suggest the presence of about 3% of clay-minerals. From Eq. 1.8 it appears that the clay-minerals are in the paramagnetic range with bulk susceptibility of $km_p = 367\ [\mu SI]$, (where I take; $km_t = -2.17\ [\mu SI]$, $km_d = -13.6\ [\mu SI]$, $c_p = 0.03\ [\mu SI]$ and $c_d = 0.97\ [\mu SI]$). This result is in agreement with known susceptibility values of clay-minerals (Borradaile and Jackson, 2004).

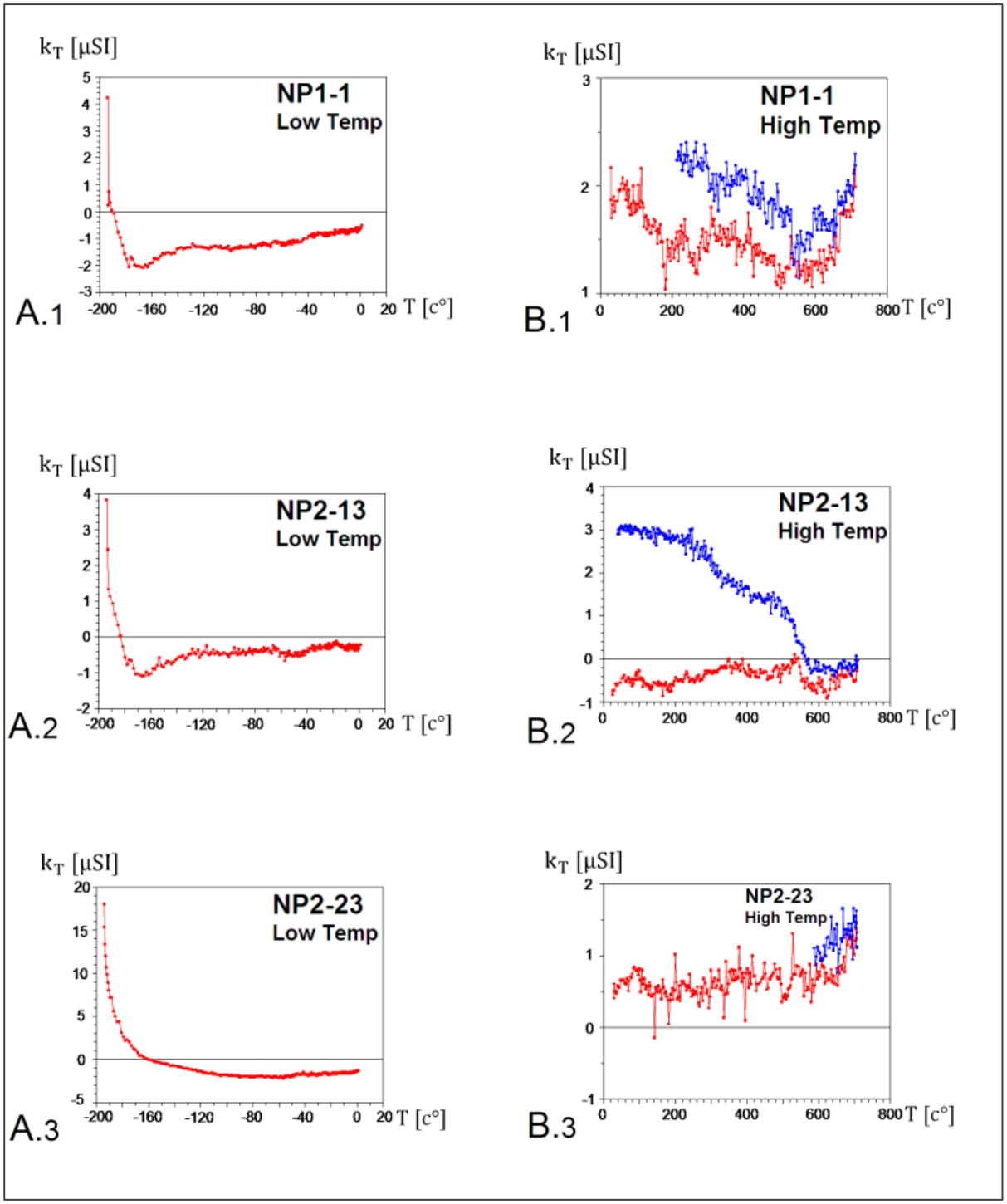

Figure 30. Thermomagnetic curves for selected samples from NP1 and NP2 sites. **kT** (temperature dependence susceptibility) versus temperature. A.1, A.2 and A.3 represent susceptibility measurements at low temperatures. B.1, B.2 and B.3 represent susceptibility measurements at high temperatures. Red color is for measurements in increasing temperatures whereas blue color is for measurements in decreasing temperatures.

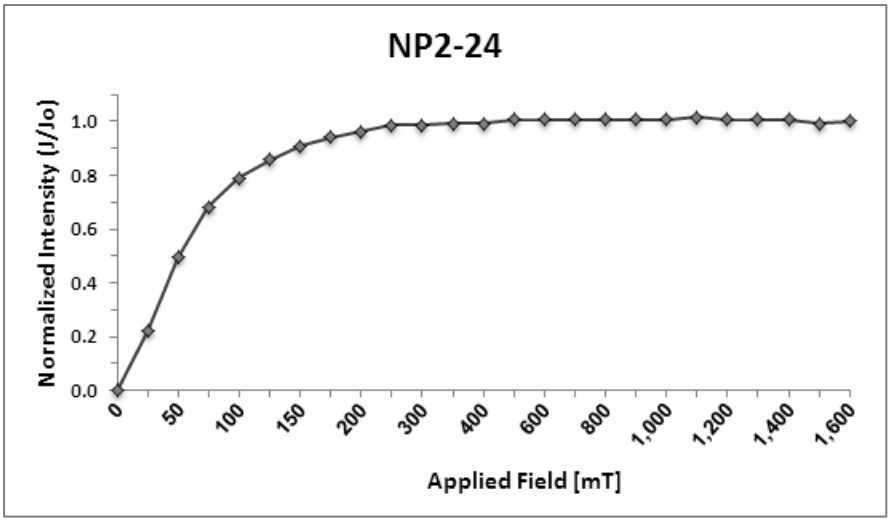

Figure 31. IRM acquisition curve of a selected sample from NP2 site. Saturation obtained just below 200 [mT] indicates magnetite.

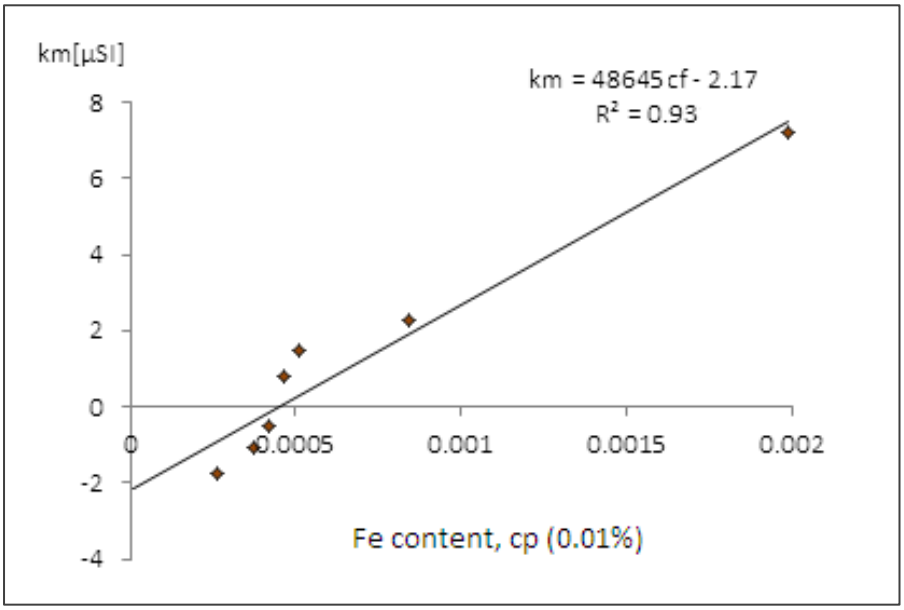

Figure 32. Bulk susceptibility (km) versus *Fe* content in 0.01% (respective percentages, cf) of selected samples from NP2 site.

3. Discussion

3.1. General

Results were obtained from repeated measurement, especially of the samples with negative susceptibility values. To estimate the measuring errors the specimen holder was measured several times before each measuring session. Samples with error greater than $100 \cdot 10^{-9}$ $[SI]$, were not taken into account.

The Bar-Kokhba rocks from the Rosh-Pinna and Mt. Gilboa areas contain extremely low contents of *Fe, Mn, Mg, Al* and *Si* (Table 3), iron content is below 300 ppm. The XRD diffraction results indicate that the Bar-Kokhba rocks consist of more than 95% calcite crystals. This and the low-field magnetic bulk-susceptibility $k_m = \sim -11[\mu SI]$ indicate that the AMS is exclusively controlled by pure calcite crystals. Therefore, the orientations of k_3 axes are co-axial with the shortening direction of the cumulative strain and are not controlled by second-phase minerals and crystal impurities.

3.2. Variations of anisotropy parameters in pure calcite-bearing rocks

The magnetic properties of the Bar-Kokhba rocks of the Rosh-Pinna and Mt. Gilboa area suggest that the AMS directly reflects calcite preferred crystal orientation. Magnetically, a single calcite crystal is anisotropic with a corrected anisotropy degree of P` $= 1.113$ (Nye, 1957; Owens and Rutter, 1978). Schmidt et al. (2006) found that the susceptibility difference of a single calcite crystal at room temperature is $\Delta k = 1.10 \pm 0.01$ $[\mu SI]$. Generally, the corrected anisotropy degree (P') and the susceptibility-difference (Δk) of deformed diamagnetic calcite-bearing rocks are expected to be lower than those of a single calcite crystal, because perfect alignments in sedimentary rocks are rare (Hrouda, 2004). The AMS magnitude of diamagnetic rocks is highly affected by the amounts of strong paramagnetic, ferromagnetic and ferromagnetic minerals. In such a case the AMS magnitude cannot be correlated with the magnitudes of strain (Borradaile and Henry, 1997). There is no correlation between the P' and Δk and *Fe* content in Bar-Kokhba rocks from the Rosh-Pinna and Mt. Gilboa area (Figure 33) and the anisotropy degree is not controlled by Fe-bearing minerals. Likewise, in the isolated diamagnetic phase of calcite (site SA1, after isolation method) the P’ values also vary in a range of 1.00 to 1.45 (Table 7). Recently, several studies suggested that the anisotropy degree parameters are associated with strain magnitudes

rather than impurities. In carbonate mylonites from the Morcles napp in Switzerland Almqvist et al. (2009) found that the increase in the anisotropy degree is associated with an increase in strain levels. Schmidt et al. (2009) experimentally showed in pure-calcite rocks that Δk generally increases with uniaxial stress under 100 [MPa] and reaches ~ 0.2 [μSI]. Levi and Weinberger (2011) found that the differences in P' (2%) and in Δk (0.2) in Bar-Kokhba rocks are related to strain magnitudes. Figure 34 shows P' and Δk versus k_m of Bar-Kokhba rocks from the Rosh-Pinna and Mt. Gilboa areas. There is no correlation between P' and Δk parameters and k_m, as is likely to be in the case of impurities. In the majority of the samples (Figure 34) P' are between 1.00 and 1.02, and Δk between 0 and 0.2 [µSI] in agreement with the anisotropy values measured in the Bar-Kokhba rocks in the Metulla area (Levi and Weinberger, 2011). Based on the present results and the aforementioned studies, it is suggested that the variations of P' and Δk in the Bar-Kokhba rocks are related to the strain magnitudes that accumulated in the rocks during the geological history.

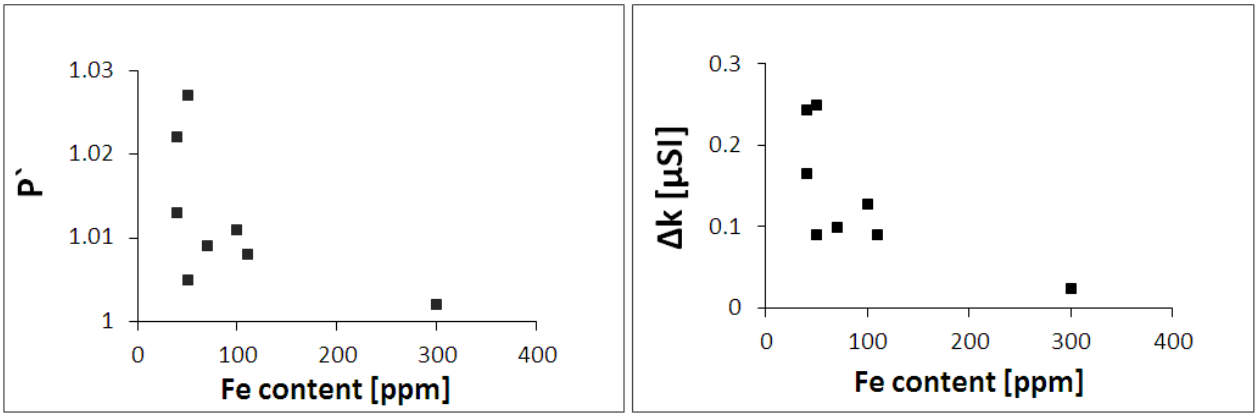

Figure 33. (Left) Corrected anisotropy degree (P') and (Right) Δk versus *Fe* content of Bar-Kokhba rocks from the Rosh-Pinna and Mt. Gilboa areas.

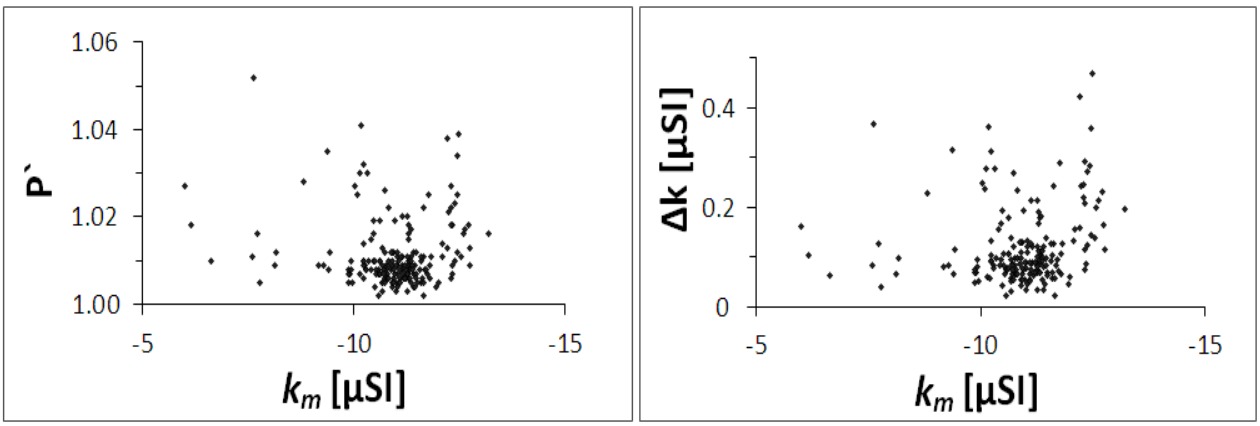

Figure 34. (left) Corrected anisotropy degree (P') and (right) Δk versus bulk-susceptibility (k_m) of Bar-Kokhba rocks from the Rosh-Pinna and Mt.

3.3. Sedimentary fabric in carbonate rocks

In the early geological history of sedimentary rocks, during diagenesis, the rocks underwent vertical-shortening due to the weight of the sediments above. The AMS is expected to reflect the strain field with well-grouped k_3 axes oriented vertical to the bedding, and scattered $k_1 \sim k_2$ axes parallel to bedding. This fabric is termed as sedimentary fabric (Fuller, 1963; Jackson and Borradaile, 1991). The sedimentary fabric reflects preferred crystal orientation that can develop by different mechanisms: (1) crystallization under non-hydrostatic stress field (Kamb, 1959); (2) plastic deformation (Hobbs et al., 1976); and (3) crystal growth in veins and dikes (for more details see section 1.4.1).

Thin-sections images of the Bar-Kokhba rocks from the Rosh-Pinna and Mt. Gilboa areas (Figure 12 and Figure 7) reveal calcite fossils and calcite cement. In MG1 the calcite cement fill of voids between the shells and the inside cavities. It is also recognized by its bright appearance (indicative of large crystals). The calcite cement formed after the arrangement of the shells, and, hence, it is reasonable to assume, that the crystals grew under the pressure of the sediments above (a few centimeters at least of sediments above). As a result, a preferred crystal orientation may have been developed by the mechanism of crystallization under non-hydrostatic stress field. Hence, it is suggested that a sedimentary fabric can be acquired by crystallization of calcite cement in the early stages of diagenesis. If the lithostatic pressure is high enough, then a continued process of plastic deformation might also develop and the mechanism of crystal growth in veins is not appropriate to the present sedimentary fabrics.

3.4. Tectonic fabrics of carbonate rocks

After diagenesis, preferred crystal orientation and a new magnetic fabric in carbonate rocks can develop due to deformation events. Under tectonic conditions with dominant horizontal shortening the calcite crystal c-axes are expected to be coaxial with the shortening axis (Figure 3d). If the horizontal strain component is lower than the vertical component then a tectonic vertical-shortening fabric is developed (Figure 3b).

The AMS of the Bar-Kokhba rocks from the Rosh-Pinna and Mt. Gilboa areas are characterized by tectonic fabrics with different magnetic patterns (Figure 10, Figure 14). The P' and Δk values are lower by at least one order of magnitude than the parameters of single calcite crystal (P'=1.113 and $\Delta k = 1.10\ [\mu SI]$ for single crystal (Owens and Rutter, 1978; Schmidt et al., 2006)).

3.5. Isolation of magnetic sub-phases

3.5.1. Sub-phases in the Bar-Kokhba Formation

The diamagnetic phase was isolated from the total AMS of site SA1 (section 1.5, Figure 4). The diamagnetic sub-fabric (Figure 23) is defined as having a tectonic origin with horizontal-shortening fabric. The paramagnetic phase (Figure 22b), formed by second-phase minerals (mainly *Fe* bearing minerals), is probably related to chemical alteration that evolved during the young surface weathering processes. The paramagnetic sub-fabric is classified as sedimentary fabric, suggesting that sedimentary fabric of chemical alteration origin can develop without the loading of lithostatic pressure. The linear correlation between the *Fe* content in the rock (cp) and bulk susceptibility (k_m) has a low R^2 value (Figure 19). According to Eq. 1.6, it suggests that *Fe* bearing minerals content is not the only factor influencing k_m, but also the presence of other minerals (such *Mn* bearing minerals). For instance, sample SA1-8 has a lower *Fe* content than sample SA1-2 but a much higher k_m value (Table 6). In this case, the linear fit gives an index for estimating the amount of paramagnetic minerals that influence the magnetic properties and masks the AMS of the diamagnetic calcite minerals.

The inclinations of the k_3 axes in the paramagnetic sub fabric are sub-vertical, whereas the k_3 axes in the diamagnetic sub-fabric are sub-horizontal. Figure 35 shows the relations between the k_3 inclinations of samples from the SA1 site versus the *Fe* content in *ppm*, estimated from the linear fit. The results suggest that above *Fe* content of 500 ppm the diamagnetic sub-fabric is masked and the paramagnetic-sub fabric controls the total AMS.

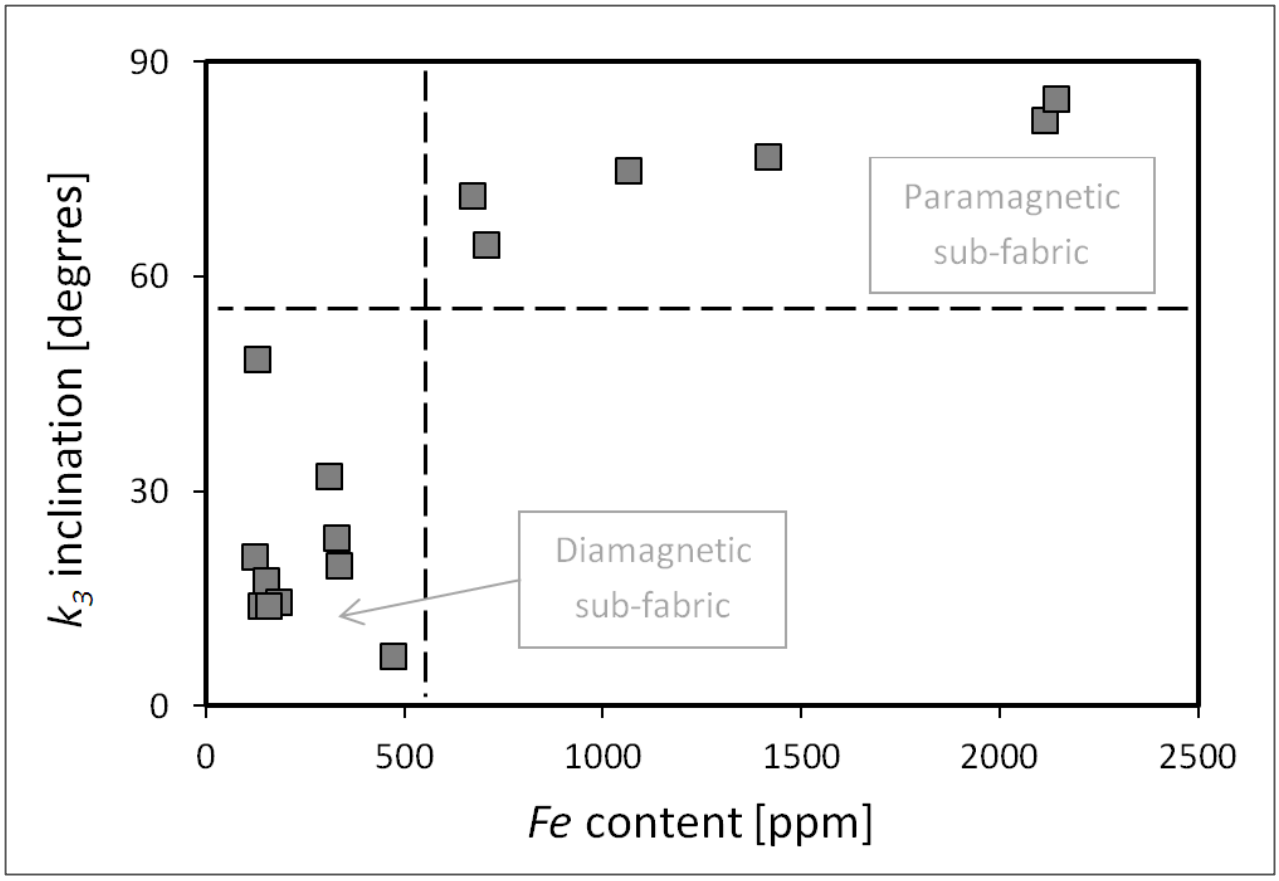

Figure 35. k_3 inclination versus *Fe* content in ppm, of samples from SA1 site. The Fe contents are estimated from the linear fit (Figure 19). Two samples were not taken into account due to incompatibility.

3.5.2. Sub-phases in the Timrat Formation

The AMS of samples from the Timrat Formation consists of three magnetic phases: 1) diamagnetic phase of calcite crystals; 2) paramagnetic phase of clay-minerals; and 3) ferrimagnetic phase of PSD to small MD magnetite grains. The identification of the three sub-phases was carried out by the isolation method, applying integrative experimental technics. AARM measurements indicate anisotropic fabric of the magnetite ferrimagnetic phase, and therefore have no influence on the principal axes of the AMS. AMS studies in clay-rich sediments and mud rocks found a correlation between principal magnetic axes k_3 and maximum shortening axis (Cifelli et al., 2004; Mattei et al., 1997; Pares et al., 1999). Therefore, the similar respond of diamagnetic calcite crystals and paramagnetic clay-minerals to strain results in a contribution of the clay-minerals to the AMS fabric of calcite-bearing rocks. In conclusion, although the AMS of the Timrat Formation consists of three magnetic phases it is suggested that the AMS principal axes are mainly controlled by the orientation of the calcite axes. This conclusion shows that the AMS of calcite-bearing rocks is a good strain indicator, even in carbonate rocks with weak diamagnetic to weak paramagnetic susceptibility.

The total bulk susceptibility becomes zero in cases where the magnetic susceptibilities cancel each other. Previous studies (Hamilton et al., 2004; Hrouda, 2004) suggest that, when the bulk-susceptibility is close to zero, the anisotropy parameters are unreliable and should be omitted from further analysis, in particular the high values of P' close to zero susceptibility (see *Appendix II*). Nevertheless, the present study shows that samples with low bulk susceptibility values have tectonic vertical-shortening fabric e.g. well grouped principal axes of the NP2 site (Figure 29a). The majority of k_3 axes of the Bar-Kokhba limestones in the Rosh-Pinna area is oriented in the horizontal direction (Figure 10 and Figure 11). The layers of the Timrat Formation are located below the layers of the Bar-Kokhba Formation, which means that the rocks of the NP2 site were subjected to equally, or more, influence of tectonic stress fields. It is well known (Hobbs et al., 1976) that in carbonate rocks preferred crystal orientation is associated with plastic deformation like development of glide systems and dislocations in the crystal structure and calcite twines. Therefore, I suggest that the Timrat and the Bar-Kokhba formations response differently to same stress regime and produce different AMS fabrics. It could be that the Bar-Kokhba and Timrat formations respond differently, because they have different mechanical properties.

3.6. Strain field in the Rosh-Pinna area

Figure 36 shows P' and Δ*k* values of the Bar-Kokhba rocks in the Rosh-Pinna area. The EP3 site, in the east parts of the Rosh-Pinna area and which is located close to a suspected segment of the DST, (Figure 2) indicates the strongest anisotropy and also shows the most grouped principal susceptibility axes (Figure 10). This means that the strain magnitude in the EP3 site is higher than that of the other sites in the Rosh-Pinna area. Because P' and Δ*k* values vary from one place to another and in most cases they are not associated with a distinct structure, it is suggested that the strains in the Rosh-Pinna area are heterogeneous.

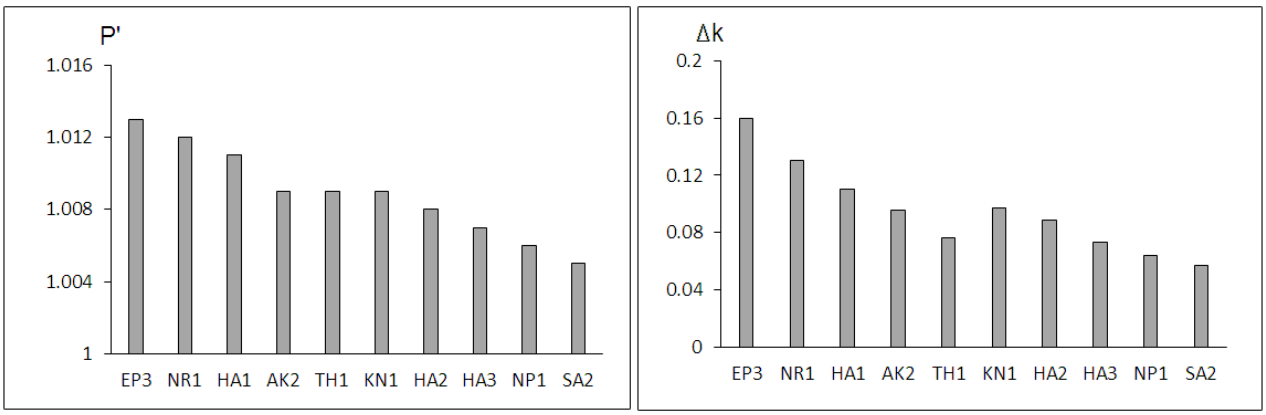

Figure 36. (Left) Corrected anisotropy degree (P') of sampling sites in the Rosh-Pinna area. (Right) Susceptibility difference (Δk) of sampling sites in the Rosh-Pinna area.

The mean vector of the k_3 axes of the Rosh-Pinna sites shows the post-Eocene finite shortening directions (Figure 37). Based on statistical analyses of the k_3 axes in the Rosh-Pinna area the mean horizontal shortening is 007° (Figure 11). This direction is sub-parallel to the strikes of the main segments of the DST system in the study area (Figure 1). The ~N-S horizontal shortening is also in agreement with a local horizontal shortening direction of 013°-193° that was suggested by Eyal (1996), who measured stylolites in one site of the Eocene rocks in the Rosh Pinna area.

Based on analysis of mega and meso-structures in the Tiberias province, Ron and Eyal (1985) suggested a stress field with maximum compression (σ_1) in the NNW – SSE direction. They suggested that this stress field is compatible with the lateral shear along the DST. According to the stress trajectory of their map (Figure 38), the stress directions vary locally between NNW and NNE directions next to segments of the DST. For example, in the Rosh-Pinna area the stress direction is rotated clockwise relative to that in Tiberias.

Assuming that stress and strain axes are coaxial, the stress direction to ~N-S is in agreement with the AMS of the Eocene rocks.

The sub-parallelism of the ~N-S trending horizontal shortening to the DST strike may be explained by the deflection process. Garfunkel (1981) showed that the directions of the principal stresses adjacent to the DST are probably deflected toward the fault trace. He suggested that this process along the DST system is dominant mainly close to "free boundaries" that form in rhomb-shape grabens. In the Rosh-Pinna area I recognize this deflection by the orientation of the horizontal shortening direction.

Recently, Levi and Weinberger (2011) measured the magnetic properties of the Bar-Kokhba and Kefar-Giladi formations in the Metulla area. They found three distinct horizontal shortening directions: 1) NW – SE shortening axis related to the pure left-lateral motion along the DST during the Neogene; 2) W – E shortening axis related to strain partitioning along the strike-slip motion during the Pleistocene to Recent; and 3) NNE shortening axis related to the early stage of the DST branching in the area. In contrast to the Metulla area, no evidence for E-W shortening was found in the Rosh-Pina area. In only one site, TH1 which is located on the structural border between Hula-Valley and Rosh-Pinna area, the k3 axes suggest E-W shortening similar to that of Levi and Weinberger (2011). Therefore it is suggested, that the strain field that probably form pre and during the Pleistocene-to-recent in the Metulla area was different in the Rosh-Pinna area.

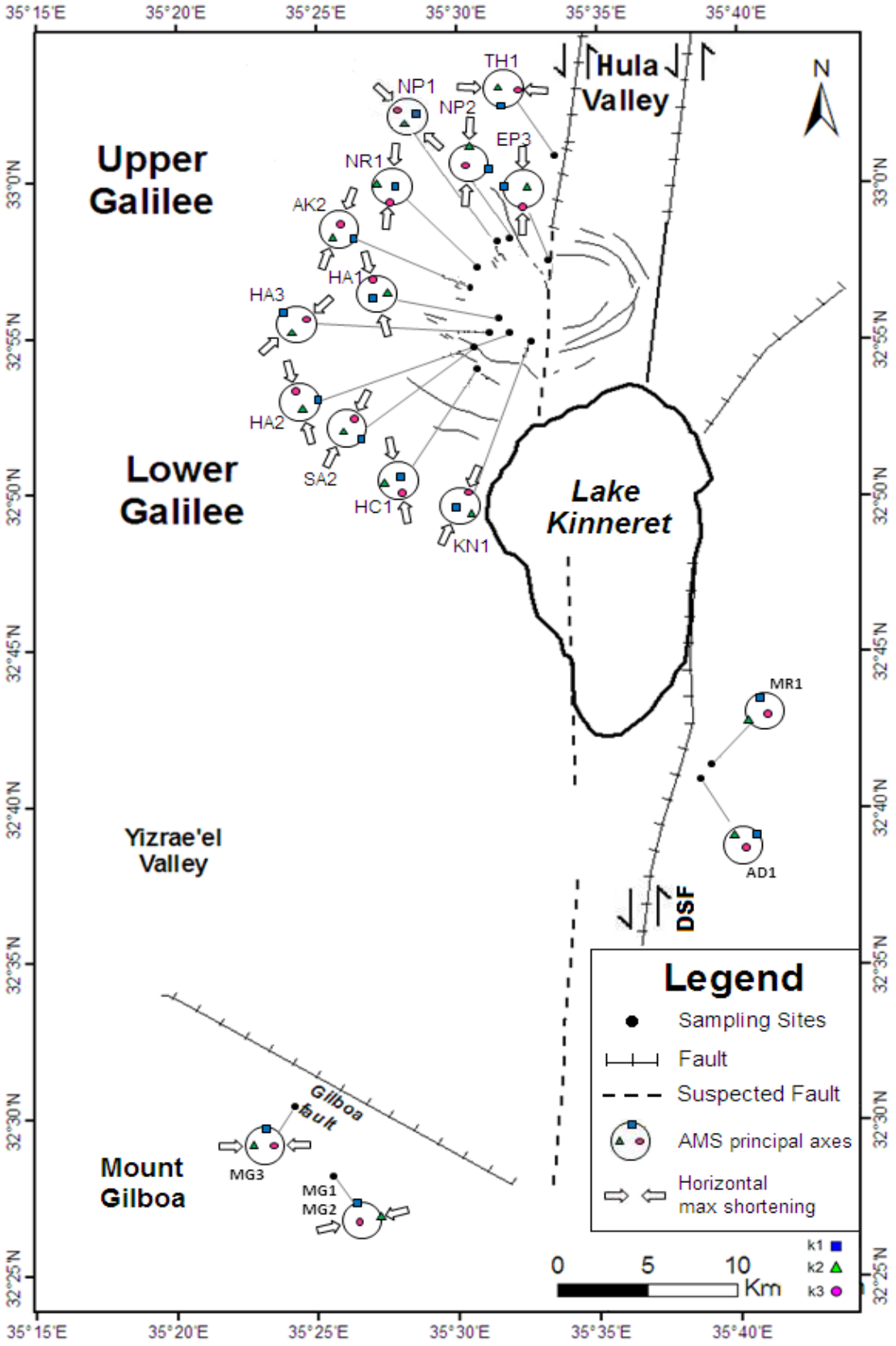

Figure 37. Map of the main fault segment of the Dead-Sea Transform (DST) and stereograms of AMS princial axes. Arrows mark the inffered horizontal shortening directions at the sites.

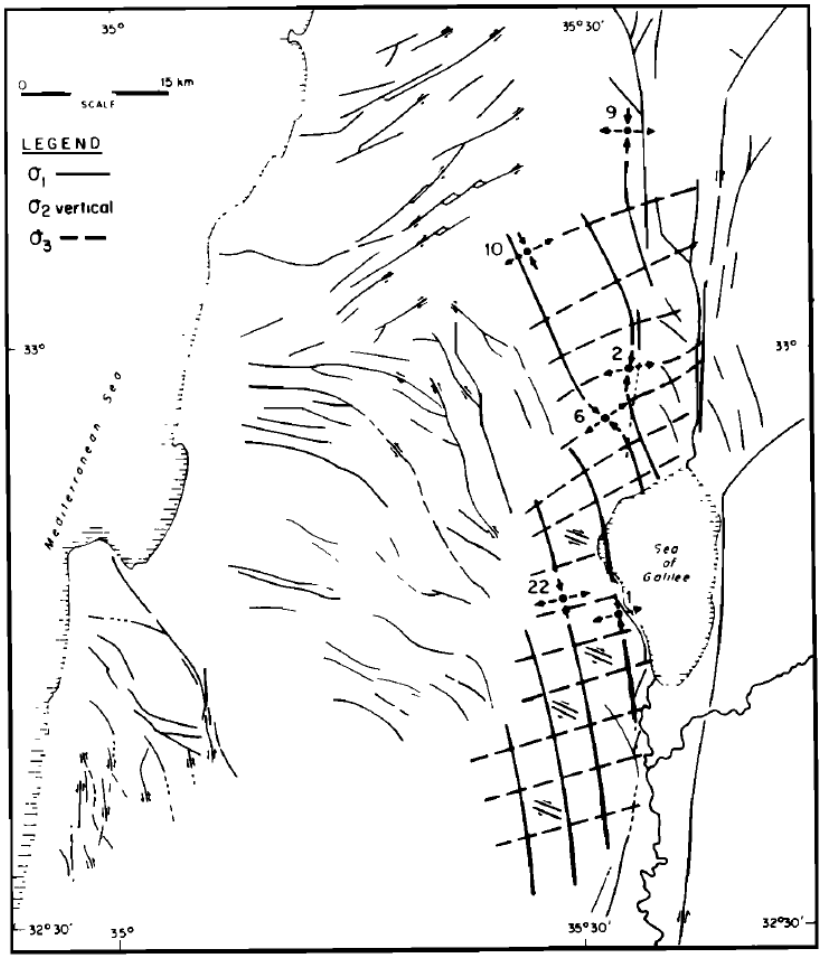

Figure 38. A stress trajectory map along the DST after Ron and Eyal (1985).

4. Conclusions

The main conclusions of this study are:

1. The Bar-Kokhba rocks in the Rosh-Pinna and in Mt. Gilboa areas are controlled by calcite diamagnetic phase and therefore can be considered as almost pure calcite-bearing rocks. The average low-field bulk-susceptibility of the rocks is $k_m = -10.95 \pm 1.01$ [μSI].
2. The orientations of k_3 axes in the Bar-Kokhba rocks are co-axial with the maximum shortening axes.
3. Variations of P' and Δk parameters of the Bar-Kokhba rocks indicate the relative magnitudes of the finite strains that have accumulated in the rocks over the geologic time.
4. The isolation method shows that the AMS of the Bar-Kokhba rocks is mostly controlled by the diamagnetic phase when the paramagnetic *Fe* minerals content is below 500 ppm.
5. The magnetic properties of the Timrat Formation are controlled by three different magnetic phases; diamagnetic, paramagnetic and ferrimagnetic. The results of the isolation method suggest that the principal axes of the total AMS are related to the diamagnetic sub-fabric of calcite.
6. The Timrat and the Bar-Kokhba formations response differently to same stress regime and produce different AMS fabrics.
7. The strain in the Rosh-Pinna area is heterogeneous, as rises from the AMS anisotropy parameters P' and Δk of the Bar-Kokhba rocks.
8. Based on the orientation of k_3 axes of the Bar-Kokhba rocks, the maximum horizontal shortening direction in the Rosh-Pinna area is ~N-S.

5. Appendix

5.1. Appendix I: Shape anisotropy of diamagnetic rocks

In general, magnetic anisotropy is controlled by grain shape anisotropy and crystal anisotropy (Borradaile and Jackson, 2010). In order to evaluate the source of magnetic anisotropy in diamagnetic rocks I will consider the effect of grain shape anisotropy.

Shape anisotropy occurs due to the demagnetization field (H_d), which forms inside the magnetized material and tends to demagnetize it (Cullity, 1972). Suppose a bar is magnetized by a magnetic field applied from left to right and subsequently removed. Then a north pole is formed at the right end and a south pole at the left, as shown in Figure 39(a). H lines radiating from the N pole and ending at the S pole, constitute a field inside the bar, which acts from N to S and therefore tends to demagnetize the bar; this field is called the "demagnetization field", H_d. The total field B inside the substance will be $B = -H_d + 4\pi M$, (where M is the magnetization) because H_d is the only field acting. The field inside the bar therefore is less than $4\pi M$ but is in the same direction, because H_d can never exceed $4\pi M$ in magnitude. These vectors are indicated in Figure 39(b), in which the B field of the bar is sketched. The demagnetizing field along a short axis is stronger than along a long axis or in other words, the applied field along a short axis has to be stronger to produce the same true field inside the specimen. Thus shape alone can be a source of magnetic anisotropy. From magnetostatic energy considerations it follows that the demagnetizing field of a body is proportional to the magnetization which creates it:

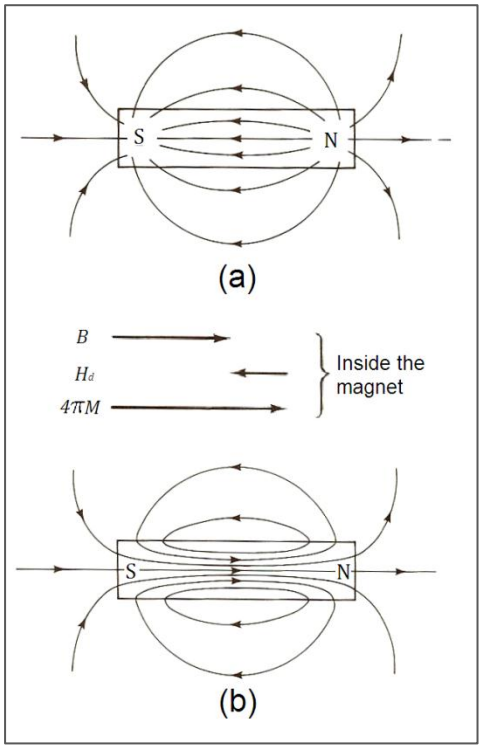

Figure 39. Fields of a bar magnet in zero applied field: (a) *H* field, and (b) *B* field. The vectors in the center indicate the values of these quantities at the center of the magnet (Cullity 1972).

$$H_d = NM \qquad .4.1$$

where N is called the "demagnetizing factor" that mainly depends on the shape of the body. Demagnetizing factors for ellipsoids have been given by Stoner (1945) and Osborn (1945) defining general ellipsoid with three unequal axes a, b and c the results are as follow:

i. Prolate spheroid with axes length, $a = b \neq c$, $^{c}/_{a} \equiv r$ then,

$$N_c = \frac{4\pi}{r^2-1}\left[\frac{r}{\sqrt{r^2-1}}\ln\left(r+\sqrt{r^2-1}\right)-1\right] \quad .4.2$$

$$N_a = N_b = \frac{4\pi - N_c}{2} \quad .4.3$$

where N_a, N_b and N_c are the demagnetizing factors along axes a, b and c respectively.

ii. Prolate spheroid with axes length, $a \neq b = c$, $^{c}/_{a} \equiv r$ then,

$$N_a = \frac{4\pi r^2}{r^2-1}\left[1-\frac{1}{\sqrt{r^2-1}}\sin^{-1}\left(\frac{\sqrt{r^2-1}}{r}\right)\right] \quad .4.4$$

$$N_b = N_c = \frac{4\pi - N_a}{2} \quad .4.5$$

where N_a, N_b and N_c are the demagnetizing factors along axes a, b and c respectively.
The magnetic susceptibility κ of a material is given by the ratio of the magnetization M and the field H which creates it :

$$\kappa = \frac{M}{H} \quad .4.5$$

Supposing an applied field H_0 then considering the demagnetization field as well, we get the total H field acting on the specimen:

$$H = H_0 + H_d \quad .4.6$$

Rearranging:

$$\kappa = \frac{M}{H_0 - NM} \quad .4.7$$

Using the above equations we can estimate the shape anisotropy degree P, $(\kappa_{max}/\kappa_{min})$ for specific prolate and oblate substances in a known magnetic field. In Figure 40 the estimation for diamagnetic substance with bulk susceptibility of -12 [μSI] measured in a magnetic field of 300 $[^{A}/_{m}]$ is presented where the horizontal axis of the graph represents the ratio between the long and short axes of the ellipsoid (r). One can see that even for a very eccentric ellipsoid the magnetic shape-anisotropy degree is very low, on the order of 10^{-4}. The crystal anisotropy degree of calcite is on the order of 10^{-1} ($P = 1.113$) (Nye, 1957). It follows that the AMS of a low magnetic rock is controlled almost entirely by crystal anisotropy and not by grain shape anisotropy.

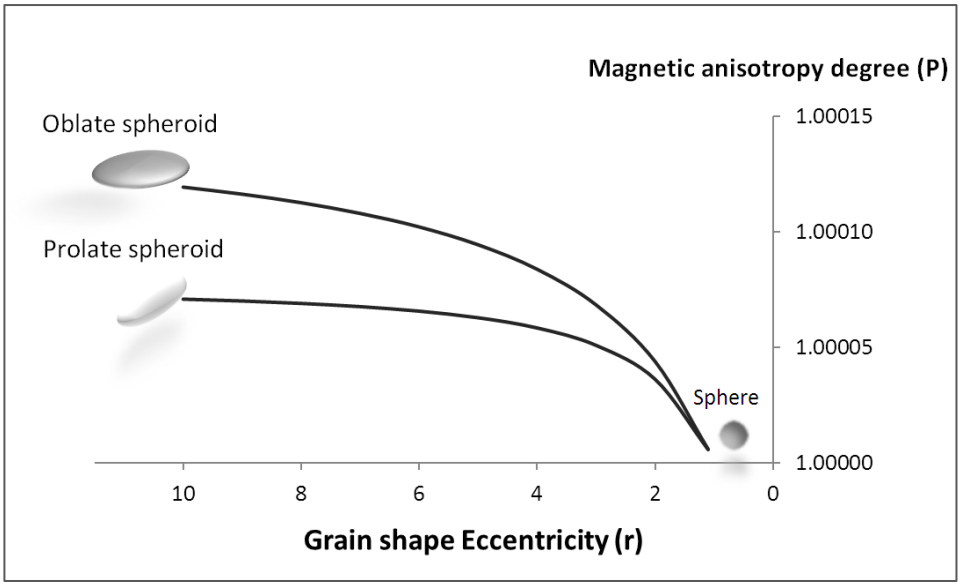

Figure 40. Magnetic anisotropy degree (P) versus grain shape eccentricity for diamagnetic calcite grains. The calcite grains subjected to a field of $\mathbf{300}\ [^{\boldsymbol{A}}/_{\boldsymbol{m}}]$ vs grain shape eccentricity.

5.2. Appendix II: Limitations of P' parameter

From Figure 18 and Figure 28 one can see that the corrected anisotropy degree, P' parameter, is increasing intensively inverse to k_m in the region of $km \to 0$. For natural anisotropy ellipsoid $\mathrm{P`} = \mathrm{P}$, where for rotational anisotropy ellipsoid $\mathrm{P`} = \mathrm{P}^{1.155}$ (Jelinek, 1981). The anisotropy degree is defined as the ratio between maximum susceptibility and minimum susceptibility, $\mathrm{P} = k_1/\mathrm{k}_3$ when principal susceptibilities referred in the absolute (unsigned) values. We can present the anisotropy degree P parameter as a function of maximum susceptibility k_1 and the strength of the anisotropy $\Delta k = k_1 - k_3$.

$$\mathrm{P} = \frac{k_1}{\mathrm{k}_3} = \frac{1}{1-\frac{\Delta k}{k_1}} \qquad .4.8$$

It is clear that always $k_1 > \Delta k$, but when k_1 becomes zero then Δk becomes zero as well, therefore:

$$\lim_{k_1 \to \Delta k} \mathrm{P} = \infty \qquad .4.9$$

This theoretical discussion explains the inverse increase of P' with k_m, shown in Figure 18. One can see where $k_m < 5$, then P' starts to grow intensively. The Δk parameter, on the other hand, is steady in the zero susceptibility vicinity. Therefore I suggest the Δk parameter be used to describe the scatter of principal susceptibilities for low magnetic response rocks such as the Eocene chalk formations in northern Israel.

5.3. Appendix III: Computer program for analytical isolation method

Matlab script. Program for isolating diamagnetic sub-fabric from AMS measurements.

```
clc
clearall

% Program for estimating a diamagnetic tensor from group of samples

% Using: readdata
%        parasub
%        decincarray
%        decinctxt
%        parameters

% kp -  Para/ferromagnetic normed tensor in Geo coordinates system
% kmp - bulk susceptibility of Para/ferromagnetic tensor (norming factor)

kp=[1.0043  1.00551 0.99019 0.00057 0.00036 0.00183]; %SA1-10 normed row tensor
kmp=34858;                          % estimated bulk susceptibility

ktfile='SA1_combine.txt';      % text file of AMS data of  the sample Anisoft42 format
data=importdata(ktfile);       % importing text file of AMS data
[kt kmt]=readdata(data.data); % [kt kmt]-array of row normed tensors and bulks

cpfile='cp_SA1.txt';           % text file of respective weights of Para/ferromagnetic
cp=load(cpfile);               % importing text file of respective weights
[kd,kmd]=parasub(kt,kmt,kp,kmp,cp);  % estimating diamagnetic sub-fabric
                                     % [kd,kmd] - diamagnetic normed row tensors and bulks

kddecinc= decincarray(kd);     % Declination and Inclination in Geo system of kd principal axis
decinctxt(kddecinc);           % Printing Declination and Inclination on text file
parameters(kd,kmd)             % Calculating anisotropy parameters and mean vector.
                               % Printing on text file
```

```
% readdata  - Program for reading AMS data from anisoft 42 text file

function [k,km]= readdata(data)

% data - imported text file of AMS measurement using anisoft 42
%k - normed susceptibility tensors
%km - bulk susceptibilities

N=size(data,1);
for i=1:N
    for j=14:19
        k(i,j-13)=data(i,j);
    end
end

for i=1:N
    km(i,1)=data(i,1);
end

return
```

```
% parasub - a program that subtract a tensor from tensors array

function[kd,kmd]=parasub(kt,kmt,kp,kmp,cp)

% input:
% kt  - array of row normed tensors
% kmt - array of bulk susceptibilities
% kp  - row normed tensor
% kmp - bulk susceptibility
% cp  - array ,  respective weights of Para/ferromagnetic

% output:
% kd 6xN every line contain a row normed tensor
% kmp 1xN every line contain bulk susceptibility

% use sabtraction1_1
```

```
m=size(kmt,1);
if (m~=size(cp))
    disp 'worng cf size'
    return
end

count=0;
for j=1:m
        count=count+1;
        [kd(count,:),kmd(count,1)]=subtraction1_2(kt(j,:),kmt(j),kp,kmp,cp(j));
end
return

function [kd,kmd] = subtraction1_2(kt,kmt,kp,kmp,cp)

%   input:
%   kt 1x6   Normed tensor from total site
%   kmt      Bulk susceptibility, norming factor of kt
%   kmp      Bulk susceptibility of Para/ferromagnetic
%   cp       respective weights of Para/ferromagnetic

% output:
%   kd 1x6   Normed tensor from diamagnetic site
%   kmd      Bulk susceptibility, norming factor of kd

Kt=abs(kmt)*kt;
Kp=abs(kmp)*kp;
Kd=  (  (1/(1-cp)) * Kt )  -  (  (cp/(1-cp)) * Kp   )  ;

% converting row tensor to 3x3 matrix form
K(1,1)=Kd(1);        K(1,2)=Kd(4);        K(1,3)=Kd(6);
K(2,1)=K(1,2);     K(2,2)=Kd(2);        K(2,3)=Kd(5);
K(3,1)=K(1,3);     K(3,2)=K(2,3);     K(3,3)=Kd(3);

[V,D]=eig(K) ;              % eignvectors and eignvalues of the matrix
kmd=(D(1,1)+D(2,2)+D(3,3))/3;
if kmd>0  ,   kd=1/kmd*Kd;  , end
if kmd<0  ,   kd=-1/kmd*Kd;  , end

return
-------------------------------------------------------------------------------------------------------------------------------
% decincarray a program that gives the Declination and Inclination of tensors array

function[out]= decincarray(k)

% input:
% k - tensors array, every row must contains a susceptibility tensor (k11 k22 k33 k12 k23 k13)

% output:
% the output is a matrix, every line is the declination and inclination of
% the eigenvectors of the susceptibility tensor in the Geo system
% every line in out matrix (k1dec k1inc k2dec k2inc k3dec k3inc)

% use the function decintvector

n=size(k,1);

for i=1:n
    tensor=k(i,:); % vector form
    matrix=[tensor(1) tensor(4) tensor(6) ; % matrix 3x3 form
                      tensor(4) tensor(2) tensor(5) ;
                      tensor(6) tensor(5) tensor(3)];

    [V,D]=eig(matrix); % eignvectors and eignvalues of the matrix

    if D(1,1) > D(3,3)
    [dec,inc]=decincvector(V(1,1),V(2,1),V(3,1));  %   declination and inclination of max eigenvector
    out(i,1)=dec; out(i,2)=inc; % writing the values to the output matrix

    [dec,inc]=decincvector(V(1,2),V(2,2),V(3,2));  %   declination and inclination of int eigenvector
    out(i,3)=dec; out(i,4)=inc; % writing the values to the output matrix

    [dec,inc]=decincvector(V(1,3),V(2,3),V(3,3));  %   declination and inclination of min eigenvector
    out(i,5)=dec; out(i,6)=inc; % writing the values to the output matrix
    end
```

```
    if D(1,1) < D(3,3)
    [dec,inc]=decincvector(V(1,3),V(2,3),V(3,3));  %   declination and inclination of max eigenvector
    out(i,1)=dec; out(i,2)=inc; % writing the values to the output matrix

    [dec,inc]=decincvector(V(1,2),V(2,2),V(3,2));  %   declination and inclination of int eigenvector
    out(i,3)=dec; out(i,4)=inc; % writing the values to the output matrix

    [dec,inc]=decincvector(V(1,1),V(2,1),V(3,1));  %   declination and inclination of min eigenvector
    out(i,5)=dec; out(i,6)=inc; % writing the values to the output matrix
    end
end

return


% decincvector - calculating Declination and Inclination of a vector

function [D,I]=decincvector(x,y,z)

% x point to the North
% y pount to the East
% z point vertical


if x>0 && y>=0
    D=atan(y/x);
    if z<0
        D=D-pi;
    end
end
if x>0 && y<0
    D=atan(y/x)+2*pi;
    if z<0
        D=D-pi;
    end
end
if x<0
    D=atan(y/x)+pi;
    if z<0
        D=D-pi;
    end
end

D=(180/pi)*D;
if D<0
    D=360+D;
end

arg=z/(((x^2)+(y^2)+(z^2))^0.5);

I=(pi/2)-acos(arg);
if z<0
    I=-I;
end

I=(180/pi)*I;

return
-----------------------------------------------------------------------------------------------------------------------------------------------

% decinctxt - exporting text file with declinations and inclinations designed for stereonet program

function[]= decinctxt(decinc3)

% input:
% decinc3  -  an array of declination and inclination
% decinc3  (k1dec k1inc k2dec k2inc k3dec k3inc)

N=size(decinc3,1);
fid=fopen('kmax.txt','wt');
fprintf(fid,'%c%c \n','TP');
for i=1:N
    fprintf(fid,'%f    ',decinc3(i,1));
    fprintf(fid,'%f  \n',decinc3(i,2));
end
```

```
fclose(fid);

fid=fopen('kint.txt','wt');
fprintf(fid,'%c%c \n','TP');
for i=1:N
    fprintf(fid,'%f    ',decinc3(i,3));
    fprintf(fid,'%f  \n',decinc3(i,4));
end
fclose(fid);

fid=fopen('kmin.txt','wt');
fprintf(fid,'%c%c \n','TP');
for i=1:N
    fprintf(fid,'%f    ',decinc3(i,5));
    fprintf(fid,'%f  \n',decinc3(i,6));
end
fclose(fid);

return
```

```
% parameters - calculating anisotropy parameters of susceptibility tensors
estimating mean tensor printing anisotropy parameters and mean tensor on text file

function[]= parameters (kq,kmq)

% input:
% kq - tensors array, every row must contains a susceptibility tensor (k11 k22 k33 k12 k23 k13)

% Using:   eigrow
%          meantensor2
%          decinctensor

 n=size(kq,1);
 fid=fopen('parameters.txt','wt');
 fprintf(fid,'   Sample            km            L          F          P         U  \n');

 kkm=0;LL=0;FF=0;PP=0;UU=0;
 for i=1:n
     tensor=kq(i,:); % vector form

     [V,D]=eigrow(tensor); % eignvectors and eignvalues of the tensor
     D=abs(D);

     if D(1,1) > D(3,3) ,    max=D(1,1);int=D(2,2); min=D(3,3);  ,     end
     if D(1,1) < D(3,3)  ,   max=D(3,3);int=D(2,2); min=D(1,1);  ,     end

    L=max/int;F=int/min;P=max/min;U=(2*int-max-min)/(max-min);
    fprintf(fid,'        %3.0f.             %3.2fE-06   %1.3f    %1.3f   %1.3f   %1.3f
\n',i,kmq(i),L,F,P,U);
     kkm=kkm+kmq(i);LL=LL+L;FF=FF+F;PP=PP+P;UU=UU+U;
 end
 fprintf(fid,'                          - - - - - - - - - - - - - - - - - - - - - - - - - - - - - - - - - - - - \n');
 fprintf(fid,'      Ave.             %3.2fE-06   %1.3f    %1.3f   %1.3f   %1.3f
\n',kkm/n,LL/n,FF/n,PP/n,UU/n);


[k,km]=meantensor2(kq,kmq);
dcm=decinctensor(k);
 [V,D]=eigrow(k) ;% eignvectors and eignvalues of the tensor
 D=abs(D);
      if D(1,1) > D(3,3) ,    max=D(1,1);int=D(2,2); min=D(3,3);  ,     end
      if D(1,1) < D(3,3)  ,   max=D(3,3);int=D(2,2); min=D(1,1);  ,     end
  L=max/int;F=int/min;P=max/min;U=(2*int-max-min)/(max-min);
  fprintf(fid,'      Mean           %3.2fE-06   %1.3f    %1.3f   %1.3f   %1.3f  \n',km,L,F,P,U);


  fprintf(fid,'\n\nMean Tensor \nDec/Inc:\nk1  %3.1f / %2.1f   \nk2  %3.1f / %2.1f     \nk3  %3.1f / %2.1f
\n',dcm);

return



% eign values and vectors 0f row tensor

function[V,D]=eigrow(k)
```

```
% 3x3 matrix form
K(1,1)=k(1);         K(1,2)=k(4);         K(1,3)=k(6);
K(2,1)=K(1,2);      K(2,2)=k(2);         K(2,3)=k(5);
K(3,1)=K(1,3);      K(3,2)=K(2,3);      K(3,3)=k(3);

[V,D]=eig(K); % eignvectors and eignvalues of the matrix
Return


% meantensor2 - Estimating a mean tensor from  group of specimens

function [k, km] = meantensor2(kq, kmq)

% kq - arrey of tensors every  specimen is a row
%kmq  -  bulk susceptibilities
N=size(kq,1);
% mean tensor 1x6
k(6)=0;
for j=1:6
  for i=1:N
      k(j)=k(j)+kq(i,j);
  end
  k(j)=k(j)/N;
end
k;
km=mean(kmq);

return


% decinctensor - a program that gives the Declination and Inclination of tensor

function [out] = decinctensor (k)

% k - a row tensor (k11 k22 k33 k12 k23 k13)
% out file is a row contain the declination and inclination of
% the eigenvectors of the susceptibility tensor in the geograph system
% out  -   (k1dec k1inc k2dec k2inc k3dec k3inc)

% use the function decintvector

% 3x3 matrix form
K(1,1)=k(1);         K(1,2)=k(4);         K(1,3)=k(6);
K(2,1)=K(1,2);      K(2,2)=k(2);         K(2,3)=k(5);
K(3,1)=K(1,3);      K(3,2)=K(2,3);      K(3,3)=k(3);

[V,D]=eig(K) ;%         eignvectors and eignvalues of the matrix

if D(1,1) > D(3,3)

    [dec,inc]=decincvector(V(1,1),V(2,1),V(3,1));  %   declination and inclination of max eigenvector
    out(1)=dec; out(2)=inc; % writing the values to the output matrix

    [dec,inc]=decincvector(V(1,2),V(2,2),V(3,2));  %   declination and inclination of int eigenvector
    out(3)=dec; out(4)=inc; % writing the values to the output matrix

    [dec,inc]=decincvector(V(1,3),V(2,3),V(3,3));  %   declination and inclination of min eigenvector
    out(5)=dec; out(6)=inc; % writing the values to the output matrix
end

if D(1,1) < D(3,3)

    [dec,inc]=decincvector(V(1,3),V(2,3),V(3,3));  %   declination and inclination of max eigenvector
    out(1)=dec; out(2)=inc; % writing the values to the output matrix

    [dec,inc]=decincvector(V(1,2),V(2,2),V(3,2));  %   declination and inclination of int eigenvector
    out(3)=dec; out(4)=inc; % writing the values to the output matrix

    [dec,inc]=decincvector(V(1,1),V(2,1),V(3,1));  %   declination and inclination of min eigenvector
    out(5)=dec; out(6)=inc; % writing the values to the output matrix
end
return
```

---

6. References

Almqvist, B.S.G., Herwegh, M., Schmidt, V., Pettke, T. and Hirt, A.M., 2010. Magnetic susceptibility as a tool to study deformed calcite with variable impurity content. Geochemistry Geophysics Geosystems, 11.

Almqvist, B.S.G., Hirt, A.M., Schmidt, V. and Dietrich, D., 2009. Magnetic fabrics of the Morcles Nappe complex. Tectonophysics, 466(1-2): 89-100.

ArRajehi, A. et al., 2010. Geodetic constraints on present-day motion of the Arabian Plate: Implications for Red Sea and Gulf of Aden rifting. Tectonics, 29.

Ballet, O., Coey, J.M.D. and Burke, K.J., 1985. Magnetic properties of sheet silicats -2-1-1 layer minerals. Physics and Chemistry of Minerals, 12(6): 370-378.

Bartov, Y., Steinitz, G., Eyal, M. and Eyal, Y., 1980. Sinistral movement along the Gulf of Aqaba - its age and relation to the opening of the Red Sea. Nature, 285: 220-221.

Beausoleil, N., Lavallee, P., Yelon, A., Ballet, O. and Coey, J.M.D., 1983. Magnetic properties of biotite micas. Journal of Applied Physics, 54(2): 906-915.

Bishop, J.F.W., 1954. A theory of the tensile and compressive textures of face-centred cubic metals. Journal of the Mechanics and Physics of Solids, 3(2).

Bishopa, J.F.W., 1953. A theoretical examination of the plastic deformation of crystals by glide. Philosophical Magazine Series 7, 44(348).

Bishopa, J.F.W. and Hilla, R., 1951. A theory of the plastic distortion of a polycrystalline aggregate under combined stresses. Philosophical Magazine Series 7, 42(327).

Borradaile, G., 1987. Anisotropy of magnetic-susceptibility - rock composition versus strain. Tectonophysics, 138(2-4): 327-329.

Borradaile, G.J., 1988. Magnetic-susceptibility, petrofabrics and strain. Tectonophysics, 156(1-2): 1-20.

Borradaile, G.J., 1991. Correlation of strain with anisotropy of magnetic-susceptibility (AMS). Pure and Applied Geophysics, 135(1): 15-29.

Borradaile, G.J. and Alford, C., 1988. Experimental shear zones and magnetic fabrics. Journal of Structural Geology, 10(8): 895-904.

Borradaile, G.J. and Henry, B., 1997. Tectonic applications of magnetic susceptibility and its anisotropy. Earth-Science Reviews, 42(1-2): 49-93.

Borradaile, G.J. and Jackson, M., 2004. Anisotropy of magnetic susceptibility (AMS): magnetic petrofabrics of deformed rocks. Geological Society, London,Special Publications v. 238: p. 299-360

Borradaile, G.J. and Jackson, M., 2010. Structural geology, petrofabrics and magnetic fabrics (AMS, AARM, AIRM). Journal of Structural Geology, 32(10): 1519-1551.

Borradaile, G.J., Lagroix, F., Hamilton, T.D. and Trebilcock, D.A., 2010. Ophiolite tectonics, rock magnetism and palaeomagnetism, Cyprus. Surveys in Geophysics, 31(3): 285-359.

Borradaile, G.J. and Stupavsky, M., 1995. Anisotropy of magnetic susceptibility - measurement schemes. Geophysical Research Letters, 22(15): 1957-1960.

Calnan, E.A. and Clews, C.J.B., 1950. Deformation textures of face-centred cubic metals. Philosophical Magazine Series 7, 41(322).

Calnan, E.A. and Clews, C.J.B., 1951. The development of deformation textures in metals.—Part II. Philosophical Magazine Series 7, 42(331).

Chadima, M., Hansen, A., Hirt, A., Hrouda, F. and Heinrich, S., 2004. Phyllosilicate preferred orientation as a control of magnetic fabric: evidence from neutron texture goniometry and low and high-field magnetic anisotropy (SE Rhenohercynian Zone of Bohemian Massif). The Geological Society of London, 238: 361-380.

Cifelli, F., Mattei, M., Hirt, A.M. and Gunther, A., 2004. The origin of tectonic fabrics in "undeformed'' clays: The early stages of deformation in extensional sedimentary basins. Geophysical Research Letters, 31(9).

Cogne, J.P. and Perroud, H., 1988. Anisotropy of magnetic-susceptibility as a strain-gauge in the flamanville granite, NW France. Physics of the Earth and Planetary Interiors, 51(4): 264-270.

Cullity, B.D., 1972. Introduction to magnetic materials. ADDISON-WESLEY, University of Notre Dame.
de Wall, H., Bestmann, M. and Ullemeyer, K., 2000. Anisotropy of diamagnetic susceptibility in Thassos marble: A comparison between measured and modeled data. Journal of Structural Geology, 22(11-12): 1761-1771.
Dietrich, D. and Song, H., 1984. Calcite fabric in a natural shear environment, the helvetic nappes of western switzerland. Journal of Structural Geology, 6(1-2): 19-32.
Evans, M.A. and Elmore, R.D., 2006. Fluid control of localized mineral domains in limestone pressure solution structures. Journal of Structural Geology, 28(5): 939-939.
Eyal, Y., 1996. Stress field fluctuations along the Dead Sea rift since the middle Miocene. Tectonics, 15(1): 157-170.
Eyal, Y. and Reches, Z., 1983. Tectonic analysis of the Dead Sea rift region since the Late-Cretaceous based on mesostructures. Tectonics, 2(2): 39-66.
Freund, R., 1970. Rotation of strike-slip faults in Sistan, Southern Iran. Journal of Geology, 78: 188-200.
Fuller, M.D., 1963. Magnetic anisotropy and paleomagnetism. Journal of Geophysical Research, 68: 293.
Fuller, M.D. et al., 1988. NRM-IRM(S) Demagnetization plots - an aid to the interpretation of natural remanent magnitization. Geophysical Research Letters, 15(5): 518-521.
Garfunkel, Z., 1981. Internal structure of the Dead Sea leaky transform (rift) in relation to plate kinematics. Tectonophysics, 80: 81-108.
Hamilton, T.D., Borradaile, G.J. and Lagroix, F., 2004. Sub-fabric identification by standardization of AMS: an example of inferred neotectonic structures from Cyprus. Geological Society, London, Special Publications, , 238: 527-540.
Hatzor, Y. and Reches, Z., 1990. Structure and paleostresses in the Gilboa' region, western margins of the central Dead Sea rift. Tectonophysics, 180: 87-100.
Heimann, A., 1990. The development of the Dead Sea rift and its margins in the northern Israel during the Pliocene and the Pleistocene. GSI/28/90 (in Hebrew, English abstract), Golan Research Institute and Geological Survey of Israel.
Heimann, A. and Ron, H., 1993. Geometric changes of plate boundaries along part of the northern Dead Sea Transform: Geochronologic and paleomagnetic evidence. Tectonics, 12(2): 477-491.
Henry, B. and Daly, L., 1983. From qualitative to quantitative magnetic-anisotropy analysis - the prospect of finite strain calibration. Tectonophysics, 98(3-4): 327-336.
Hext, G.R., 1963. The estimation of second-order tensors, with related tests and designs. Biometrika, 50(3 and 4): 353.
Hirt, A.M., Evans, K.F. and Engelder, T., 1995. Correlation between magnetic-anisotropy and fabric for Devonian shales on the appalachian plateau. Tectonophysics, 247(1-4): 121-132.
Hirt, A.M. and Gehring, A.U., 1991. thermal alteration of the magnetic mineralogy in ferruginous rocks. Journal of Geophysical Research-Solid Earth and Planets, 96(B6): 9947-9953.
Hirt, A.M., Julivert, M. and Soldevila, J., 2000. Magnetic fabric and deformation in the Navia-Alto Sil slate belt, northwestern Spain. Tectonophysics, 320(1): 1-16.
Hirt, A.M., Lowrie, W., Clendenen, W.S. and Kligfield, R., 1988. The correlation of magnetic-anisotropy with strain in the chelmsford formation of the sudvury basin, Ontario. Tectonophysics, 145(3-4): 177-189.
Hobbs, B.E., Means, W.D. and Williams, P.F., 1976. An Outline of Structural Geology. Wiley.
Hounslow, M.W., 2001. The crystallographic fabric and texture of siderite in concretions: implications for siderite nucleation and growth processes. Sedimentology, 48.
Hrouda, F., 1982. Magnetic-anisotropy of rocks and its application in geology and geophysics. Geophysical Surveys, 5(1): 37-82.
Hrouda, F., 1993. Theoretical-models of magnetic-anisotropy to strain relationship revisited. Physics of the Earth and Planetary Interiors, 77(3-4): 237-249.
Hrouda, F., 2004. Problems in interpreting AMS parameters in diamagnetic rocks. Geological Society, London, Special Publications 2004,, 238: 49-59.

Hrouda, F., Henry, B. and Borradaile, G., 2000. Limitations of tensor subtraction in isolating diamagnetic fabrics by magnetic anisotropy. Tectonophysics, 322(3-4): 303-310.
Hrouda, F. and Jelinek, V., 1990. Resolution of ferrimagnetic and paramagnetic anisotropies in rocks, using combined low-field and high-field measurements. Geophysical Journal International, 103(1): 75-84.
Hrouda, F., Jelinek, V. and Zapletal, K., 1997. Refined technique for susceptibility resolution into ferromagnetic and paramagnetic components based on susceptibility temperature-variation measurement. Geophysical Journal International, 129(3): 715-719.
Hrouda, F. and Jezek, J., 1999. Theoretical models for the relationship between magnetic anisotropy and strain: effect of triaxial magnetic grains. Tectonophysics, 301(3-4): 183-190.
Hrouda, F., Krejci, O., Potfaj, M. and Stranik, Z., 2009. Magnetic fabric and weak deformation in sandstones of accretionary prisms of the Flysch and Klippen Belts of the Western Carpathians: Mostly offscraping indicated. Tectonophysics, 479(3-4): 254-270.
Ihmle, P.F., Hirt, A.M., Lowrie, W. and Dietrich, D., 1989. Inverse magnetic fabric in deformed limestones of the Morcles nappe, Switzerland. Geophysical Research Letters, 16(12): 1383-1386.
Jackson, M., 1991. Anisotropy of magnetic remanence - a brief review of mineralogical sources, physical origins, and geological applications, and comparison with susceptibility anisotropy. Pure and Applied Geophysics, 136(1): 1-28.
Jackson, M. and Borradaile, G., 1991. On the origin of the magnetic fabric in purple Cambrian slates of North Wales. Tectonophysics, 194(1-20): 49-58.
Jackson, M. and Tauxe, L., 1991. Anisotropy of magnetic-susceptibility and remanence-developments in the characterization of tectonic, sedimentary and igneous fabric. Reviews of Geophysics, 29: 371-376.
Jayangondaperumal, R., Dubey, A.K., Kumar, B.S., Wesnousky, S.G. and Sangode, S.J., 2010. Magnetic fabrics indicating Late Quaternary seismicity in the Himalayan foothills. International Journal of Earth Sciences, 99: S265-S278.
Jelinek, V., 1977. The Statistical Theory of Measuring Anisotropy of Magnetic Susceptibility of Rocks and its Application Geofyzika Brno.
Jelinek, V., 1978. Statistical processing of anisotropy of magnetic susceptibility measured on groups of specimens. Studia Geophysica et Geodaetica, 22(1): 50-52.
Jelinek, V., 1981. Characterization of the magnetic fabric of rocks. Tectonophysics, 79(3-4): T63-T67.
Jelinek, V., 1995. Measuring anisotropy of magnetic susceptibility on a slowly spinning specimen-basic theory. AGICO print, No 10.
Joffe, S. and Garfunkel, Z., 1987. Plate kinematics of the circum Red Sea- a re-evaluation. Tectonophysics, 141: 5-22.
Jover, O., Rochette, P., Lorand, J.P., Maeder, M. and Bouchez, J.L., 1989. Magnetic mineralogy of some granites from the French Massif Central - origin of their low-field susceptibility. Physics of the Earth and Planetary Interiors, 55(1-2): 79-92.
Kamb, W.B., 1959. Theory of preferred crystallographic orientation developed under stress. journal of Geology, 67: 153-160.
Kligfield, R.W., Lowrie, W. and Pfiffner, O.A., 1982. Magnetic properties of deformed oolitic limestones from the Swiss Alps: the correlation of magnetic anisotropy and strain. Eclogae geologicae Helveticae [0012-9402], 75.
Krenkel, E., 1924. Der Syrische Bogen. Cent. Mineral Geology Palaeontology, Abh. B, 9-10: 9: 274-281 and 10: 301-313.
Lanci, L., Kent, D.V., Biscaye, P.E. and Bory, A., 2001. Isothermal remanent magnetization of Greenland ice: Preliminary results. Geophysical Research Letters, 28(8): 1639-1642.
Latta, D.K. and Anastasio, D.J., 2007. Multiple scales of mechanical stratification and decollement fold kinematics, Sierra Madre Oriental foreland, northeast Mexico. Journal of Structural Geology, 29(7): 1241-1255.

Le Beon, M. et al., 2008. Slip rate and locking depth from GPS profiles across the southern Dead Sea Transform. Journal of Geophysical Research-Solid Earth, 113(B11): -.
Levi, T. and Weinberger, R., 2011. Magnetic fabrics of diamagnetic rocks and the strain field associated with the Dead Sea Fault, northern Israel. Journal of Structural Geology, 33(4): 566-578.
Levitte, D., 2001. Gological Map of Isreal, Zefat, Sheet 2-III. Geological Survey of Israel.
Mamtani, M.A. and Sengupta, A., 2009. Anisotropy of magnetic susceptibility analysis of deformed kaolinite: implications for evaluating landslides. International Journal of Earth Sciences, 98(7): 1721-1725.
Martin-Hernandez, F. and Ferre, E.C., 2007. Separation of paramagnetic and ferrimagnetic anisotropies: A review. Journal of Geophysical Research-Solid Earth, 112(B3).
Mattei, M., Sagnotti, L., Faccenna, C. and Funiciello, R., 1997. Magnetic fabric of weakly deformed clay-rich sediments in the Italian peninsula: Relationship with compressional and extensional tectonics. Tectonophysics, 271(1-2): 107-122.
McCabe, C., Jackson, M. and Ellwood, B.B., 1985. Magnetic anisotropy in the Trenton Limestone results of a new technique, anisotropy and anhysteretic susceptibility. Geophysical Research Letters, 12(6): 333-336.
McKenzie, D.R., Yin, Y., McFall, W.D. and Hoang, N.H., 1996. The orientation dependence of elastic strain energy in cubic crystals and its application to the preferred orientation in titanium nitride thin films. Journal of Physics-Condensed Matter, 8(32): 5883-5890.
Morrish, A.H., 1965. The Physical Principles of Magnetism. John Wiley, Hoboken, N. J.
Mullins, C.E., 1977. MAGNETIC-SUSCEPTIBILITY OF SOIL AND ITS SIGNIFICANCE IN SOIL SCIENCE - REVIEW. Journal of Soil Science, 28(2): 223-246.
Neumann, E., 1969. Experimental recrystallisation of dolomite and comparison of preferred orientations of calcite and dolomite in deformed rocks. Journal of Geology, 77: 426-438.
Nye, J.F., 1957. Physical properties of crystals: their representation by tensors and matrices.
Osborn, J.A., 1945. The demagnetizing factors of the general ellipsoid. Physical Review, 67: 351-357.
Owens, W.H. and Bamford, D., 1976. Magnetic, seismic, and other anisotropic properties of rock fabrics. Philosophical Transactions of the Royal Society of London Series a-Mathematical Physical and Engineering Sciences, 283(1312): 55-68.
Owens, W.H. and Rutter, E.H., 1978. The development of magnetic susceptibility anisotropy through crystallographic preferred orientation in a calcite rock. Physics of the Earth and Planetary Interiors, 16(3): 215-222.
Parés, J.M. and B.A., V.d.P., 2004. Correlating magnetic fabrics with finite strain: Comparing results from mudrocks in the Variscan and Appalachian Orogens. Geologica Acta, 2(3).
Pares, J.M. and van der Pluijm, B.A., 2003. Magnetic fabrics and strain in pencil structures of the Knobs Formation, Valley and Ridge Province, US Appalachians. Journal of Structural Geology, 25(9): 1349-1358.
Pares, J.M., van der Pluijm, B.A. and Dinares-Turell, J., 1999. Evolution of magnetic fabrics during incipient deformation of mudrocks (Pyrenees, northern Spain). Tectonophysics, 307(1-2): 1-14.
Patterson, M.S., 1973. Nonhydrostatic thermodynamics and its geologic application. Reviews of Geophysics, 11: 355-389.
Quennell, A.M., 1956. Tectonics of the Dead Sea rift, Congreso Geologico Internacional, 20th sesion, Asociacion de Servicios Geologicos Africanos, Mexico City, pp. 385-405.
Reches, Z., 1987. Mechanical aspects of pull-apart basins and push-up swells with applications to the Dead Sea transform. Tectonophysics, 141: 75-88.
Reches, Z. and Hoexter, D.F., 1981. Holocene seismic and tectonic activity in the Dead Sea area. Tectonophysics, 80: 235-254.
Reilinger, R. et al., 2006. GPS constraints on continental deformation in the Africa-Arabia-Eurasia continental collision zone and implications for the dynamics of plate interactions. Journal of Geophysical Research-Solid Earth, 111(B5).

Rochette, P., 1988. Inverse magnetic fabric in carbonate-bearing rocks. Earth and Planetary Science Letters, 90(2): 229-237.
Ron, H. and Eyal, Y., 1985. Intraplate deformation by block rotation and mesostructures along the Dead Sea transform. Tectonics, 4: 85-105.
Rotstein, Y. and Bartov, Y., 1989. Seismic reflection across a continental transform: an example from a convergent segment of the Dead Sea rift. J. Geophys. Res., 94: 2902-2912.
Rutter, E.H., Casey, M. and Burlini, L., 1994. Preferred crystallographic orientation development during the plastic and superplastic flow of calcite rocks. Journal of Structural Geology, 16(10): 1431-1446.
Rutter, E.H. and Rusbridge, M., 1977. The effect of non-coaxial strain paths on crystallographic preferred orientation development in the experimental deformation of a marble. Tectonophysics, Volume 39, (Issues 1-3,): Pages 73-86.
Schmidt, V., Gunther, D. and Hirt, A.M., 2006. Magnetic anisotropy of calcite at room-temperature. Tectonophysics, 418(1-2): 63-73.
Schmidt, V., Hirt, A.M., Leiss, B., Burlini, L. and Walter, J.M., 2009. Quantitative correlation of texture and magnetic anisotropy of compacted calcite-muscovite aggregates. Journal of Structural Geology, 31(10): 1062-1073.
Schmidt, V., Hirt, A.M., Rosselli, P. and Martin-Hernandez, F., 2007. Separation of diamagnetic and paramagnetic anisotropy by high-field, low-temperature torque measurements. Geophysical Journal International, 168(1): 40-47.
Schultzkrutisch, T. and Heller, F., 1985. Measurement of magnetic-susceptibility anisotropy in Buntsandstein deposits from southern Germany. Journal of Geophysics-Zeitschrift Fur Geophysik, 57(1): 51-58.
Siegesmund, S., Ullemeyer, K. and Dahms, M., 1995. Control of magnetic rock fabrics by mica preferred orientation - a quantitative approach. Journal of Structural Geology, 17(11): 1601-&.
Sneh, A. and Weinberger, R., 2006. Gological Map of Isreal, Rosh-Pinna, Sheet 2-IV. Geological Survey of Israel.
Soto, R., Casas-Sainz, A.M., Villalain, J.J. and Oliva-Urcia, B., 2007. Mesozoic extension in the Basque-Cantabrian basin (N Spain): Contributions from AMS and brittle mesostructures. Tectonophysics, 445(3-4): 373-394.
Soto, R. et al., 2009. Reliability of magnetic fabric of weakly deformed mudrocks as a palaeostress indicator in compressive settings. Journal of Structural Geology, 31(5): 512-522.
Stockhausen, H., 1998. Some new aspects for the modelling of isothermal remanent magnetization acquisition curves by cumulative log Gaussian functions. Geophysical Research Letters, 25(12): 2217-2220.
Stoner, E.C., 1945. The demagnetizing factors for ellipsoids. Philosophical Magazine Series 7, 36(263).
Tarling, H.D. and Hrouda, F., 1993. The magnetic anisotropy of rocks. Chapman and Hall,, London.
Tauxe, L. (Editor), 1998. Paleomagnetic Principles. Boston, Kluwer Academic, p 299
Taylor, G.I., 1938. Plastic strain in metals. Jour. Inst. Metal., 62: 307-324.
Tullis, J. and Yund, R.A., 1982. Grain growth kinetics of quartz and calcite aggregates. journal of Geology, 90: 308-318.
Weinberger, R., Agnon, A. and Ron, H., 1997. Paleomagnetic reconstruction of a diapir emplacement: A case study from Sedom diapir, the Dead Sea Rift. Journal of Geophysical Research-Solid Earth, 102(B3): 5173-5192.
Weinberger, R., Gross, M.R. and Sneh, A., 2009. Evolving deformation along a transform plate boundary: Example from the Dead Sea Fault in northern Israel. Tectonics, 28: -.
Weinstein, Y., 2011. Transform faults as lithospheric boundaries, an example from the Dead Sea Transform. Journal of Geodynamics, 54: 21-28.
Wenk, H.R., Kern, H., Schaefer, W. and Will, G., 1984. Comparison of neutron and x-ray diffraction in texture analysis of deformed carbonate rocks. Journal of Structural Geology, 6(6): 687-&.

Wenk, H.R., Takeshita, T., Bechler, E., Erskine, B.G. and Matthies, S., 1987. Pure shear and simple shear calcite textures - comparison of experimental, theoretical and natural data. Journal of Structural Geology, 9(5-6): 731-745.

תקציר

לשם שיפור הבנת שדה-המעותים לאורך בקע-ים-המלח בצפון ישראל, נמדדו ונחקרו התכונות המגנטיות של 400~ דוגמאות מסלעים אאוקנים מהאזורים ראש-פינה, הר הגלבוע ומצוקי האון. דיפרקציית קרני-x, ניתוח שקפים ותמונות מיקרוסקופ אלקטרונים מלמדים כי תצורת בר-כוכבא מורכבת מגבישי קלצית וכי תכולת היסודות ברזל, מנגן, מגנזיום, אלומיניום וצורן נמוכה במיוחד. נמצא כי הדוגמאות מתצורת בר-כוכבא הן דיאמגנטיות עם סוספטביליטי ממוצע של $k_m = -10.95 \pm 1.01[\mu SI]$, המעיד כי התכונות המגנטיות נשלטות ע"י גבישי קלצית גרדא. צירי k_3 של האניזוטרופיה של הסוספטביליטי המגנטי (אי.אם.אס.) מקבילים לכיווניות המועדפת של צירי-c בגבישי הקלצית ומצביעים לכיוון ההיתקצרות המקסימאלית. בעבודה הוסק כי ערכי פרמטרי האניזוטרופיה (P` ו Δk) מקושרים לערכי עוצמות המעוות המצטבר (finite strain) בסלע. מדידות ה-אי.אם.אס. של $300\sim$ דוגמאות מתצורת בר-כוכבא מאיזור ראש-פינה מצביעות על התקצרות מקסימאלית בכיוון צפון-דרום המשוייכת לפעילות לאורך בקע-ים-המלח. עוצמות המעוות באזור הן הטרוגניות בעיקרן ואינן מקושרות למבנים מקומיים.

בעבודה פותחה שיטה לבידוד הפאזות המגנטיות (magnetic phases) בסלע. ייסומה מעיד כי בסלעי קלצית, פאזה פרהמגנטית של מינרלי ברזל בתכולה של מעל 500 ppm ממסכת את הפאזה הדיאמגנטית ושולטת ב אי.אם.אס.. במקרה בוחן אחד, הפאזה הדיאמגנטית בודדה בהצלחה מה-אי.אם.אס. של סלע קרבונטי רב-פאזות, ומגלה ערכי P` בטווח שבין 1.01 ו 1.04 .

בנוסף, נחקרו התכונות המגנטיות של תצורות הקירטון האאוקניות אדולם, תימרת ומרשה ונמצאה תגובה דיאמגנטית חלשה עד פרהמגנטית חלשה. נמצא כי ה-אי.אם.אס. של תצורת התימרת מורכב משלוש פאזות מגנטיות: דיאמגנטית של קלצית, פרהמגנטית של חרסיות ופרימגנטית של גרעיני מגנטית. תוך שימוש משולב בטכניקות מגנטיות שונות בתהליך בידוד הפאזות הוערכו תרומות הפאזות השונות ל-אי.אם.אס.. בעבודה הוסק כי כיווני צירי ה-אי.אם.אס של תצורת התימרת משקפים את הכיוויניות המועדפת של גבישי הקלצית בסלע.

משרד התשתיות הלאומיות
האנרגיה והמים
המכון הגיאולוגי

תכונות מגנטיות של סלעים קרבונטיים ככלי להערכת מעוות ליד בקע-ים-המלח בצפון ישראל

רן יששכר

חיבור זה הוגש כחלק מהדרישות לקבלת התואר
"מוסמך אוניברסיטה" - M.Sc. באוניברסיטת תל-אביב
החוג לגיאופיסיקה ולמדעים אטמוספריים פלנטריים.

העבודה הוכנה בהדרכתם של:
דר' צפריר לוי, המכון הגיאולוגי, ירושלים
פרופ' רם ויינברגר, המכון הגיאולוגי, ירושלים
פרופ' שמואל מרקו, החוג לגיאופיסיקה ומדעים אטמוספריים ופלנטריים, אוניברסיטת תל-אביב

דו"ח מס' GSI/25/2013 ירושלים, תמוז תשע"ג, יוני 2013